Technische Universität München

Max-Planck-Institut für Quantenoptik

Rotational-state cooling and detection of trapped CH_3F molecules

Rosa Glöckner

Vollständiger Abdruck der von der Fakultät für Physik der Technischen Universität München zur Erlangung des akademischen Grades eines

Doktors der Naturwissenschaften (Dr. rer. nat.)

genehmigten Dissertation.

Vorsitzende(r):		Univ.-Prof. Dr. W. Zwerger
Prüfer der Dissertation:	1.	Hon.–Prof. Dr. G. Rempe
	2.	Univ.-Prof. Dr. J. Barth
	3.	Univ.-Prof. Dr. F. Merkt, ETH Zürich/ Schweiz (nur schriftliche Beurteilung)

Die Dissertation wurde am 22.12.2015 bei der Technischen Universität München eingereicht und durch die Fakultät für Physik am 30.05.2016 angenommen.

Abstract

The creation of a degenerate quantum gas of polyatomic molecules is a long standing goal in quantum science. To reach this goal, external and internal control of the molecules has to be gained. While the former is extensively studied, the latter has hardly been investigated so far. A widely applicable, comprehensive approach for controlling the rotational states of trapped polyatomic molecules is presented in this thesis. It includes the development of a rotational-state detection method, the first rotational-state cooling of polyatomic molecules and the preparation of a motionally cold ensemble in a single state. The toolbox for this approach comprises the selective driving of rotational transitions and optical pumping via vibrational transitions and only uses generic properties of symmetric top molecules.

The developed rotational-state detection method is based on state-selective removal of molecules from an electrically trapped ensemble. The trap depletion is analyzed in detail and the measured dynamics is nicely explained by a rate model. The rotational-state cooling is realized via the first implementation of optical pumping to trapped polyatomic molecules. By integrating rotational-state cooling with motional Sisyphus cooling, internal and external degrees of freedom are concurrently cooled. An additional optical pumping process prepares more than 70 % of the population in a single rotational Stark-substate. In total, starting from a room temperature gas bottle, where thousands of rotational states are populated, a motionally cold ($\approx 30\,\mathrm{mK}$) and almost pure state ensemble of about 10^6 trapped CH_3F molecules was produced in a DC electric trap using only a single laser and microwave radiation. This approach for controlling the rotational state of trapped polyatomic molecules represents a crucial step towards an ultracold molecular gas in a single internal state. An extension of the optical pumping to transfer the population into the absolute ground state could be a next step as it creates favorable conditions for studying evaporative cooling of polyatomic molecules.

Contents

Chapter 1

Introduction

Molecules can offer fascinating characteristics like a wealth of internal degrees of freedom, a large permanent electric dipole moment, and a variety of chemical properties. Intrigued by these features, research groups originating from seemingly different fields in physics unite in the very lively and rapidly developing research area of cold and ultracold molecules. This fascinating development throughout the last decade is in particular highlighted in the books [Smi08, Kre09] and special issues [Car09a, Jin12, Her13, Car15] dedicated to this field.

In order to explore the new applications of cold and ultracold molecules, the internal and external degrees of freedom of the molecules have to be controlled. Therefore, many different techniques to produce molecules at low or ultralow temperatures were developed. In this context, two temperature ranges are commonly distinguished, the cold (1 mK to few K) and the ultracold (< 1 mK) regime [Bel09b, Car09b, Lem13], whereas a more rigorous definition of cold and ultracold can be based on scattering properties of the molecules [Boh09]. The control of the internal state is equally important and can be accomplished by optical pumping, but only few implementations were demonstrated up to now. In particular, a method for control and cooling of the rotational states of trapped polyatomic molecules by optical pumping was lacking prior to this thesis.

1.1 Applications of cold and ultracold molecules

The presence of an electric dipole moment as well as a rich structure of internal states are essential for many applications in many-body physics with quantum gases, quantum information processing, controlled collisions and spectroscopy. From the perspective of this thesis those are the most important applications of cold and ultracold molecules. They are therefore discussed in more detail in the following and particular advantages of polyatomic molecules are highlighted. The large body of work on the interaction of molecules with attosecond laser pulses [Cor07] and coherent control of molecular dynamics [Sha03], will be omitted as they are beyond the scope of this thesis.

Cold collisions and quantum chemistry The particular interest in collisions at low energies, or chemical reactions at low temperatures, has several reasons [Kre08, Bel09b, Boh09, Her09, Qué12]: Controlling molecules at the quantum level requires the knowledge of their scattering properties, which can be dramatically different at ultralow temperatures. In this regime, the collision processes are expected to be dominated by quantum effects and can in particular be strongly influenced by the long-range intermolecular forces. In addition, external fields are likely to have a strong influence on the

reaction dynamics which can be used to tailor the process. The experimental study of cold collisions and chemical reactions allows to draw conclusions about the potential energy surface which can then be compared to ab-initio calculations which together yields a gain in fundamental understanding of these effects. Chemical reactions at low temperatures also provide insights about the cold chemistry in interstellar gas clouds. In these cold ($\approx 5\,\mathrm{K}$) clouds, the coldest naturally occuring chemical reactions take place. Up to date, more than a hundred molecule species were found and huge effort is put into understanding these chemical reactions in more detail [Her08, Tie13, vH11].

A large variety of cold-collisions experiments is performed with crossed or merged beams [Van12, Nar12, Jan15]. In 2006 the group of G. Meijer [Gil06] demonstrated the first observation of collisions of Stark decelerated OH radicals with a crossed cold Xe beam. They achieved collision energies from 50 to $400\,\mathrm{cm}^{-1}$ with a high state purity of the OH radials and found a clear threshold behavior. The collision energies can be further reduced by merging two beams and selecting the relative forward velocity and therewith the collision energy. With such a system, several resonances could be observed in the Penning ionization $\mathrm{He}(^3\mathrm{S}_1)+\mathrm{H}_2 \rightarrow \mathrm{H}_2^+ + \mathrm{He}$ [Hen12]. Recently, Penning ionization experiments with Ne^* and $\mathrm{CH}_3\mathrm{F}$ were performed [Jan14a]. A disadvantage of the merged beam technique, however, is the large forward velocity of both beams and therewith a short interaction time.

Trapping of molecules can dramatically increase the interaction time and therefore gives access to slow or weak processes. The first approach towards this goal is a combination of trapped ensembles and molecular beams. For example, Parazzoli [Par11] and coworkers measured the electric field dependence of elastic and inelastic cross sections for collisions of Stark decelerated ND_3 molecules with Rb atoms in a magneto-optical trap. Collisions of magnetically trapped OH molecules for the sake of evaporative cooling were studied and a large dependence of the loss rate on electric field strength was observed [Stu13].

There is also a large body of work on collisions of cold molecules with cold ions [Rot06, Bel09a, Ton10, Wil08, Hal12]. The group of T.P. Softley [Wil08], for example, studied the reaction of velocity-filtered $\mathrm{CH}_3\mathrm{F}$ with Ca^+ Coulomb crystals at single-particle sensitivity. The use of a source providing molecules at very low, tunable velocities in well-defined internal states would lead to only a few partial waves contributing to the collision and would hence drastically increase the resolution.

High-resolution spectroscopy and the study of fundamental physics It is well known that high-resolution spectroscopy of atoms or molecules constitutes a key element for experimental investigations in physics. Spectroscopy not only provides insights on the structure needed for controlled manipulation but also yields a sensitive probe to test theory. The particular advantage that comes with cold or ultracold molecules is twofold. Control of the internal states of molecules allows to prepare the ensemble in a particular internal state and slow or even stopped motion results in longer interaction times thereby increasing the spectral resolution.

A prominent example for the particular benefit of spectroscopy on molecules is the search for variations of fundamental constants, a problem that traces back as far as the work of Dirac [DIR37]. A possible variation of e.g. the fine structure constant manifests differently on vibrational, rotational and electronic transitions of molecules and thus opens compared to atoms additional possibilities for the intensive study of this

problem [Gin04, Chi09, Kaj09, Jan14b]. As an example, spectroscopy data obtained in the laboratory can be compared to measurements in the interstellar medium to put limits on the drift of the proton-to-electron mass ratio or the variation of the fine structure constant [Bag13, Tru13]. Moreover, precision spectroscopy on molecules can be exploited to put constraints on existing theories of higher dimensions [Sal15]. Those extra dimensions should become visible in a change of the gravitational strength. Molecules can probe space time on length scales of the bonding length and thereby put constraints on the compactification radii of extra dimensions.

Spectroscopy on molecules also allows measuring parity violation [Dau99, DeM08] or testing time-reversal symmetry [Hin97]. In recent years, cold polar molecules emerged as ideal candidates to measure the electron electric dipole moment (EDM) [Hud11]. Compared to atoms, the effective internal electric fields of polarized molecules are orders of magnitude larger and act thereby on the EDM of the electron, thus providing a sensitive probe. With buffer-gas cooled ThO molecules, the highest level of precision $|d_e| < 8.7 \times 10^{-29}\,\mathrm{e}\cdot\mathrm{cm}$ so far was reported [Bar14], thereby probing new physics at the TeV energy scale. However, to boost the sensitivity even more, further cooling of the molecules is needed [Tar13].

Quantum information processing Due to their long range dipole-dipole interaction and the rich internal structure, molecules are considered to be ideal candidates for quantum information processing. Already in 2002, D. DeMille [DeM02] proposed the use of polar molecules as qubits. They are held in a one-dimensional array of traps with the dipole moment pointing up or down relative to an external electric field. This system possesses many advantages: a field gradient allows for addressing individual sites, the dipole-dipole interaction provides a way to quickly create entanglement and these arrays appear feasible to scale up to obtain large networks. The entanglement of these arrays of molecules was studied by Q. Wei and coworkers [Wei10, Wei11a, Wei11b]. In [Wei11b] they especially investigate the entanglement of polar symmetric top molecules as candidate qubits thereby pointing out the advantage resulting from a first-order Stark shift: an effective dipole moment that is nearly independent of the field strength.

Another approach is the combination of molecules with solid-state systems [Rab06, And06], where the molecules serve as optical interfaces and provide the long-term storage, overcoming the key issue of rapid decoherence in solid-state systems. In particular, typical transition frequencies between rotational states of molecules are often in the microwave regime allowing for a strong coupling with microwave photons confined by a strip-line resonator. Preparing these molecules in a crystalline one-dimensional dipolar chain is studied as a candidate for a high-fidelity quantum memory in reference [Rab07]. This approach protects the molecular qubits from the damaging effects of short-range collisions.

Yelin, Kuznetsova and coworkers studied schemes for robust quantum computation with polar molecules [Yel06] and provided an analysis of the experimental feasibility of polar-molecule-based phase gates [Kuz08]. They in particular address the task of switching "on" and "off" the strong dipole interaction of polar molecules using hyperfine states. De Vivie-Riedle and coworkers [Tes02] developed schemes for quantum computation with vibrationally excited states. Each normal mode of polyatomic molecules can be used to define quantum bits and they discuss how to employ this idea for the

polyatomic molecule acetylene (C_2H_2). First experimental results in this direction of quantum computation with molecules have been obtained with Li_2 [Val02] and iodine molecules [Hos10] based on population transfer with shaped ultrashort laser pulses. Cooling and trapping of molecules with the prospect of individual addressing of single molecules, however, is necessary to scale up the system [Hos10].

Quantum many-body physics The achievements in cooling the motion of atoms and controlling their internal degrees of freedom has opened a beforehand unimaginable playground. One of the intensively studied areas is the work on many-body physics, e.g. simulating solid state physics, studying phase transitions or research on low-dimensional systems [Blo08]. The dynamics in these experiments is usually determined by the character of the interparticle interaction, which in non-polar atomic systems is typically an s-wave isotropic short range interaction described by the scattering length a.

Already in 2000 it was found that the properties of a Bose-Einstein condensate change dramatically if the interactions are dominated by long-range and anisotropic dipole-dipole forces [San00]. Since then, quite a number of proposals for new physics with dipole-dipole interaction came up, like new quantum phases [Gór02, Mic07] or new toolboxes for lattice-spin models [Mic06, Ort09] which are nicely reviewed in [Lah09, Tre11, Bar12].

The first and fascinating observation of dipolar behavior in a quantum gas was made with chromium atoms, which have a large magnetic moment of several Bohr magnetons in their ground state [Gri05, Stu05]. Compared to the magnetic dipole moments of atoms, polar molecules posses much larger dipole moments and thus allow to deeply advance into the dipole-dipole interaction dominated regime. However, the production of an ensemble of polar molecules near quantum degeneracy remains a challenge and has only been achieved by assembling ultracold atoms, as first demonstrated by the group of J. Ye and D. Jin [Ni08]. The same group also realized the first lattice spin model with ground-state polar molecules [Yan13]. Despite recent progress [Mos15], realizing a degenerate quantum gas of molecules in an optical lattice with high filling remains an open goal.

Despite these challenges and the technical effort, assembling ultracold alkali atoms seemed for long times the only feasible method to produce ultracold molecules and thus many of the proposals mentioned above focus on diatomic molecules. However, recent proposals demonstrate that polyatomic molecules and in particular symmetric top molecules have clear advantages compared to diatomic molecules [Wal13, Wal15]. In particular the dipole-dipole interaction of symmetric top molecules in a static electric field due to their linear Stark shift corresponds to the dipole-dipole interaction of magnetic dipoles in a magnetic field. This correspondence does not exist for alkali dimers revealing the benefits of symmetric top molecules for simulating quantum magnetism.

1.2 Producing ensembles of cold polyatomic molecules

The various applications of cold and ultracold molecules have driven the development of new and very diverse experimental approaches to produce these molecules. The techniques which are applicable to polyatomic molecules are summarized below. In particular the effects of these methods on the internal-state distribution is discussed.

Owing to the focus on polyatomic molecules, a discussion of the production of ultracold molecules by assembling ultracold alkali-atoms is omitted, despite the fact that this method reaches the lowest temperatures [Ni09, Mos15] . Another promising technique that is not discussed is laser cooling of molecules. This approach can be applied to certain diatomic molecules [Di 04] and resulted recently in a few thousand sub-mK SrF molecules in a magneto optical trap [Nor15].

Velocity filtering A technique that is applicable to a wide range of polar molecule species is velocity filtering. The concept is simple: Every thermal gas contains a small fraction of molecules with very low energy. These molecules can be filtered using velocity-selective trapping, e.g. a static electric quadrupole guide that only guides this low energy faction. This method does not cool, but nevertheless provides a simple and very robust method to continuously produce molecules at about 1 K [Ran02, Jun04, Mot09] with a flux of about 10^{10}/s. Cold polar molecules produced by velocity filtering can easily be trapped by suitable electric traps [Rie05]. This technique is therefore particularly well suited to be combined with the microstructured DC electric trap [Eng11] used in this thesis.

The internal state distribution of the guided molecular beam depends on the rotational constants of the molecule species and the applied trapping field. It was first investigated via depletion spectroscopy by Motsch et al. [Mot07] and a good agreement of expected and measured rotational state distribution was found. Investigations of the rotational state populations inside a hexapole guide were performed by B. Bertsche and coworkers [Ber10, Ber11] and also showed a rather broad distribution covering tens of rotational states.

Deceleration techniques For decelerating molecules after supersonic expansion, various methods are intensively studied [Hog11]. One of the advantages of this technique is its applicability to several small polyatomic molecules species as e.g. NH_3,ND_3, H_2CO, CH_3F. However, it is important to note, that the cooling takes place due to collisions during the supersonic expansion and not during the deceleration. The deceleration shifts the center-of-mass velocity to lower velocities in the laboratory frame which due to phase space arguments directly sets limits on the achievable temperatures and molecule numbers with this method.

Deceleration is e.g. based on the interaction of polar molecules with time-varying electric field to slow neutral molecular ensembles [Bet99, Van12]. These Stark decelerators have also been built on a chip [Mee09] or in the form of traveling traps [Ost10]. Deceleration of molecules can also be based on Rydberg-Stark states [Yam04] and on magnetic [Nar12], microwave [Mer12] or optical fields [Ful04]. A continuous deceleration of polar molecules was recently achieved with a centrifuge decelerator [Che14].

Trapping of decelerated polyatomic molecules was demonstrated by several groups. Traveling-wave decelerators have, for example, been used to trap ammonia molecules. In a subsequent adiabatic cooling, temperatures below 1 mK with few molecules were achieved [QP14]. Meng at al. [Men15] used in 2015 a traveling wave decelerator to slow CH_3F molecules to rest, the heaviest and most complex molecule decelerated to rest till then. They were able to trap 2×10^4 CH_3F molecules at a temperature of about 40 mK.

The internal distribution of the decelerated ensembles depend on the collisions during the supersonic expansion and the properties of the deceleration. These collisions effectively cool the rotational state of the molecules, whereas the vibration is poorly cooled [vdM05]. The resulting state distribution is further reduced by the state-selective deceleration process and often results in high rotational-state purities. However, an experimental analysis by the group of Lewandowski showed, that Stark deceleration can be inefficient in producing molecules in a single rotational state [Fit12] and further filtering or internal cooling might be needed.

Buffer-gas cooling A method capable to cool the internal and external degree of freedom of a wide variety of molecule species is buffer-gas cooling, nicely reviewed in [Hut12]. Molecules are cooled by collisions with a cryogenic gas like He or Ne inside a cryogenic cell. A small hole allows the formation of a molecular beam together with the buffer-gas. The buffer-gas density has a strong influence on the beam formation: For low buffer-gas densities, the molecular beam almost matches a Maxwell-Boltzmann distribution. Unfortunately, the slow molecules are missing in the beam. In addition, the low pressure results in a low molecule number due to freezing of the molecules on the walls of the cell. For higher buffer-gas densities, the wind of the buffer-gas leads to a better extraction of molecules from the cell, but results in a higher forward velocity of the molecular beam. A cell design for good extraction of molecules with small forward velocities is under current study.

If there are sufficient inelastic collisions with the buffer gas, the internal distribution thermalizes with the buffer gas. Typically the rotational degree of freedom thermalizes equally fast as the motional degree, however, the vibrational relaxation is less efficient [Hut12]. The rotational-state distribution has been studied in several experiments [Van09, Twy14] proving that the rotational state can efficiently be cooled to the lower rotational states for the molecules ND_3 or H_2CO. However, for larger molecules with small rotational constants, even at cryogenic temperatures a huge number of states are still populated and further filtering or internal cooling is needed to achieve pure state ensembles.

Optoelectrical Sisyphus cooling This is the cooling method employed in this thesis, and it can be used to cool polyatomic molecules to sub-mK temperatures [Zep09, Zep12, Pre15]. In the current implementation, it proceeds in an electric trap, which is loaded via velocity filtering. As discussed above, velocity filtering provides molecules at temperatures below 1 K, but with a rather broad rotational-state distribution containing hundreds of states even for relatively light molecules such as CH_3F. Sisyphus cooling, however, only cools molecules populating two neighboring (freely chosen) rotational states. Thus the number of cooled molecules could be significantly enhanced by rotational-state cooling. Narrowing the rotational-state distribution is in particular a prerequisite for applying Sisyphus cooling to molecule species with a small rotational constant, where the initial rotational-state distribution is even broader. In addition, Sisyphus cooling does not produce an internally pure-state ensemble. To reach this goal, an additional method for controlling the internal state is needed.

1.3 Internal cooling of molecules

The fascinating applications of cold and ultracold molecules require a further internal-state control than the one provided by the discussed cooling methods so far. Both, narrowing the population distribution by internal-state cooling and preparing the molecules in well-defined and freely-chosen quantum states can be accomplished by optical pumping. The extremely useful technique of optical pumping is one of the first methods that were used to manipulate atoms with light. It was developed by the 1966 Nobel laureate Alfred Kastler in 1950 [Kas50] and shortly afterwards experimentally observed [Bro52, Haw53]. Since then, optical pumping has been a versatile tool for many applications in quantum optics and was in particular used for internal-state preparation.

Optical pumping of molecules for the purpose of internal state cooling has been demonstrated by the group of P. Pillet in 2008 [Vit08, Sof09]. Photoassociated Cs_2 molecules initially populating several vibrational states were pumped to the vibrational ground state with a shaped femtosecond laser pulse. In combination with a narrowband cw laser, the vibrational and rotational states were concurrently cooled into the respective ground states with up to 40 % efficiency [Man12, Man13]. Vibrational cooling of a heteronuclear molecule, photoassociated NaCs, via optical pumping was achieved in 2012 in the group of N. P. Bigelow [Wak12]. Population transfer by optical pumping, without the purpose of narrowing the distribution, has also been used to pump Stark-decelerated metastable CO into the absolute internal ground state [Blo11] or to efficiently load CaF [Lu14] or NH [Rie11] molecules into a magnetic trap.

In summary there are only a few implementations of optical pumping of cold neutral molecules, despite the fact that there is a huge need for internal state control of molecules and that optical pumping is a widely used technique for atoms. In particular, an implementation for polyatomic molecules was still lacking prior to this thesis. It is hampered by the much more complex internal structure of molecules compared to the atomic species typically used in quantum optics. Optical pumping of molecules could, for example, lead to rapid trap loss due to population transfer to untrapped states or even to the dissociation of molecules while driving electronic transitions.

Compared to atoms, however, the multitude of internal states also brings new possibilities for manipulation as for example driving vibrational transitions to manipulate the rotational state. Optical pumping of molecules via vibrational transitions has been concurrently demonstrated for the molecular ions HD^+ [Sch10] and MgH^+ [Sta10] in 2010, achieving 78 % and 36 % ground-state population, respectively. One advantage of using molecular ions is their long storage time which enables driving vibrational transitions despite the orders of magnitude slower decay rate compared to electronic ones. Second, the trapping is independent of the internal state of the ions and therefore optical pumping cannot lead to losses of the ions. Handling these two issues, however, allows one to implement optical pumping via vibrational transitions also for trapped neutral molecules as will be demonstrated in the course of this thesis.

1.4 Outline of this thesis

In this thesis, a comprehensive approach of controlling cold polar molecules is presented. Based on previous work [Eng13, Zep13] which demonstrated a method to motionally cool trapped polyatomic molecules to sub-mK temperatures [Pre15] via an

optoelectrical Sisyphus mechanism, this thesis adds a key missing element: control of the internal states. Note that parts of this thesis have been published beforehand in the publications [Glö15b, Glö15a].

The experimental and theoretical foundations of this thesis are given in chapter 2. In particular, the properties of the employed molecule fluoromethane (CH_3F) are discussed and the experimentally exploited internal states and transitions are introduced. Furthermore, a short summary of the theoretical concepts of rotational-state control is given and the experimental setup is briefly described. The key element of the experimental setup, the DC-electric homogeneous-field trap, is investigated in detail in chapter 3. In particular, a new method for measuring the electric-field distribution is presented. This analysis is used to discuss the ability to resolve individual rotational and vibrational transition, a prerequisite for controlled manipulation of the internal states by radiation fields. In addition, any investigation of internal-state control is impossible without means to detect the internal state. Chapter 4 presents a widely applicable method for rotational-state detection based on state-selective removal of molecules from the trapped ensemble. In particular, the dynamics of this depletion is analyzed experimentally and compared to results from a rate model. Chapter 5 presents the major result of this thesis, the first rotational-state cooling of trapped polyatomic molecules via optical pumping. It can be integrated seamlessly with motional Sisyphus cooling providing a concurrent cooling of the internal and motional degrees of freedom of polyatomic molecules. By a subsequent additional optical pumping process, a motionally cooled ensemble can be prepared in a single rotational M substate, achieving a cold and almost pure state ensemble of polyatomic molecules. Finally, the outlook in chapter 6 provides an overview about possible further experiments and discusses the applicability of the approach to other molecule species.

Chapter 2

Experimental and theoretical foundations

This chapter summarizes the experimental and theoretical basics of this thesis. In particular, the molecule of choice, fluoromethane (CH_3F), is introduced and the important properties of symmetric top molecules are discussed in section 2.1. An overview about the experimental setup and the basic elements of the experimental sequences used in this thesis is presented in section 2.2. Section 2.3 of this chapter introduces the exploited rotational states and gives an overview about all transitions that are driven in this thesis. Finally, the theoretical concepts of the presented rotational-state control are discussed in section 2.4

2.1 The molecule CH_3F

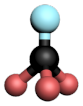

All experimental results presented in this thesis are obtained with the polar molecule fluoromethane (CH_3F). It is a prototypical symmetric top molecule and has a very large inversion barrier and thus a negligible inversion splitting. In addition, the hyperfine levels with opposite parity are coupled already at low electric fields of less than 1 V/cm resulting in a linear Stark shift [Bul91]. CH_3F is therefore well suited for simulating quantum magnets [Wal13, Wal15] and in addition is used to study chemical reactions [Bul91, Wil08] or nuclear spin conversion in molecules [Nag96]. For the purpose of the experiments performed in this thesis, the favorable selection rules for vibrational and rotational transitions of symmetric top molecules are of particular importance.

The fascinating theory of molecules and molecular spectra is explained in detail in several textbooks. In particular the series of Herzberg [Her45], *Microwave Spectroscopy* by Schawlow and Townes [Tow55] and *Molecular Symmetry and Spectroscopy* by Bunker and Jensen [Bun06] can be recommended. In this brief introduction, the focus is on the employed rotational and vibrational states. Electronically excited states of the closed shell molecule CH_3F are not considered at all. Because of the lack of strict selection rules for the vibrational quantum number, any electronic excitation would lead to the loss of internal state control and in addition contains the risk of rapid predissociation. Hence, for all experiments presented in this thesis, only vibrational and rotational transitions are used.

Rotational states of a symmetric top molecule The rotational state of a symmetric top molecule is described by three quantum numbers: the total angular momentum J, its projection onto the molecular symmetry axis K, and the projection on the electric

constant	symbol	value
dipole moment	μ	1.85 D
rotational constants	A_0	155.352 GHz
	B_0	25.536 GHz
centrifugal distortion	D_J	60.217 kHz
	D_{JK}	439.57 kHz
	D_K	2106.923 kHz

Table 2.1: Summary of molecular constants for CH_3F [Hüt10, Lid90].

field axis M. In the following, the rotational state will be denoted by $|v; J, \mp K, \pm M\rangle$, the $\pm$ signs being chosen such that $\mp K$ is positive. This notation effectively ignores the sign of K, reflecting the fact that states with K, M and $-K$, $-M$ are identical under inversion symmetry. The opposite sign for K and M allows low-field-seeking states to be expressed with positive state indices. v denotes the vibrational quantum number of the used v_1 mode.

In the case of no interaction with external fields the rotational energy is given by

$$\begin{aligned} E_{J,K}/h = \quad & B_0 J\,(J+1) + (A_0 - B_0)\,K^2 \\ & -D_J J^2(J+1)^2 - D_{JK} J(J+1)K^2 - D_K K^4 + \ldots \end{aligned} \tag{2.1}$$

Here, the first two terms correspond to the rigid rotor approximation with rotational constants B_0 and A_0 and the last three are small first-order corrections due to centrifugal distortions.

In the presence of an electric field the degeneracy of the M states is lifted according to the first order Stark effect,

$$\Delta\nu = -\frac{\mu\mathcal{E}}{h}\frac{KM}{J(J+1)}. \tag{2.2}$$

Here μ is the permanent electric dipole moment and $\mathcal{E}$ is the electric field strength. For typical electric fields in the experiment, this splitting is on the order of tens to hundreds of MHz and depends on all three rotational quantum numbers J,K and M. The associated molecular constants of CH_3F are summarized in Tab. 2.1.

Vibrational states To describe the vibration of a molecule it can be regarded as an N-body harmonic oscillator, where N is the number of nuclei. The vibrational energy is then given by $(3N-6)$ normal coordinates Q_r each of them describing a collective normal mode of vibration. The normal coordinates of CH_3F span the representation $\Gamma_Q = 3A_1 \oplus 3E$ of the molecular symmetry group $C_{3v}(M)$. Thus CH_3F has three non-degenerate vibrational modes and three degenerate ones which are listed in Fig. 2.1.

A comparison of the transition energies and the temperatures at our experiment immediately shows that the molecules almost exclusively populate the vibrational ground state which is often the case for small polyatomic molecules. Thus no vibrational cooling is needed and the sufficiently fast spontaneous decay of the vibrational excited states allows implementing optical pumping via vibrational transitions. In this work, Q-Branch vibrational transitions at the v_1-mode at 2996 cm^{-1} are driven. The corresponding excited state has a spontaneous decay rate of about 15 Hz [Eng13].

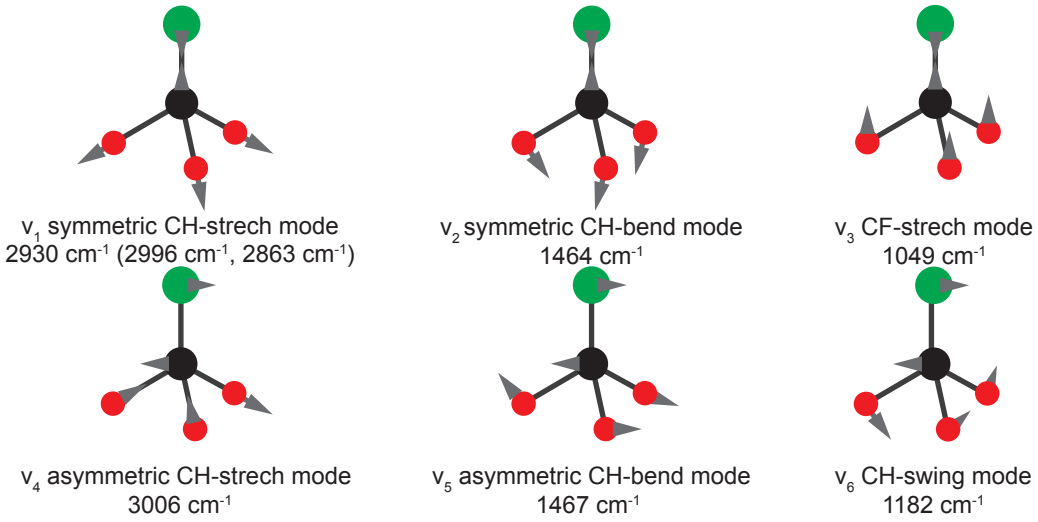

Figure 2.1: Vibrational modes of CH_3F. A Fermi resonance of the v_1 and the $2v_5$ mode leads to a splitting for the v_1 symmetric strech mode [Gra81]. In this thesis, purely the v_1 mode at $2996\,\mathrm{cm}^{-1}$ is used to drive vibrational transitions. The spontaneous decay rate of this mode is about 15 Hz.

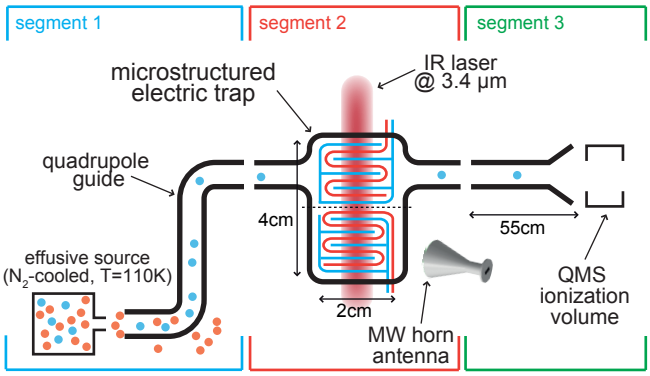

Figure 2.2: Experimental setup. Molecules are loaded from a thermal liquid-nitrogen cooled source into the trap via an electric quadrupole guide. For detection, the molecules are guided to a quadrupole mass spectrometer.

2.2 Experimental setup and sequence

All experiments proceed in a DC-electric trap providing trapping times of up to 30 s and a trap depth of about 1 K. Its unique design allows one to apply a tunable homogeneous electric field in a large fraction of the trap volume [Zep13]. Figure 2.2 shows the integration of the trap into the experimental setup where the individual parts are described below. Additional information about the setup can be found in [Mie10, Pre12, Eng13].

The source Cold polar molecules at about 1 K are produced via velocity filtering [Ran02, Jun04]. Starting from a room temperature gas bottle the molecules are

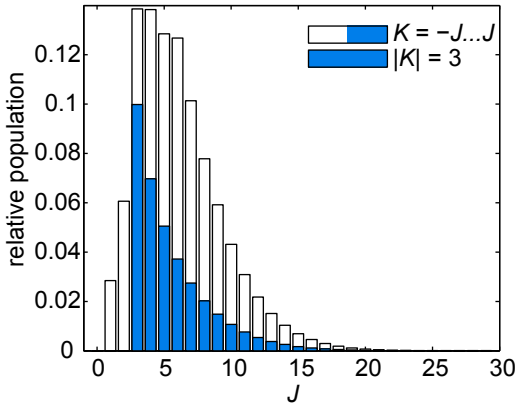

Figure 2.3: Rotational-state distribution for CH_3F in the electric quadrupole guide for velocity filtering from a thermal source at a temperature of 110 K.

precooled to 110 K in the liquid nitrogen cooled nozzle to reduce the internal and external temperature of the molecules. From the nozzle, the molecules are injected into a DC-electric quadrupole guide providing a trapping field of $\mathcal{E}_{load} = 30\,\mathrm{kV/cm}$, where the low energy fraction of the molecules ($\lesssim 1\,\mathrm{K}$) is guided to the electric trap. All measurements were performed with a molecule pressure at the nozzle of 4 Pa resulting in a small boosting parameter [Mot09].

The thermal population of rotational states in the liquid-nitrogen cooled nozzle can be calculated using Maxwell-Boltzmann statistics as no external fields are present in the nozzle. However, the population in the electric quadrupole guide differs as the trapping force depends on the molecular state, and the Maxwell-Boltzmann distribution has to be weighted with the Stark shift squared [Mot09]. The resulting population distribution is shown in Fig. 2.3. We find the highest population in the lowest rotational J states of the $|K| = 3$ manifold.

CH_3F offer a few great advantages for this type of source. First, it can be bought in a gas bottle and thus no chemical process for the production of the molecules is needed. Second, a rather narrow rotational state distribution is loaded into the trap. Finally, CH_3F has large dipole moment of 1.85 D which results in strong interactions with the electric fields resulting in favorable trapping properties.

The detection of molecules The molecules are unloaded via a second electric quadrupole guide and detected with a quadrupole mass spectrometer (QMS). The detection efficiency of the QMS is about 10^{-4}. Molecule detection with a QMS is a simple and robust technique, but does not give access to information about the internal state of the molecules. However, in combination with state-selective depletion, detecting the internal states of molecules is possible. This method of rotational-state detection is described in chapter 4. The employed settings at the QMS are given in Tab. 2.2.

The OPO laser system A widely tunable single mode optical parametric oscillator (OPO), Aculight Argos SF-15, is operated at a wavelength of 3.4 μm and provides the infrared (IR) radiation needed to drive vibrational transitions of our molecules. The frequency of the pump (1064 nm) and the signal (1555 nm) is stabilized to a frequency

parameter	value	parameter	value
SEM voltage	2400 V	mass	32.9 a.u.
resolution	120	ion source type	crossbeam
detector type	Ion-counter	emission current	0.6 mA

Table 2.2: Settings used at the QMS (Pfeiffer Vacuum QHG700+QMH410-3). The considerably reduced background of the QMS at the mass of CH_3F is a notable technical advantage of the choice of this molecule species.

comb allowing for sub-MHz frequency precisions. In addition, the frequency of the idler is measured with a wave meter at a precision of about 20 MHz.

The frequencies of the employed vibrational transitions lie within 20 GHz (see below). Fortunately, the frequency of the pump can be mode-hop-free tuned by up to 100 GHz with a suitable high voltage applied to a piezoelectric crystal at the fiber Bragg grating of the seed laser. In addition, the signal frequency can be tuned by several hundred MHz by varying the cavity length with a mirror mounted on a piezoelectric crystal. A fast ramp and relock system was designed and implemented [Pre12] and allows one to ramp and relock the frequency of the pump and signal within less than 10 ms. Hence, the frequency of the idler can be changed with a rate that is fast compared to the spontaneous decay rate of the vibrational excited state. This technique is used for a quasi-continuous driving of several vibrational transitions with only one laser source.

Microwave radiation To drive the rotational transitions of interest in our molecule, microwave (MW) radiation at about 200 GHz and 300 GHz is needed. A MW-synthesizer (Aeroflex 2218 OEM Modular Synthesizer) provides MW radiation with frequencies ranging from 500 MHz up to 18.4 GHz. A switch directs the radiation to two amplifier multiplier chains (AMC) which multiply the frequency by x12 or x24. The power of the resulting MW radiation is about 2 mW at 200 GHz and about 15 mW at 300 GHz. The radiation is directed onto the trap with horn antennas outside of the vacuum chamber.

For most applications, it is necessary to drive several rotational transitions simultaneously. Fortunately, the MW-synthesizer can switch the output frequency within about a μs. Thus, all needed frequencies be cycled and one total cycle is about 20 ms long often including a dark time. This is fast compared to the driving rate of the rotational transitions and hence the transitions can be regarded to be driven quasi-simultaneously. In the following it is assumed that the power used to drive the individual rotational transitions can be set by the duty cycle of the corresponding frequency. This assumption is based on the discussion, that the driving of transitions can be described by rates (see section 2.4). However, e.g. doubling the length of a MW pulse by doubling the duty cycle leads only to twice the effective power if even during these pulses coherent processes can be ignored. Thus the molecules have to be in different electric fields during the pulse which might fail for slow molecules or short pulses. The distance which the molecules move during one pulse can in a first guess be compared to the periodicity of the micostructures of 200 μm (see section 3.1). The total output power of the AMCs can also be reduced by applying a voltage at the user controlled attenuation port.

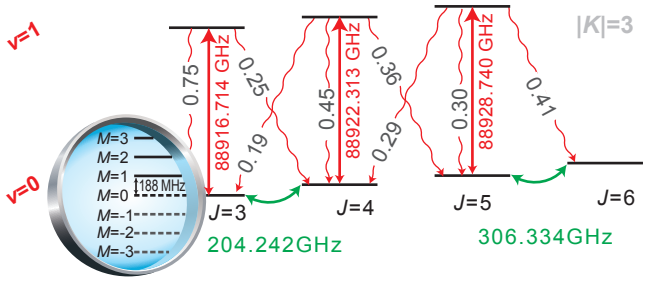

Figure 2.4: Summarized level scheme showing the relevant internal states of CH_3F. Transition frequencies are given for zero electric field. As indicated by the zoom, the rotational states split in an electric field according to the linear Stark effect. Only the low-field seeking states (positive M values) are trapped with the DC electric trap.

Experimental sequence The experimental setup consists of three segments as shown in Fig. 2.2. The voltages in each segment can be controlled individually allowing different configurations for loading molecules to the trap, storage of molecules in a closed trap and unloading molecules to the QMS [Eng11]. In the majority of the measurements presented in this thesis, the trap was loaded for 16 s. Motional and/or rotational cooling of molecules can already be applied during the loading. The time for storage differed for the individual experiments. If applicable, state-sensitive depletion for the purpose of state detection (chapter 4) was implemented at the end of the storage time directly before unloading and detecting the molecules for 12 s. The timings of the sequences are given together with the data and appendix A provides an overview about experimental steps.

2.3 The level scheme

Exploited internal states The level scheme shown in 2.4 is the basis of all internal state manipulation in this thesis. The choice of the rotational states was based on the high relative population (see Fig. 2.3). It was found that the lowest rotational states $J = 3, 4$ with $|K| = 3$ are best populated with $\approx 17\,\%$. Additional $9\,\%$ of the molecules populate the rotational states $J = 5, 6; |K| = 3$. The high population is of great advantage, as it allows manipulating a large fraction of the trapped ensemble when addressing these states. Note that the rotational states split in an electric field according to the linear Stark effect and only the low-field seeking states (positive M values) are trapped with the DC electric trap.

Figure 2.4 also indicates all driven rotational and vibrational transitions and the branching ratios for the spontaneous decay. The current setup allows the driving of the rotational transition $J = 3 \leftrightarrow J = 4$ and $J = 5 \leftrightarrow J = 6$ with MW radiation. For these pure rotational transitions, the selection rules are

$$\Delta K = 0 \qquad \Delta M = 0, \pm 1 \qquad \Delta J = 0, \pm 1 \qquad (\Delta J = 0 \text{ only for } K \neq 0). \tag{2.3}$$

Driving Q-Branch vibrational transitions benefits from the close vicinity of the transition frequencies: all needed transition frequencies lie within the tuning range of the OPO which allows one to quasi-simultaneously drive these transitions with the same laser source. By exciting the v_1 vibrational mode, the dipole moment oscillates along

the molecular symmetry axis. Thus, K cannot be changed during excitation or the spontaneous decay which leads to the same selection rules as for the pure rotational transitions.

Blackbody radiation Another, however, non-intended population transfer is caused by blackbody radiation. This population transfer leads to a repopulation of states during the internal state manipulation. The effect of blackbody radiation can then only be neglected if the timescale for repopulation is much slower than the time needed for manipulation. In the past, the effect of blackbody radiation on molecular states was associated with blackbody induced driving of rotational transitions [Hoe07]. CH_3F, however, has a relatively small rotational constant B_0 and thus blackbody induced transitions between rotational states can in good approximation be neglected for experiments described in this thesis. For transitions between vibrational states the transition strengths for various vibrational modes of a molecule can vary over a large range and each vibrational mode has to be considered individually. Indeed, the v_3 CF-stretch vibration in CH_3F lies at $1049\,\mathrm{cm}^{-1}$ and has a spontaneous decay rate of about $13\,\mathrm{Hz}$ [Per74]. At room temperature this leads to blackbody rate of $\Gamma_{bb} = 0.075\,\mathrm{Hz}$, which is relevant on the timescales of the experiments. Note that only dipole allowed transitions contribute and can therefore only lead to a change of the M and J values with K being conserved.

2.4 Theoretical concepts of rotational-state control

As indicated in the level scheme in Fig. 2.4 all rotational-state manipulation processes are based on driving rotational and vibrational transitions. To understand the concept of the here presented rotational-state manipulation, two basic processes have to be considered: First, population can selectively be transferred to untapped states. This transfer leads to a removal of molecules from the trapped ensemble, a process that is denoted depletion. It is particularly used for the rotational-state detection method in chapter 4. The second basic process is population transfer between trapped states. Here, coupling two states with MW radiation leads to an equalization of the population. In addition, optical pumping is used to accumulate the population within chosen states. In particular, optical pumping allows one to implement rotational-state cooling and to prepare the ensemble in single M substate (see chapter 5). These core concepts are described with simple examples below.

For an analysis of the state manipulation, it is important to know, how these processes can be described. In this thesis, all coherent processes are ignored and the population transfer is described with rate equations. This assumption can be validated by the experimental parameters: The MW rate is at most on the order of hundreds of Hz and has to be compared to the Stark broadening in the central trap region of many MHz. The argument for the infrared radiation is slightly different. Although the laser intensity might locally be high enough to drive coherent processes, the molecules pass the small laser beam only once in a while in the large trapping volume.

The toolbox for rotational-state control In the following, the main ingredient of the toolbox for rotational-state control are discussed. Figure 2.5(a) shows the most

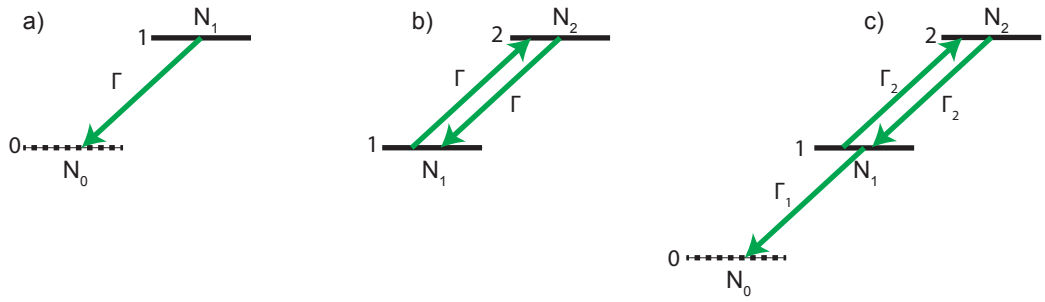

Figure 2.5: Concepts for rotational-state control by driving rotational transitions. (a) Removal of molecules from state 1 by driving a transition to an untrapped state. (b) Coupling two rotational transitions for equalizing the population. (c) A combination of (a) and (b) with consequences as discussed in the main text.

simple example of an depletion process. Specifically, two rotational states are coupled with MW radiation. The state 0 is considered as an untrapped state and thus all the population N_1 of state 1 is transferred to state 0 but not the other way around. As this loss of molecules can be described by rates, the remaining population is simply given by $N_1(t) = \exp(-\Gamma \cdot t) \cdot N_1(t = 0)$, with t being the time for which the MW radiation is applied and Γ being the driving rate. In order to deplete all molecules in N_1, $\Gamma \cdot t$ has to be sufficiently large to neglect the remaining population in state 1 and the process is then considered to be saturated. Figure 2.5(b) shows a second important process, the coupling of two trappable rotational states with MW radiation for the sake of equalizing the population. As well known, solving the corresponding rate equations yields $N_2(\Gamma \cdot t) = (1 - \exp(-2\Gamma \cdot t))/2$ for $N_2(t = 0) = 0$ and thus saturates at a relative population of $N_2(\infty) = N_1(\infty) = 0.5$.

In the experiment it now often necessary to couple several rotational states to one untrapped state with e.g. a ladder of MW couplings. The simplest example of such a ladder is a combination of the two examples in (a) and (b) as given in Figure 2.5(c). This situdation is already slightly more complicated as illustrated in the following. We consider $\Gamma = 1\,\mathrm{Hz}, t = 5\,\mathrm{s}$ for the two processes in (a) and (b). For these parameters, both are almost saturated as the population distribution differs by less than one percent from the one for $t = \infty$. Choosing $\Gamma_1 = \Gamma_2 = 1$ and t=5 s for the model in (c), however, results in still more than 15 % of the population being in the state 1 or 2. Even with the optimal ratio of $\Gamma_1 = 1.5 \cdot \Gamma_2$ ($\Gamma_1 + \Gamma_2 = 2$) the population in the state 1 or 2 improves only by less than one percent. Thus, for an implementation of such a or a bigger ladder in the experiment, all MW driving rates are adjusted to be equal (see section 3.5 for details of the implementation). In most presented experiments, it is necessary to drive all involved transitions with such a rate, that the transitions can be considered to be saturated. Thus, many of the characterization measurements shown in this thesis determine the needed MW power or time for a saturated driving of the transitions.

The other ingredient of the toolbox is the driving of vibrational transitions. The core concept can be explained by the examples in Fig. 2.6. First, the Stark splitting in the vibrational excited state is almost the same as in the ground state. Thus all depicted IR transitions within each scheme have in good approximation the same frequency and

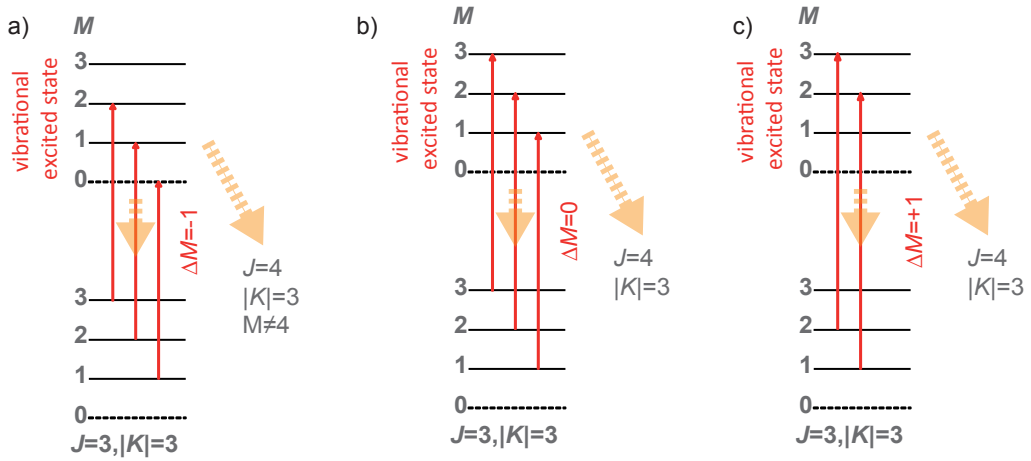

Figure 2.6: Concepts for rotational-state control by driving vibrational transitions. The concepts are explained in the main text by the example of driving a $\Delta J = 0$ transition from the $J = 3, |K| = 3$ state with $\Delta M = -1$ (a), $\Delta M = 0$ (b), and $\Delta M = +1$ (c).

are thus driven simultaneously for $\Delta J = 0$ transitions. Second, the spontaneous decay can transfer population back to $J = 3, |K| = 3$ and due to the selection rule $\Delta J = 0 \pm 1$ also to $J = 4, |K| = 3$. The selection rule $\Delta K = 0$ however, forbids a decay to states with $J < 3$.

In Fig. 2.6(a), a $\Delta M = -1$ vibrational transition is driven thereby lowering the M quantum number. Together with the spontaneous decay ($\Delta M = 0, \pm 1$), this leads to a successive removal of molecules from the $J = 3, |K| = 3$ states to either the untrapped $M = 0$ states or to $J = 4, |K| = 3$ with $M < 4$. In particular the highest $M = 4$ substate of $J = 4, |K| = 3$ cannot be populated, which will be used for implementing a single M substate detection in chapter 4. Driving a $\Delta M = 0$ transition as in Fig 2.6(b) also results in a depletion of the population in the states with $J = 3, |K| = 3$, but on a slower timescale as more spontaneous decay events are needed. In particular, most of the population is transferred to $J = 4$ which will be used for implementing rotational-state cooling in chapter 5. A $\Delta M = +1$ transition on average increases the M quantum number, see Fig 2.6(c). In particular, the state $|0; 3, 3, 3\rangle$ is the only dark state within $J = 3, |K| = 3$ and thus all the population either accumulated in this state or is transferred to $J = 4$. This process shows the basic principle of a preparation of the population in single rotational states as will be discussed in chapter 5.

Rate model Some of the processes for rotational-state control are analyzed using rate equations in the following. These rate equations have the usual form

$$\dot{p}_i(t) = \sum_j \Gamma_{i,j} p_j(t) \tag{2.4}$$

where p_i is the population in state i and $\Gamma_{i,j}$ is the rate for driving a transition from a state i to a state j. The solution of such a coupled system is given by

$$P(t) = \exp(\Gamma \cdot t) \cdot P(t = 0) \tag{2.5}$$

with $P(t) = \{p_1(t), p_2(t), ...\}$ and the matrix $\Gamma = (\Gamma_{i,j})$. These rate equation systems easily involve hundred states and thus all results presented in this theses are obtained by numerical calculations and not analytically.

To determine Γ several contributions have to be taken into account: rotational states coupled with MW, vibrational transitions driven via the laser, the spontaneous decay from the vibrational excited states, and blackbody induced driving. For large molecule densities, two-body inelastic collisions could also lead to population transfer. However, with the density in the trap estimated to be in the range $10^6 - 10^7\,\mathrm{cm}^{-3}$ [Zep12], this is not an issue in the present experiment.

Unlike for the spontaneous decay and the blackbody induced population transfer the driving of the MW and IR transitions depends on the applied power. The appropriate rates for the model are determined as follows: For IR transitions, the driving rate is much faster than any other relevant process in the trap and in particular it is much faster than the spontaneous decay rate of 15 Hz. The exact rate hence does not influence the end result as long as it is sufficiently large, and a value of 1 kHz was chosen. For rotational transitions, the discussion is more elaborated as e.g. the electric field distribution has to be considered. The driving rate $\Gamma_{i,j}^{MW}$ with which a rotational transition from state i to state j is driven is derived in section 3.5.

In addition to the coupling matrix Γ, the initial rotational-state distribution inside the electric trap has to be calculated. The used population distribution is shown in Fig. 2.3. For the initial population distribution in the rate models, the rotational states $J = 1$ to $J = 8$ with all possible K and M values are included unless stated differently.

Chapter 3

Spectral resolution inside the homogeneous-field electric trap

The main ingredient of the experiment is a DC homogeneous-field electric trap. The first storage of molecules with this type of trap was demonstrated in 2011 [Eng11] achieving trapping times of about 10 s. In 2012 it was used to implement motional cooling of polyatomic molecules using a Sisyphus scheme [Zep12] (see also section 5.2).

The trap was carefully designed to dramatically reduce the problem of Stark broadening and thus to significantly increases the spectral resolution compared to, e.g., quadrupole traps. However, Stark spectroscopy performed by simply scanning one MW frequency showed rather broad features. This chapter presents a new method for a detailed investigation of the electric-field distribution. With this method, the spectrum of a single rotational transition is measured which allows one to extract the electric-field distribution. A comparison of the simulated and the measured distribution verifies the expectations of a narrow electric-field distribution. This analysis is of particular importance for the characterization of internal-state detection and manipulation of trapped molecules. The consequences of the electric-field distribution of the trap for state-selective driving of rotational and vibrational transitions are discussed at the end of this section.

3.1 The electric trap

The design concept and theoretical considerations about the electric-field distribution are given in great detail in [Zep13]. Here the major aspects of the trap are briefly summarized. A drawing of the trap is given in Figure 3.1. It consist of two microstructured capacitor plates facing each other with a distance of 0.3 cm. A voltage difference between the capacitor plates leads to a homogeneous electric field inside the trap. The voltages applied to the two plates are in the following denoted by $\pm V_{Offset}$. Additionally applied high voltage differences at the neighboring electrodes of the microstucture

V_{Offset}	V_{μ}	V_{Ring}	$\mathcal{E}_{hom}$	comment
±90 V	±1800 V	+5400 V	815 V/cm	most often used configuration
±70 V	±1400 V	+1400 V		unloading of molecules cooled to $T \approx 150$ mK
±15 V	±300 V	+300 V		unloading of molecules cooled to $T \approx 30$ mK
±450 V	±1800 V	+5400 V	3.11 kV/cm	used for measurements in Fig 3.5(b) and Fig. 5.4.

Table 3.1: Voltage configurations used in this thesis. The electric-field strength in the homogeneous electric-field region of the trap is given as measured below.

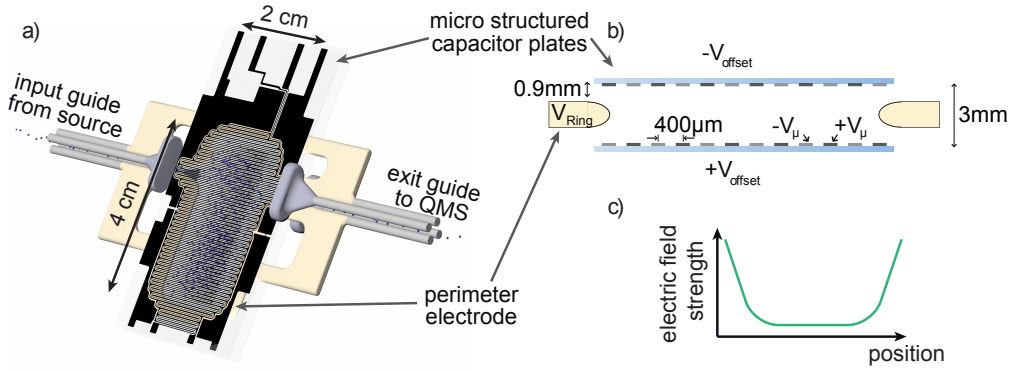

Figure 3.1: The electric trap. a) A drawing of the trap consisting of two microstructured capacitor plates and a surrounding perimeter electrode. The microstructured plates are made out of a 250 nm thick chromium layer on glass and were fabricated by IMT Masken und Teilungen AG. To improve the high voltage performance, the whole microstructure is coated with Cyclotene. b) Schematic picture of a cross section trough the trap perpendicular to the axis given by the guides. c) Schematic electric-field strength depending on the position between the two microstructured plates.

($\pm V_\mu$) create the needed trapping fields which decay exponentially toward the trap center. This design leads to a box-like potential as indicated in Fig. 3.1(c). A perimeter electrode (V_{Ring}) ensures three dimensional trapping and is connected to the loading and unloading quadrupole guides. The voltage configurations used in this thesis are given in Tab. 3.1 together with the electric-field strength of the homogeneous-field region $\mathcal{E}_{hom}$ measured below.

3.2 The scheme for measuring the electric-field distribution

The electric-field distribution is investigated by measuring a spectrum of the single MW transition $|0;3,3,3\rangle \leftrightarrow |0;4,3,4\rangle$. The line shape of this transition has several contributions, e.g. the natural line width, Doppler broadening, and Stark broadening. However, the natural line width of a MW transition is many orders of magnitude smaller than of an optical transitions as the spontaneous decay rate scales with the transition frequency cubed. Also the Doppler broadening scales with the frequency and is in the order of a few tens of kHz. Hence, the line shape of this transition is almost exclusively given by the Stark broadening and thus reflects the electric-field distribution. The extracted electric-field distribution can then be used to calculate the line shape of any other transition of interest.

The scheme for measuring the MW spectrum is based on measuring the loss of the population in the single M substate $|0;4,3,4\rangle$ via the $|0;3,3,3\rangle \leftrightarrow |0;4,3,4\rangle$ rotational transition. As depicted in Fig. 3.2, driving IR transitions from $J = 3$ with $\Delta J = 0$ and $\Delta M = -1$ (red vertical arrows) and coupling all $|0;3,3,M \neq 3\rangle \leftrightarrow |0;4,3,M+1\rangle$ rotational transitions with microwaves (horizontal orange arrows) leads to depletion of all states within the manifold except the $|0;4,3,4\rangle$ state (see also section 4.1.3). Thus, by adding a fourth MW frequency (dashed green line), any additional depletion can only be caused by the depletion of the $|0;4,3,4\rangle$ state via the target transition

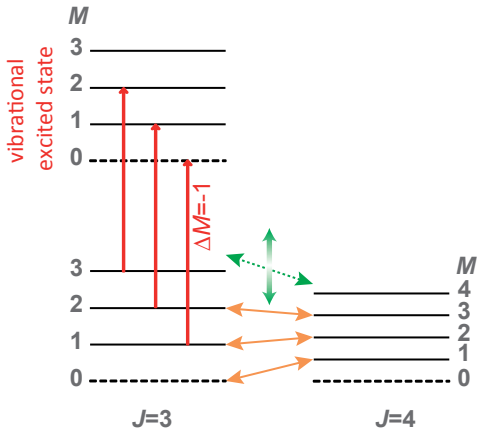

Figure 3.2: Level scheme for Stark spectroscopy of the rotational transition $|0;3,3,3\rangle \leftrightarrow |0;4,3,4\rangle$. The line shape is predominantly given by the Stark broadening inside the trap and can be converted into an electric-field distribution as described in the main text.

$|0;3,3,3\rangle \leftrightarrow |0;4,3,4\rangle$. To obtain the line shape of the transition this MW frequency is varied. The target transition $|0;3,3,3\rangle \leftrightarrow |0;4,3,4\rangle$ is always driven resonantly at the corresponding electric field values thereby probing the probability for a molecule to be at a position in the trap with the given electric-field strength. This probability is essentially the electric-field distribution.

Based on the fact that this process can be described by rates, a simple theoretical model can be used to extract the electric-field distribution from the data. First, the rate Γ with which molecules are depleted from the $|0;4,3,4\rangle$ state using a specific MW frequency is proportional to the effective driving power P of the applied frequency. Second, it is also proportional to the probability $\rho(\mathcal{E})$ to find an electric-field strength $\mathcal{E}$ inside the trap at which the transition frequency is resonant to the applied MW frequency. This assumption implies that the probability distribution for the molecule in the electric field is constant which is valid as long as the total energy of the molecules is much larger than the potential energy. Thus this assumption is good for measuring the peak of the electric field distribution but will fail at some point for the high-electric field part of the distribution. In total we find $\Gamma \propto \rho(\mathcal{E}) \cdot P$. Based on the expectation that the number of molecules N remaining in the state $|0;4,3,4\rangle$ is given by $N \propto \exp(-\Gamma \cdot T)$ with T being the depletion time, the electric-field distribution can be calculated via $\rho(\mathcal{E}) \propto \log(N)/P$.

3.3 Experimental optimizations

This section discusses additional measurements that are needed to obtain the electric-field distribution. First, an example of the necessary optimization of the used MW power is given. Second, the above assumed exponential behavior of the depletion is verified.

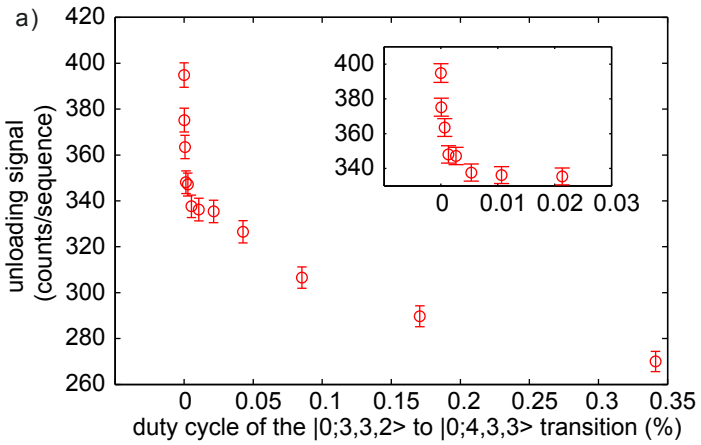

b)

duration(s)	experimental step
21	Sisyphus cooling to 150 mK
1	accumulation
2	optical pumping
2	depletion with variation of the MW power
12	unloading and molecule detection

Figure 3.3: Power scan of the MW frequency driving the rotational transition $|0;3,3,2\rangle \leftrightarrow |0;4,3,3\rangle$. a) Experimental result. The power is scanned by varying the duty cycle of the applied frequency as discussed in section 2.2. The optimal power is determined by the first and fast depletion process which is saturated at a duty cycle of about 0.005 % b) Summary of the experimental sequence.

3.3.1 Determination of the microwave power

For the above explained scheme to work the driving of the MW transitions $|0;3,3,M\rangle \leftrightarrow |0;4,3,M+1\rangle$ with $M < 3$ (orange solid arrows) have to be saturated. This is needed so that the populations of the states $|0;4,3,M < 4\rangle$ are almost completely removed and hence increasing the driving rate of these transitions does not lead to more depletion. It is thus ensured, that the addition of the fourth MW frequency results only in a depletion of the $|0;4,3,4\rangle$ state via the target transition $|0;3,3,3\rangle \leftrightarrow |0;4,3,4\rangle$. To saturate the MW transitions $|0;3,3,M\rangle \leftrightarrow |0;4,3,M+1\rangle$ with $M < 3$, the applied MW power has to be adjusted. In the following, a typical measurement for such an optimization of the MW power is shown for the $|0;3,3,2\rangle \leftrightarrow |0;4,3,3\rangle$ rotational transition.

Experimental sequence First, the molecules are cooled to about 150 mK by optoelectrical Sisyphus cooling (see section 5.2) for improved statistics. Afterwards, one second of accumulation is applied to equally distributes the cooled molecules between the $|0;3,3,3\rangle$ and $|0;4,3,4\rangle$ states. To transfer as much population to the $|0;4,3,3\rangle$ state as possible two seconds of optical pumping are applied. Specifically, the infrared transitions $|0;3,3,M\rangle \leftrightarrow |1;3,3,M\rangle$ are driven which transfers population to the $J = 4$ state via the spontaneous decay. To avoid accumulation in the $|0;4,3,4\rangle$ state, the MW transition $|0;3,3,3\rangle \leftrightarrow |0;4,3,4\rangle$ are additionally driven and thus the population is transferred either to untrapped states or to the lower $M \leq 3$ states within $J = 4$. After this preparation of the ensemble, the scheme for measuring the MW power dependence of driving the $|0;3,3,2\rangle \leftrightarrow |0;4,3,3\rangle$ transition is applied. Specifically, the IR transitions $|0;3,3,M\rangle \leftrightarrow |1;3,3,M-1\rangle$ are driven thereby depleting the population in $J = 3, |K| = 3$. In addition, the $|0;3,3,2\rangle \leftrightarrow |0;4,3,3\rangle$ MW transition is driven which is expected to cause an additional depletion of the $|0;4,3,3\rangle$ state. The amount

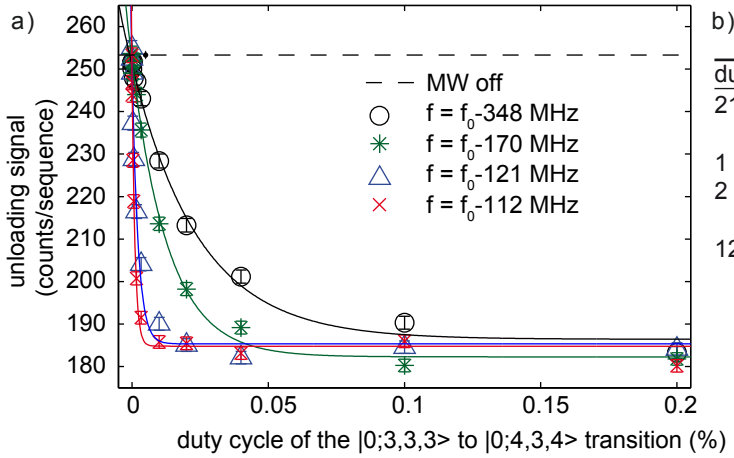

Figure 3.4: Power scan of the MW frequency driving the rotational transition $|0;3,3,3\rangle \leftrightarrow |0;4,3,4\rangle$ used for measuring the electric-field distribution below. a) Experimental result together with exponential fits for different detunings from the the transition frequency at zero electric field f_0. The power is scanned by varying the duty cycle of the applied frequency. The behavior fits well with an exponential validating the theoretical approach described in the main text. b) Summary of the experimental sequence.

of depletion depends thereby on the power of the applied MW frequency. This power is scanned by varying the duty cycle of the MW frequency as explained in chapter 2.2.

Results Figure 3.3 shows the result of the measurement. The depletion clearly occurs with two different power scales. The inset shows a zoom of the first and fast decrease which is caused by driving the $|0;3,3,2\rangle \leftrightarrow |0;4,3,3\rangle$ transition thereby depleting the population of the $|0;4,3,3\rangle$ state as expected. The additional slow process can be attributed to driving the close-lying other transitions $|0;3,3,M\rangle \leftrightarrow |0;3,3,M+1\rangle$ ($M \neq 2$) in the inhomogeneous electric-field regions of the trap. This driving of the target transition in the inhomogeneous electric-field regions is in particular the reason for not choosing the MW power to be large as possible. Although this driving has no influence on the measured line shape, it reduces the population in $|0;4,3,4\rangle$ and thus the measured signal, which would have to be compensated with longer measurement times to obtain the same statistics. As the fast process saturates at a duty cycle of about 0.005 % this value can be chosen to ensure a saturated driving of the rotational transition $|0;3,3,2\rangle \leftrightarrow |0;4,3,3\rangle$. The microwave power of the $|0;3,3,1\rangle \leftrightarrow |0;4,3,2\rangle$ was determined in the same way.

3.3.2 Verification of exponential behavior

The model for extracting the electric-field distribution from the MW spectrum assumes an exponential dependence of number of depleted molecules on the depletion time. This dependence is experimentally measured in the following, validating the theoretical approach. Instead of varying the depletion time, the power of the microwave radiation

is varied to avoid influences of blackbody radiation induced population transfer or of long storage times.

Experimental sequence A molecular ensemble is cooled to 150 mK with a subsequent second of accumulation. During the two seconds of depletion a scheme similar to the one for measuring the MW spectrum is applied. Specifically, a $\Delta M = -1$ vibrational transition from $J = 3$ is driven together with the $|0; 3, 3, M \neq 3\rangle \leftrightarrow |0; 4, 3, M + 1\rangle$ rotational transition depleting all states within the manifold except the $|0; 4, 3, 4\rangle$ state (see scheme in Fig. 3.2). In addition, a fourth MW frequency is added of which the MW power is scanned. This scan is repeated for four different MW frequencies: on resonance (red cross), close to the resonance (blue triangle) and far off (green star and black circle). The frequency is given as a detuning from the zero electric field transition frequency between $J = 3 \leftrightarrow J = 4$ of $f_0 = 204.242\,\mathrm{GHz}$.

Results Figure 3.4 shows the results of the measurements together with exponential fits. The good agreement of the exponential fitting with the data justifies to assume the depletion of the rotational state $|0; 4, 3, 4\rangle$ via the transition $|0; 3, 3, 3\rangle \leftrightarrow |0; 4, 3, 4\rangle$ to be well approximated with an exponential. As expected, the depletion is fastest for the MW frequency, that is resonant in the homogeneous electric-field region of the trap (red cross) and gets slower for larger detunings.

3.4 MW Spectrum and extracted electric-field distribution

This section discusses the measured electric-field distribution for two different trapping configurations. In particular the overall shape is compared with a simulated electric-field distribution. The dependence of the peak position and width are discussed qualitatively.

Experimental sequence As before, a molecular ensemble cooled to 150 mK with a subsequent second of accumulation is used. Before unloading 2 s of depletion is applied as explained above (sec. 3.2). As the occurrence probability of the electric field values varies by more than an order of magnitude, two MW frequency scans are performed. First, a higher power of the scanning MW is used (duty-cycle of the $|0; 3, 3, 3\rangle \leftrightarrow |0; 4, 3, 4\rangle$ transition is 2.2 %, see Fig. 3.4 for comparison). It is adjusted to measure the flanks of the line shape but leads to a complete depletion at the peak. Second, a narrow scan around the peak value is performed with about ten times less power which allows one to resolve the peak.

Simulation of the electric-field distribution A numerical simulation of the electric-field distribution allows one to compare the measurement with expectations. For that purpose the electric fields were simulated on a grid. To simplify the simulation of the large trapping volume with the small structures of 200 μm on the microstructured capacitor plates, the simulation was done in two steps. First, the electric field of the ring electrode was simulated while the microstructures were replaced with metal plates. In particular, both plates were set to zero voltage. Afterwards, the electric field of the microstructure was simulated which needs a much higher resolution than

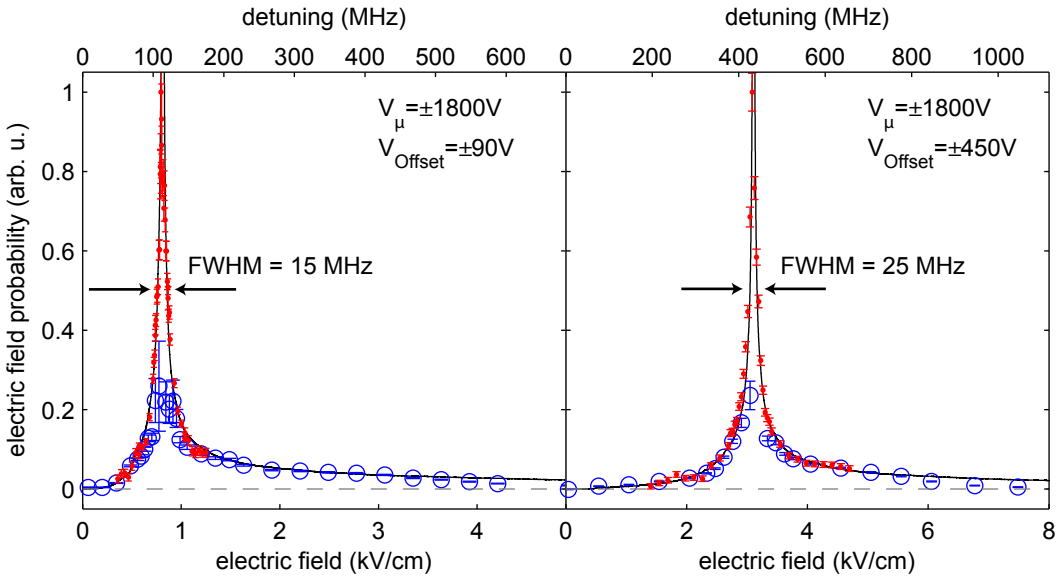

Figure 3.5: Measured and simulated (black line) electric-field distribution in the electric trap. The spectral line shape of the single MW transition $|0;3,3,3\rangle \leftrightarrow |0;4,3,4\rangle$ is measured to obtain the electric-field distribution. For comparison with the simulation the measured depletion signal is converted into the electric-field distribution as explained in the main text. The frequency scale for the unconverted data on the top axis is given relative to the zero electric field frequency 204.242 GHz of the transition $J = 3, |K| = 3 \leftrightarrow J = 4, |K| = 3$. To resolve the flanks, the spectrum is measured with a higher MW power (blue circles). In addition, a narrow scan at lower power around the peak value (red dots) is performed.

the simulation of the fields of the ring electrode. To simplify the calculation, only one slice perpendicular to the plates was simulated. The thickness of the slice is chosen such that one periodicity of the structure is simulated. An array of these slices then gives in good approximation the electric field of the microstructure. Both fields, the one obtained from the microstructure and the one from the ring electrode, were finally added to calculate the electric-field distribution.

Results and comparison with the simulated electric-field distribution The result of the measurement and the simulation are shown in figure 3.5 for two different electric field configurations. The measurements have been converted into the electric-field distribution using the theoretical approach described above. The result fits nicely to the simulation where only a small horizontal scaling by less than 5 %, attributed to inaccuracies in the simulation, is needed to overlap the two.

The peak position is mainly given by the offset field due to the voltages applied to the capacitor plates. Results shown in Fig. 3.5(a) were measured with a typical offset voltage between the capacitor plates of ±90 V and (b) with ±450 V. The resulting FWHM is roughly 100 V/cm at a peak position of 815 V/cm in (a) and 120 V/cm at 3.11 kV/cm in (b), corresponding to a relative width of 12 % and 4 %, respectively. This shows that the electric field is homogeneous in a large fraction of the trap volume.

In addition to the low homogeneous field, also higher electric fields for trapping are present in the trap. These trapping fields lead to the long tail of the distribution. This long tail has consequences for the ability to resolve single transitions in any of the experiments. In particular, transitions which would be separated by hundreds of MHz in the homogeneous field region of the trap are Stark shifted into resonance. Even though the driving rate of such transitions is substantially suppressed, the residual driving can still cause unwanted effects. An analysis of the consequences for the rotational-state detection based on rates is provided in section 4.1.

The excellent agreement of the measurement and the simulation shows that the electric-field distribution is well understood. In particular, it proves that the single MW transition $|0;3,3,3\rangle \leftrightarrow |0;4,3,4\rangle$ is driven as shape and peak position of the spectrum scale with trap voltages as expected. When discussing the theoretical model for extracting the electric field distribution from the measurement (section 3.2), is was stated that the assumption of $\Gamma \propto \rho(\mathcal{E})$ might fail for high electric fields as the limited kinetic energy of the molecules prevents them from reaching these high-field regions of the trap. Indeed, the measurement lies below the electric-field distribution for high electric fields.

3.5 Rotational-state selectivity

The previous analysis of the spectral resolution yields a basis for a discussion of the J,K and M selectivity of rotational and vibrational transitions inside the trap. For this purpose one has to consider whether there are other transitions close to the ones that are intended to be driven. Afterwards the frequency separations have to be compared to the spectral resolution. General considerations were given in section 2.1. Here, a detailed analysis for the MW transitions $|0;3,3,M\rangle \leftrightarrow |0;4,3,M\pm1\rangle$ and $|0;5,3,M\rangle \leftrightarrow |0;6,3,M\pm1\rangle$ is presented as well as for the IR Q-branch transitions from the $J=3$, $J=4$ and $J=5$ with $|K|=3$ states used for the rotational-state detection schemes in chapter 4 and the internal state manipulation in chapter 5.

Driving rotational transitions The rotational states mainly used in this thesis are the lowest four states $J=3,4,5,6$ of the $|K|=3$ manifold. In the experimental setup used in this thesis, the rotational transition $J=3 \leftrightarrow J=4$ and $J=5 \leftrightarrow J=6$ can be driven with MW radiation as described in section 2.2. Based on the selection rules (equation 2.3) and the rotational energy of a symmetric top molecule (equation 2.1) the transition frequencies can be calculated and the result is plotted in Fig. 3.6 for all possible $|K|$ and M values and a typical electric-field strength. The frequency for driving rotational transitions between J and $J+1$ states is in first approximation given by $\nu_0 = 2B_0(J+1)$, and hence differs by at least $2B_0$ for different J. A dependency on $|K|$, however, is only introduced by small corrections due to centrifugal distortion and the Stark shift of the M sublevels, where both shifts are much smaller than B_0. Resolving the J quantum number with microwaves is thus substantially easier than discriminating different $|K|$ or M. Still, the rates at which the addressed and non-addressed transitions are driven can be quite different, thus allowing for resolving the K or the M quantum numbers.

Any population transfer within this thesis can be described by rate equations as

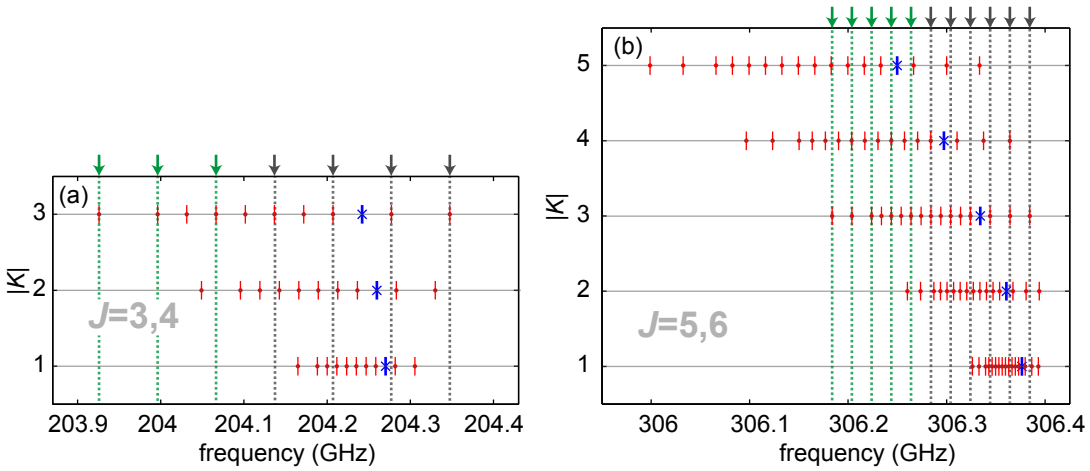

Figure 3.6: Rotational transition frequencies for different K-values for the $J = 3 \leftrightarrow J = 4$ MW transitions (a) and the $J = 5 \leftrightarrow J = 6$ MW transitions (b). All transition frequencies are calculated for the typical homogeneous electric field in the trap. The blue crosses indicate the frequencies for zero electric field for the individual K states and the red dots represent the frequencies of the Stark-shifted dipole-allowed transitions between M substates. The arrows at the top mark as an example the transition frequencies needed for microwave depletion (section 4.1.1) in the $|K| = 3$ manifold and the dashed lines are guides to the eye. For infrared depletion(section 4.1.2) only the highest four (a) or six (b) frequencies are needed.

motivated in section 2.4. The rate at which the addressed and non-addressed transitions are driven can be calculated as explained in the following: Two components influence the rate $\Gamma_{i,j}^{MW}$ with which a rotational transition from state i to state j is driven: The wanted driving of this transition in the homogeneous field region of the trap (if applicable) and the unwanted driving of this transition in the inhomogeneous electric field regions due to other applied MW frequencies. For both processes the rate can be calculated with the following assumptions. Applying a single fixed MW frequency ν is considered, which does not necessarily match the transition frequency from state i to state j in the homogeneous electric-field region. First of all, the rate $\Gamma_{i,j}^{MW}$ is then proportional to the effective driving power P of the applied MW frequency. Second, it is proportional to $c_{i,j}$, the square of the Clebsch Gordan coefficient for transitions between state i and state j. Third, the rate $\Gamma_{i,j}^{MW}$ is proportional to the spectral line shape function $\rho_{i,j}(\nu)$ of the given transition. This can be written in terms of a coefficient $d_{i,j} = \left(\frac{KM_j}{J_j(J_j+1)} - \frac{KM_i}{J_i(J_i+1)}\right)$ for the differential Stark shift of the transition and the electric-field distribution $\rho(\mathcal{E})$ as follows. With $\nu = \nu_0 + \frac{\mathcal{E}_{i,j}\,\mu}{h} \cdot d_{i,j}$ where $\mathcal{E}_{i,j}$ is the electric field where the transition takes place, we have $\rho_{i,j}(\nu) = \rho(\mathcal{E}_{i,j})\frac{d\mathcal{E}_{i,j}}{d\nu} \propto \rho(\mathcal{E}_{i,j})\frac{1}{d_{i,j}}$. ν_0 denotes the transition frequency in the absence of any electric fields. The rate $\Gamma_{i,j}^{MW}$ for the single MW frequency is thus given by

$$\Gamma_{i,j}^{MW} \propto \rho(\mathcal{E}) \cdot \frac{c_{i,j}}{d_{i,j}} \cdot P. \tag{3.1}$$

transition	frequency
$\|0;3,3,M\rangle \leftrightarrow \|1;3,3,M\rangle$	88916.7138(3) GHz
$\|0;4,3,M\rangle \leftrightarrow \|1;4,3,M\rangle$	88922.3126(3) GHz
$\|0;5,3,M\rangle \leftrightarrow \|1;5,3,M\rangle$	88928.7400(3) GHz
$\|0;6,3,M\rangle \leftrightarrow \|1;6,3,M\rangle$	88935.8872(3) GHz

Table 3.2: Vibrational transition frequencies measured via saturated absorption spectroscopy without applying an electric-field.

To obtain the total rate with which the rotational transition from state i to state j is driven, the contributions for the various applied MW frequencies have to be summed up.

One particular consequence is discussed in the following. If several rotational transitions have to be driven with the same rate in the homogeneous electric-field region of the trap, the effective power, adjusted via the duty cycle (see chapter 2.2), of the MW frequencies is chosen according to $P_{i,j} \propto \frac{d_{i,j}}{c_{i,j}}$. Thus, a rotational transition with large Stark shifts and low Clebsch Gordan coefficient needs way more effective power. For example, to drive the $|0;3,3,3\rangle \leftrightarrow |0;4,3,2\rangle$ transition with the same rate as the $|0;3,3,3\rangle \leftrightarrow |0;4,3,4\rangle$ transition, an about 80 times higher MW power is needed. A comparison with the measured electric-field distribution in Fig 3.5(a) reveals that a MW frequency applied to drive the $|0;3,3,3\rangle \leftrightarrow |0;4,3,2\rangle$ transition will despite the rather large frequency separation of 226 MHz always drive the $|0;3,3,3\rangle \leftrightarrow |0;4,3,4\rangle$ transition in the inhomogeneous field region with an even 3.5 times higher rate. However, cooling the motional degree of freedom of the molecules is a possibility to reduce or hinder the unwanted driving of the $|0;3,3,3\rangle \leftrightarrow |0;4,3,4\rangle$ transition in the inhomogeneous field region as high electric fields cannot be reached by cold enough molecules anymore.

Driving vibrational transitions Q-branch IR transitions are more randomly distributed than the discussed rotational transitions because the rotational constants of the excited states can be quite different for different vibrational states. Couplings between vibrational modes can additionally shift the transition frequencies. Thus each vibrational transition has to be investigated individually. IR transition frequencies of the v_1 vibrational mode of CH_3F are provided in [Gra81] and were verified via saturated absorption spectroscopy in a room temperature cell. The transition frequencies of the most important transitions were determined with sub-MHz resolution using a frequency comb and are given in Tab. 3.2.

It was found that luckily the Q-branch IR transition from the $J = 3, |K| = 3$ state is well isolated, with the closest relevant transition from a different state being several GHz away (see figure 3.7). The spectral resolution is clearly better than this and thus the driving of this transition is K and J selective. The IR transition from the $J = 5, |K| = 3$ state is less isolated, as the $J = 8, |K| = 2$ transition lies close by. However, according to the calculation in figure 2.3 only about 0.6 % of the molecules loaded into the trap populate this state. The IR transition from the $J = 4, |K| = 3$

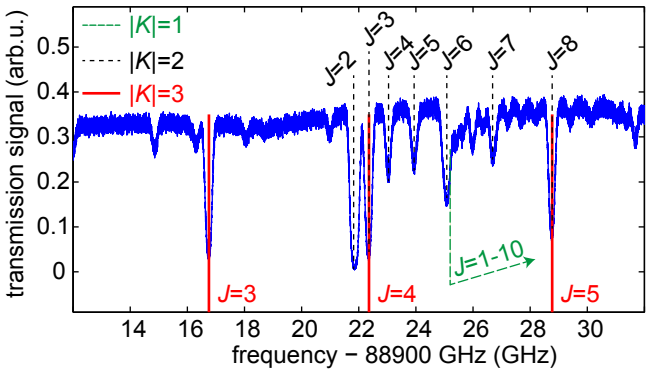

Figure 3.7: Doppler-broadened absorption spectrum of the v_1 vibrational mode of CH_3F obtained with a room temperature cell. The measurement is shown in the vicinity of the relevant transitions. The transition frequencies for $|K| = 1$ lie quite close together and increase for higher J, as indicated by the arrow. It could be verified that all transitions in the Q-branch with $|K| = 4$ to 12 lie well outside the shown frequency range [Gra81]. All non-identified lines thus correspond either to higher J, K states or to other vibrational modes and can be neglected for the optical pumping schemes. The transitions from $J = 3$ and $J = 5$ for $|K| = 3$ are well isolated, with only the transitions from states with $J > 8$, $|K| = 1$ and $J = 8, |K| = 2$ lying in the vicinity of the transition from $J = 5$, $|K| = 3$.

state is even less isolated. In particular the $J = 2, 3, 4$ states with $|K| = 2$ are close by and these states are populated by about 9.7 % of the molecules.

Despite the fact that driving IR transitions can in special cases be regarded as being perfectly J and K selective, resolving M is hardly possible while using the Q-branch. The Stark shifts of the vibrational excited states are almost the same as in the ground state and therefore the Stark shift does not lead to a separation of transitions with different M quantum numbers.

3.6 Discussion

A new method for investigating the spectral resolution in an electric trap was presented in this chapter. The approach is based on measuring the line shape of single MW transition and extracting the electric-field distribution. The measurement shows that the electric fields are indeed homogeneous in a large fraction of the trapping volume. This results in a spectral resolution which is sufficient for implementing a rotational-state selective detection based on state-selective depletion (see next chapter) and for the implementation of rotational state control via optical pumping (see chapter 5).

The spectral resolution inside the trap can be greatly advanced by narrowing the electric-field distribution and by a better suppression of the long tail. As discussed in detail in [Zep13] a redesign with e.g. a reduced microstructure periodicity or modulation of the microstructure width could be a solution toward this goal. For all spectroscopic purposes sufficiently cooling the motion of the molecular ensemble also increases the spectral resolution. First, molecules are hindered to probe the long tail of the distribution which hinders the unwanted driving of transitions in the high-electric

field regions of the trap. Second, cooling allows one to reduce the trapping fields. As the electric field distribution scales with the voltages, the Stark broadening then is reduced.

Chapter 4

Rotational-state detection

A prerequisite for internal-state cooling and control is the ability to state-selectively detect molecules. Unfortunately, commonly used techniques for rotational-state detection of cold molecules such as resonance-enhanced multi photon ionization (REMPI) [Ant78, Twy14, Ber10] and laser-induced fluorescence (LIF) [Kin77] rely on the excitation of electronic states. Especially for polyatomic molecules, however, the excitation of electronic states can lead to rapid predissociation [Her66], causing an enormous line broadening and thus a loss of state selectivity. In addition, almost all electronic transitions lie in the ultraviolet (UV), some in the deep UV and the generation of laser light at these frequencies can be experimentally challenging.

A rotational-state detection technique that is suitable for a large variety of molecular species, especially polyatomic ones, is described in this chapter. The method is based on state-selective depletion of trapped molecules. In contrast to previous experiments [Mot07], this depletion method does not incorporate electronic excitations but uses instead vibrational and rotational transitions to transfer the molecules from the rotational state of interest to an untrapped state. A big advantage of this method is that the detection of the molecules themselves can be accomplished by state-insensitive techniques e.g. the ionization in quadrupole mass spectrometer.

This chapter is organized as follows: In section 4.1 schemes for detecting the population of rotational states of symmetric top molecules are discussed. The focus lies on two complimentary schemes. One exclusively uses rotational transitions the other one is based on a combination of rotational and vibrational transitions. Both schemes are discussed for the four lowest J states of the $|K| = 3$ manifold in CH_3F. The key challenge for the experimental realizations of the described detection schemes is to resolve all three symmetric top rotational quantum numbers J, K and M during the depletion. Based on the discussion of the spectral resolution in chapter 3, the dynamics of the depletion is examined using rate equations.

An experimental analysis of the detection method is provided in section 4.2. First a potential caveat of the state-detection method is discussed in section 4.2.1. An excellent agreement between the measurements and results of the rate model is obtained and presented in section 4.2.2. Both confirm that discriminating the J quantum number is relatively easy, while discriminating K and M is more difficult. Still, a signal that only depends on the population of molecules in states with a single K can be achieved by using a combination of depletion schemes. Section 4.2.3 gives results for the detection of molecules exclusively populating a single M substate, characterized by single J, K and M quantum numbers. As a final result, the quality of the detection methods is investigated in section 4.2.4. In particular, the results of the various depletion schemes

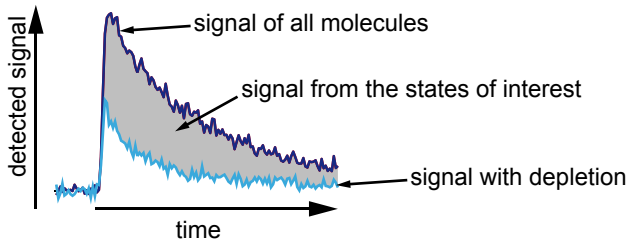

Figure 4.1: Schematic presentation of the idea for state detection via state-selective depletion. To obtain a state-selective signal, two measurements are performed. First, the signal caused by all molecules that populate the trap is recorded (black line). In the second measurement, molecules populating the states that we want to detect are selectively removed (depleted) from the trapped ensemble prior to the unloading and detection with the QMS. The remaining molecules lead to the second signal (blue line). The difference yields a signal that is proportional to the number of removed molecules and that is therefore state-selective (gray shaded area).

are compared to one another as well as to the expected relative populations inside the trap.

4.1 Depletion schemes

The general idea of all detection methods shown in this thesis is to selectively remove (deplete) molecules in states which we want to detect from the trapped ensemble (see Fig. 4.1). Unloading the rest of the ensemble from the trap to the QMS and detecting the molecules gives a background signal. This background signal can then be subtracted from the signal of a measurement without depletion resulting in a state-selective signal. The state-selective removal is realized with two methods which are based on the considerations in section 2.4 and involve the driving of rotational and/or vibrational transitions. As the molecular parameters (e.g. the rotational constants, or vibrational transition frequencies, or spontaneous decay rates) can vary over a large range, the individual advantages of the two methods can be used for different rotational states or molecular species. Although the approach for detecting the rotational states can be applied to many rotational states, it will be explained with a focus on the four lowest J states of the $|K| = 3$ manifold in CH_3F (compare section 2.3).

4.1.1 Microwave depletion

The scheme for MWD The transition frequency between rotational states depends on the quantum numbers J and to some extent on K and M (see section 2.1). The first detection method, microwave depletion (MWD), takes advantage of this. By driving microwave transitions between neighboring rotational J states, sets of rotational states are selectively depleted.

Figure 4.2 shows the implementation of MWD for the rotational states $J = 3, 4, |K| = 3$(a) and $J = 5, 6, |K| = 3$(b). All rotational transitions $|0; J, 3, M\rangle \leftrightarrow |0; J+1, 3, M\pm1\rangle$ with $J = 3$(a) or $J = 5$(b) are driven thereby addressing all trappable M substates. This couples all M substates of each set to the untrapped $M = 0$ states, successively

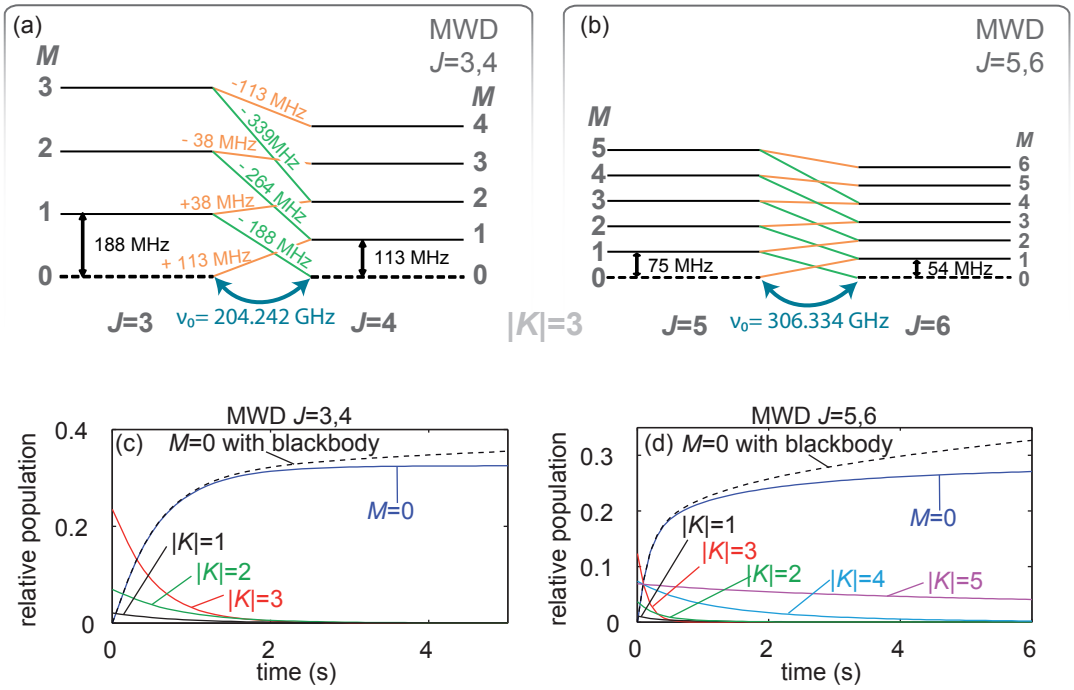

Figure 4.2: Microwave depletion (MWD). Level scheme for MWD for the rotational states $J = 3, 4, |K| = 3$(a) and $J = 5, 6, |K| = 3$(b). Untrapped negative M sublevels are omitted. Stark shifts are plotted to scale and all involved transition frequencies are calculated for a typical electric field in the homogeneous field region of the trap ($\mathcal{E} = 815\,\mathrm{V/cm}$ with $V = \pm 1.8\,\mathrm{kV}$ applied to the microstructures and an offset of $V = \pm 90\,\mathrm{V}$ applied between the capacitor plates; see chapter 3 for details). ν_0 is the MW transition frequency between the neighbouring J states for zero electric field (bent blue arrows). The applied MW transitions between the M substates are marked in green and orange and the corresponding frequencies specify the detuning from ν_0. (c) and (d) show the results of rate models for MWD as explained in the main text.

removing these states from the trapped ensemble. Note that all transition frequencies are calculated to be driven in the homogeneous-field region of the trap. The key question is now, whether this depletion is indeed rotational-state selective or whether other states are depleted too. Based on the discussion is section 3.5 it is obvious, that an unintended addressing of states with a different J quantum number can be excluded, however, resolving $|K|$ seems to be difficult.

Analysis of MWD based on rate equations The knowledge of the electric-field distribution allows one to analyze the rotational-state selectivity of MWD with rate equations (see section 2.4 for more details of the rate model). In particular, the timescales of the depletion of the states of interest with $|K| = 3$ and of unwanted states with $|K| \neq 3$ can be identified. In addition, population transfer caused by blackbody radiation is included. This population transfer leads to a repopulation of states during the depletion and thus to an enhanced number of depleted molecules. The effect of blackbody

radiation can then only be neglected if the timescale for repopulation is much slower than the depletion.

The experimental implementation of MWD in the states with $J = 3, 4$, $|K| = 3$ involves seven frequencies, and an efficient depletion can be achieved by driving the corresponding seven transitions with an equal rate (compare section 3.5). These seven frequencies are implemented in the rate model and the initial-state distribution is the same as in Fig. 2.3. Figure 4.2(c) shows the result of the rate model. The timescale of the depletion process depends purely on the total applied MW power and is chosen to match the experimental data in section 4.2.2. As can be seen immediately, states with $|K| = 1, 2$ and $|K| = 3$ are depleted on almost the same timescale and it is thus impossible to obtain a $|K|$ dependent MWD depletion signal with the current spectral resolution. By including population transfer caused by blackbody radiation an increase of the population with $M = 0$ (dashed black curve) can be observed on long timescales.

The analysis is repeated for MWD of the $J = 5, 6$, $|K| = 3$ states and the result is given in Fig. 4.2(d). Again states with $|K| < 3$ are depleted on the same timescale as the $|K| = 3$ states. In contrast, states with $|K| > 3$ are less affected due to the larger frequency separation (see Fig. 3.6). Including blackbody radiation in the rate model results, as before, in an increase of the population with $M = 0$ (dashed black curve) on long timescales.

4.1.2 Infrared depletion

The second detection method uses optical pumping via a vibrational excitation to deplete the population of the addressed states. These vibrational transitions typically lie in the infrared and this method is hence entitled infrared depletion (IRD). The scheme for depletiong the populatin in the states $J = 3, 4, |K| = 3$ is shown in Fig. 4.3 (left side). A $\Delta M = -1$ Q-branch vibrational transition from $J = 3, |K| = 3$ is driven to pump the population to lower lying M substates, thus successively transferring the population to the untrapped $M = 0$ states. In addition, a spontaneous decay leading to population transfer to the states $J = 4, |K| = 3$. As a detection via depletion is only useful if the population of the chosen set of states is entirely transferred to untrapped states, the rotational states with $J = 4, |K| = 3$ must additionally be depleted. This can be achieved with appropriate microwave couplings as shown in Fig. 4.3. IRD in $J = 3, 4, 5, 6, |K| = 3$ additionally needs the driving of the vibrational transition from $J = 5, |K| = 3$ and MW coupling between $J = 5, |K| = 3$ and $J = 6, |K| = 3$. The concurrent driving of both vibrational transitions is realized by cycling the two needed IR laser frequencies with the fast ramp and relock system described in section 2.2.

Analysis of IRD based on rate equations As for MWD, rate equations are used to quantify the dynamics of IRD. The inset in Fig. 4.3 shows the results of a rate model for IRD for the states $J = 3, 4$, $|K| = 3$. In contrast to MWD the highest possible timescale for depletion is not given by the power of the IR or MW radiation but is set by the spontaneous decay rate of the vibrational excited state. After about 2 s all molecules of the $J = 3, 4$, $|K| = 3$ manifold are depleted.

Compared to MWD, IRD uses only four MW transitions. These transitions have small differential Stark shifts and large Clebsch Gordan coefficients and thus need a relatively low MW power to be driven at a faster rate than the spontaneous decay.

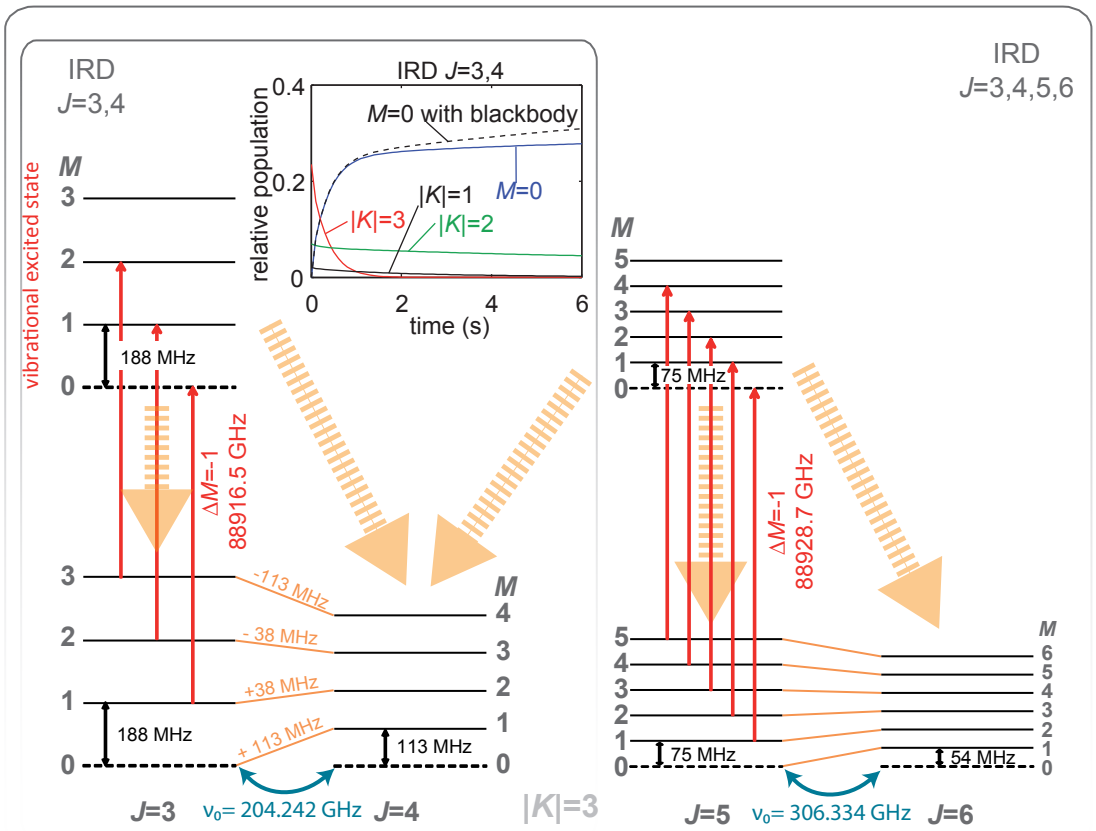

Figure 4.3: Infrared depletion (IRD). The laser addresses the first vibrational excited state of a parallel vibrational mode while driving a $\Delta J = 0$, $\Delta M = -1$ transition (red arrows). The spontaneous decay (big orange arrows) leads to a population transfer to lower lying M states. In the process the $J \pm 1$ states get populated, which are coupled to the J state using microwaves (orage lines). The left side shows the level scheme for IRD for the rotational states $J = 3, 4, |K| = 3$ and the whole figure for IRD in $J = 3, 4, 5, 6, |K| = 3$. The inset gives the result of a rate model for IRD in $J = 3, 4, |K| = 3$.

Thus states with $|K| = 1, 2$ are still depleted but on a much slower timescale than for MWD. This has mainly two consequences. First, the moderate increase of depleted molecules on long timescales is here unlike for MWD not only given by repopulation of the states due to blackbody radiation but also by the slow depletion of states with $|K| \neq 3$. Second, IRD provides a detection method which is compared to MWD less influenced by the depletion of states with $|K| \neq 3$.

Optimization of the MW power for IRD For MWD the total MW power was chosen to be maximal as this yields the fastest depletion. The timescale for IRD is, however, given by the spontaneous decay rate and compared to this rate, the driving rate of the rotational transitions should be fast. In the following, the optimization of the MW power is discussed for IRD in $J = 3, 4, |K| = 3$. Molecules are loaded for 16 s into the trap and are stored for three seconds before unloading and detection. During the last

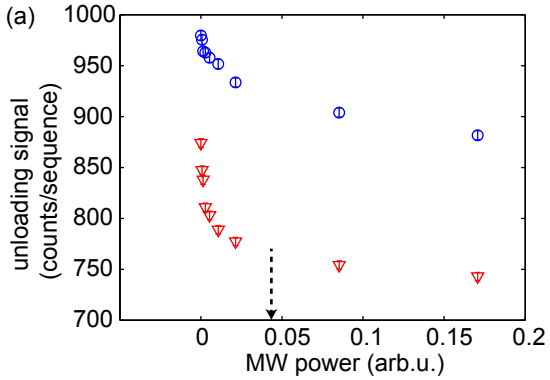

(b)

duration(s)	experimental step
16	trap loading
1	storage
2	depletion
12	unloading and molecule detection

Figure 4.4: Optimization of the MW power for IRD in $J = 3, 4, |K| = 3$. (a) The MW power of the four needed frequencies is scanned by varying the duty cycle. Two measurements are performed, the full IRD scheme (red triangles) and a measurement without IR radiation (blue circles). The arrow marks the finally chosen value. (b) Summary of the experimental sequence.

two seconds of storage IRD for in $J = 3, 4, |K| = 3$ is applied where the MW power of the four frequencies is scanned by varying the duty cycle as discussed in section 2.2. Note that the relative power of the four frequencies is fix to drive all transitions with the same rate. The result of this measurement is shown in Fig. 4.4(a) (red triangles). A fast depletion process is measured which can in comparison to the rate model be attributed to the depletion of molecules populating the states $J = 3, 4, |K| = 3$ whereas the slow decay comes from molecules populating the states $J = 3, 4, |K| < 3$. Thus, a too high MW power leads to more unwanted depletion of states with $|K| \neq 3$. The chosen value is marked by an arrow in Fig. 4.4(a).

The statement that the MW radiation alone depletes molecules is verified by repeating the measurement without applying the IR radiation. Indeed, the unloading signal decreases with increasing MW power (blue circles). Note that this depletion has its origin not only in the depletion of states with $J = 3, 4, |K| < 3$, but also couples the states within $J = 3, 4, |K| = 3$ to the untrapped states in the inhomogeneous electric field region of the trap.

4.1.3 Single rotational M substate detection

Up to now we have discussed the depletion of sets of states while addressing all trapped M substates. Now the detection of the population of a single M substate $|0; J, K, M\rangle$ is considered. While a depletion of a single M substate alone is only possible for $M = 1$, for $M > 1$ it is at least theoretically possible to deplete two sets of rotational states which differ by the M substate of interest.

As an example, the detection of the M substate $|0; 4, 3, 4\rangle$ using MWD and IRD (see figures 4.2 and 4.3) is discussed. In both cases the MW coupling $|0; 3, 3, 3\rangle \leftrightarrow |0; 4, 3, 4\rangle$ is the only one that addresses the $|0; 4, 3, 4\rangle$ state. The population of this state is detected by running the whole experimental sequence twice: The depletion (MWD or IRD) is applied once with driving the $|0; 3, 3, 3\rangle \leftrightarrow |0; 4, 3, 4\rangle$ transition and once

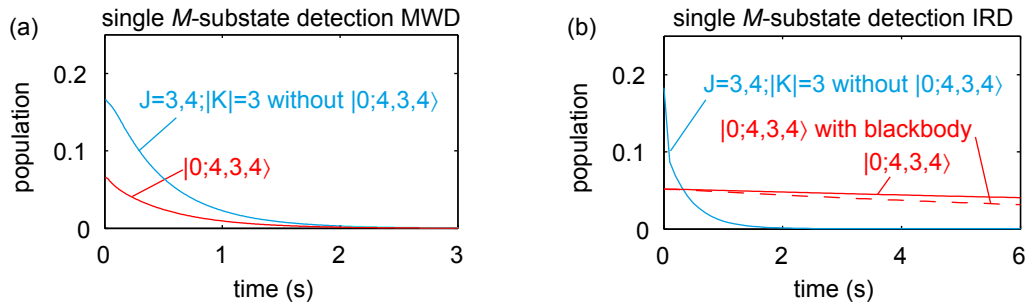

Figure 4.5: Implementation of MWD (a) or IRD (b) without driving the $|0;3,3,3\rangle \leftrightarrow |0;4,3,4\rangle$ transition, used for detection of the population in the single M substate $|0;4,3,4\rangle$ (see main text). The population remaining in the trap is plotted for the state of interest $|0;4,3,4\rangle$ and for all other states of the manifold $J = 3,4,|K| = 3$.

without. The difference of both measurements yields the population in the $|0;4,3,4\rangle$ state.

An extension to other single M substates is possible but at the same time more challenging due to experimental limitations. Using MWD any M substate can be detected by coupling all M substates up to the desired M substate and measuring twice as explained above. However, to be able to implement this scheme, a sufficient spectral resolution is needed to resolve all individual transitions. In the case of IRD one has to keep in mind that spontaneous decay can lead to population transfer to the state of interest.

Analysis of the single M substate detection based on rate equations The rate models allow to test whether it is possible to deplete all molecules within the states described by $J = 3,4$, $|K| = 3$ apart from the $|0;4,3,4\rangle$ state. Figure 4.5 shows the result of a MWD (a) and an IRD (b) simulation where the coupling of the $|0;3,3,3\rangle \leftrightarrow |0;4,3,4\rangle$ transition is not applied. The results presented in (a) show that for MWD the $|0;4,3,4\rangle$ state is depleted at a similar rate as the rest of the $J = 3,4$, $|K| = 3$ states and thus a single M substate detection is not possible. This is primarily due to the high power needed to drive the $|0;3,3,3\rangle \leftrightarrow |0;4,3,2\rangle$ transition (compare discussion in section 3.5).

In contrast, using IRD, the detection of the population of the single M substate $|0;4,3,4\rangle$ is possible and was in fact used to measure the electric-field distribution in section 3.4. The population of the $|0;4,3,4\rangle$ state is still depleted but on a much slower timescale. Blackbody radiation causes the unwanted loss of population from the single M substate to further increase. However, these effects only result in a slight systematic underestimation of the population.

4.2 Experimental results

In the following, experimental results for the state-selective detection methods MWD and IRD are presented. However, first, a potential caveat of the state-detection method is discussed. Then, measurements of the depletion time dependence are presented and compared to the results of the rate model from the previous section. Subsequently, the

population of the $|0;4,3,4\rangle$ state is measured, achieving the main goal of the rotational state detection: discriminating the population of a single rotational M substate described by single J, K and M quantum numbers. A time dependent saturation measurement is used to estimate the error of the single M substate detection.

Knowing the relevant timescales, finally the quality of the depletion techniques is investigated: It is first examined to which extent the methods yield the same result. Second, measured and expected relative state populations are compared. Third, it is proven that all molecules populating the states of interest can be depleted.

4.2.1 Effect of unloading on the state-selective detection

Before presenting experimental results a brief discussion about a potential caveat of the state-detection method is given. In our setup, molecules are detected outside the trap with a QMS and the efficiency for unloading the molecules from the trap and guiding them to the QMS depends on the kinetic energy and the Stark shift of the molecules. Thus, the rotational-state distribution at the QMS is correlated to but not necessarily identical to the rotational-state distribution inside the trap.

Knowing the rotational-state distribution at the position of the QMS is of interest for many applications, e.g., a transfer of molecules to a different kind of trap or crossed-beam collision experiments. Quantitative investigations of in-trap populations, however, require the unloading efficiency to be taken into account. In the most general case, this would require to determine the unloading efficiency as a function of the kinetic energy and the Stark shift of the molecules for various applied trap voltages. A full analysis of this topic, however, is beyond the scope of this thesis. Nevertheless, below two cases where quantitative results for state populations inside the trap can be obtained with considerably less effort are described. Almost all measurements shown in this thesis fall into these two categories, allowing the effect of the unloading efficiency to be ignored.

First, the trap unloading efficiency can to good approximation be ignored for direct loading and unloading of molecules to and from the trap with no intermediate manipulation other than the complete depletion of the population in the states of interest needed for rotational-state detection. In this case, the mean energy of molecules in a given state is to good approximation proportional to its Stark shift due to the use of velocity filtering as the molecule source. The ratio of energy to Stark shift is thus nearly independent of the molecular state. The same holds for the unloading efficiency which depends predominantly on this ratio, so that the relative state populations are nearly unaffected by the unloading process.

Second, if an experimental process prior to the state-selective detection changes neither the relative populations among a given set of states nor the kinetic energy of the molecules in these states, the unloading efficiency for these molecules remains constant. In this case, a change of the state-selectively measured signal for these states implies a directly proportional population change inside the trap. This fact is used to measure population changes in a single M sublevel in section 4.2.3 (the "given set of states" being the single M sublevel). Moreover, it is used for quantitative investigation of population changes caused by optical pumping inside the trap in section 5.3.

In addition to the quite general considerations above, the results of a first measurement for the characterization of the unloading efficiency is given in Fig. 4.6(a). The

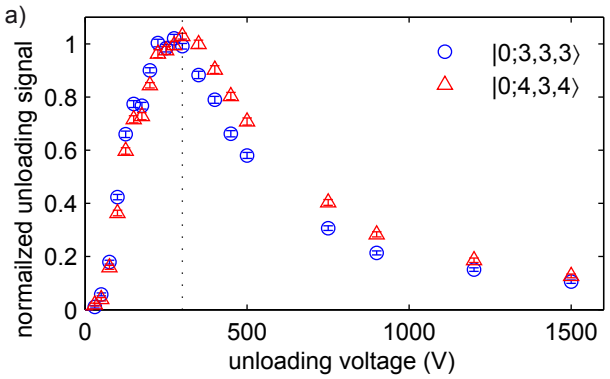

b)

duration (s)	experimental step
37	RSC + Sisyphus cooling
2	SSP
12	unloading and molecule detection

Figure 4.6: Unloading particular rotational states. (a) Measured normalized unloading signal versus the unloading voltage applied at the the ring electrode of the trap and the unloading electric quadrupole guide. The dotted line shows the value that is used throughout this thesis for unloading molecules at $\approx 30\,\mathrm{mK}$. Vertical bars denote the 1σ statistical error. (b) Summary of the experimental sequence (see appendix A for more information about the individual experimental steps)

normalized unloading signal of a Sisyphus cooled molecular ensemble pumped either to the single M sublevel $|0;3,3,3\rangle$ or to $|0;4,3,4\rangle$ (see section 5.3) is measured versus the unloading voltage at the ring electrode of the trap and the unloading electric quadrupole guide. The trapping voltage applied to the microstructure is kept constant at $V_\mu = \pm 300\,\mathrm{V}$ with a voltage difference between the capacitor plates of $V_{Offset} = \pm 15\,\mathrm{V}$. The measurement shows a clear maximum mainly due to two processes. Too low voltages cause trap losses of molecules and too high voltages prevent the molecules from entering the exit guide. The overall form is discussed in detail in [Eng13, Zep12]. As both ensembles have the same kinetic energy distribution the unloading efficiency differs only due to the different Stark shifts of the two states. The curve for the rotational state $|0;4,3,4\rangle$ is slightly shifted to higher unloading voltages due to the lower Stark shift. Nevertheless, by adjusting the unloading voltage to $V_{Ring} = \pm 300\,\mathrm{V}$ (dotted line), both rotational states are unloaded with maximal efficiency.

4.2.2 Measurement of the time dependence

Measurements of the time dependence of the depletion process are presented in this subsection. Specifically, these measurements yield the timescale needed for depletion which can then be compared to other timescales such as the population transfer caused by blackbody radiation or the trap lifetime. In addition, it is found that the predictions from the rate model agree well with the measurement results, explaining the effect of blackbody radiation and unwanted depletion of wrong K-states. For both problems solutions are discussed in the following subsection. In particular, with a variation of IRD a detection signal can be obtained which is independent of the population in wrong K-states.

Comparison of rate model and experiment For a comparison of the results obtained via the rate model with experimental data, one has to keep in mind that several

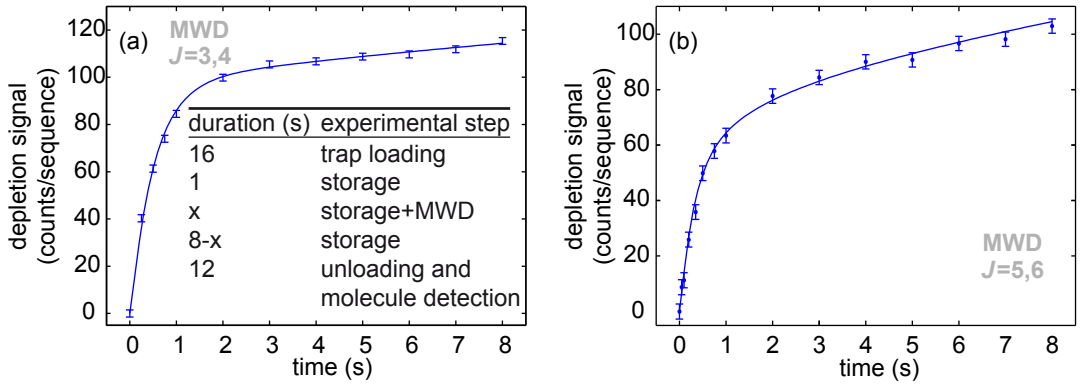

Figure 4.7: Experimental results and comparison to the rate model for MWD. A saturation measurement of MWD is shown for the $|0; J, 3, M\rangle$ states with $J = 3, 4$ in (a) and $J = 5, 6$ in (b). The inset in (a) gives a summary of the experimental sequence used to obtain the data in (a) and (b). The time where MWD is applied is varied from x=0 to 8 s. Both measurements show two timescales. The fast increase in (a) is given by the depletion of the entire $J = 3, 4$ states, including also the unintended depletion of states with $|K| = 1, 2$. The slow increase results from blackbody induced population transfer, see main text for details. (b) shows the same behavior except for a more pronounced slow increase. In addition to blackbody induced population transfer, this is due to the slow depletion of states with $|K| > 3$.

experimental effects such as the unloading efficiency (see section 4.2.1) or trap losses are not included. As an example: a molecule initially populating a high M substate is transferred to a lower M state during depletion. In the experiment this molecule is less well trapped and a higher loss rate is observed. In addition, the unloading filters the molecules according to their Stark shift. Both effects are not reproduced in the rate model. However, as the MW driving rate is a fitting parameter, the losses in the experiment might be simulated by choosing a higher MW driving rate in the rate model.

Experimental sequence All saturation measurements were performed with a similar experimental sequence. Molecules are loaded without any manipulation for 16 s. The state-selective depletion then is applied for varying amounts of time after the first second of storage. The total storage time, however, is always the same (9 s for MWD; 7 s for IRD) which allows one to ignore trap losses. Finally, the molecules are unloaded and detected with the QMS.

Microwave depletion for $\mathbf{J = 3, 4, |K| = 3}$ MWD is implemented according to the scheme discussed in section 4.1.1. The result of the saturation measurement and the rate model for the $J = 3, 4$, $|K| = 3$ states are presented in Fig. 4.7(a) and show an excellent agreement. To fit the rate model to the data only two fit parameters were used: The first one is the total power of the microwaves. This is a single fit parameter as the effective power of the individual applied MW frequencies is set according to $P_{i,j} \propto \frac{d_{i,j}}{c_{i,j}}$ (see section 3.5). The second one is a vertical scaling parameter to match the population given by the rate model to the depletion signal.

The saturation measurement shows two timescales, as expected from the rate model. The fast increase is the depletion of the $J = 3, 4$ states, where the unwanted $|K| = 1, 2$ states are depleted almost equally fast as the $|K| = 3$ states of interest. A better separation can only be achieved with a more homogeneous electric field in the trap. Thus signal contributions due to the $|K| = 1, 2$ states are, at the moment, only limited by the population of these states. The calculation of the population distribution as presented in section 2.1 shows that 72 % of the molecules in the $J = 3, 4$ manifold populate the $|K| = 3$ state. Thus using MWD the measured number of molecules populating states with $J = 3, 4$ $|K| = 3$ is at most overestimated by 40 %.

The slow increase in Fig. 4.7(a) is a result of blackbody induced population transfer. Whereas the timescale for the depletion via MWD is purely limited by the total MW power, the timescale of blackbody induced population transfer is given by the temperature of the setup. Thus the timescales of both processes are independent and a sufficient separation is achievable.

The saturation measurement can now be used to choose the depletion time for state-selective detection. While measuring the full saturation curve gives additional information, measuring only a single point is sufficient for many purposes and requires substantially fewer measurements. Hereby one has to find a compromise: On the one hand, too long depletion times lead to larger errors due to the population transfer caused by blackbody radiation. On the other hand, the depletion of the states of interest should be saturated. In this thesis, 2 s are picked for further measurements. Here the influence of blackbody radiation on the detection result is on the order of a few percent and is thus almost negligible.

Microwave depletion for $\mathbf{J = 5, 6, |K| = 3}$ A MWD measurement of the population within the $J = 5, 6, |K| = 3$ states and the corresponding rate model is shown in Fig. 4.7(b). The overall shape of the curve is similar to the one in Fig. 4.7(a) and again agrees nicely with the rate model. However, compared to Fig. 4.7(a), (b) shows a much more pronounced increase at longer depletion times. This is because in the manifold of states with $J = 5, 6$ only about 40 % of the molecules populate the states with $|K| = 3$. Moreover, as discussed in section 4.1.1, the states with $|K| > 3$ contribute on top of the blackbody radiation to the slow increase of the signal. The error for detecting the population of states with $|K| = 3$ is here larger than for the $J = 3, 4$ states, and MWD should only be used to discriminate the total angular momentum J.

Full infrared depletion The rate model and the experimental result of the saturation measurement for the states with $J = 3, 4$, $|K| = 3$ using IRD are given in Fig. 4.8(a). The implementation is realized according to the scheme discussed in section 4.1.2. This leads to the blue curve (blue diamonds) which is in good agreement with the rate model. This method is denoted full IRD in contrast to K-selective IRD described below.

As already discussed above, the driving of the infrared transitions is J and K selective and the unwanted depletion of states with $|K| = 1, 2$ is purely caused by the MW radiation. This timescale is however much slower than the depletion of the states with $|K| = 3$. Thus, in contrast to MWD, the unintended depletion of states with $|K| = 1, 2$ also contributes to the slow increase of the depletion signal, which is of great advantage: By picking two seconds of depletion for further experiments, the detection signal is less

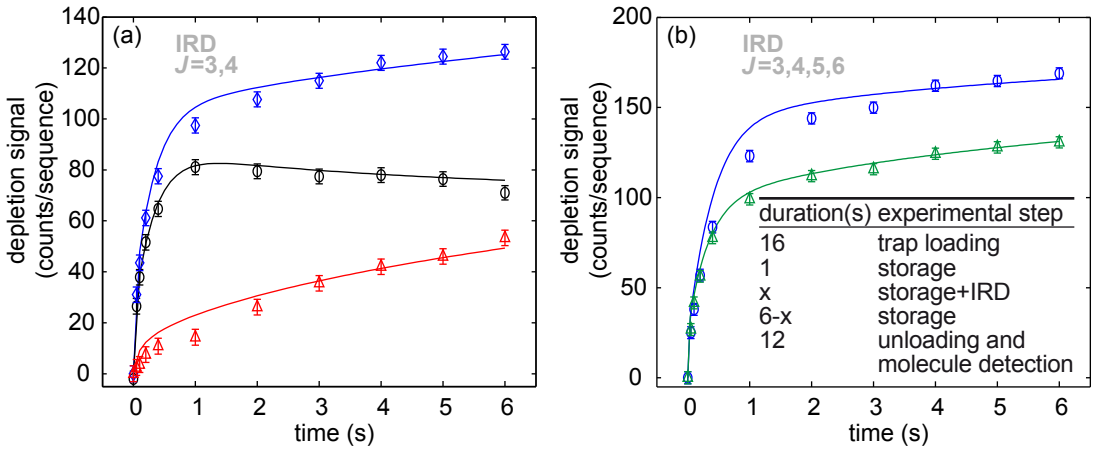

Figure 4.8: Saturation measurement and comparison to the rate model for IRD. (a) The blue diamonds show the result of an IRD saturation in the states with $J = 3, 4$, $|K| = 3$ according to the scheme shown in Fig. 4.3. The red triangles represent a reference measurement, without applying the laser. The difference of the two (black circles) yields a $|K|$-selective IRD measurement as explained in the main text. (b) IRD saturation of the states with $J = 3, 4, 5, 6$ and $|K| = 3$. The difference of the full IRD signal (blue) and the measurement with the laser only applied to the $J = 3$ state (green) yields the K-selective signal of molecules populating the states with $J = 5, 6$ and $|K| = 3$. The inset gives a summary of the experimental sequence for the data shwon in (a) and (b). The time where IRD is applied is varied from x=0 to 6 s

influenced by the unintended depletion of states with $|K| = 1, 2$, thus reducing the error.

$|\mathbf{K}|$-selective infrared depletion The influence of the unintended depletion of states with $|K| = 1, 2$ on the detection signal can completely be eliminated by subtracting out the influence of the MW radiation. For that, the depletion effect of the microwaves is examined with a reference measurement. Here the four MW frequencies for IRD were applied but the laser was left off (Fig. 4.8(a) red triangles). As both measurements (the full IRD and reference measurement) are equally affected by the unintended depletion of states with $|K| \neq 3$, the difference of both measurements yields a $|K|$-selective measurement (black circles). The drawback of this K-selective IRD is a slightly reduced signal as the reference measurement also includes some depletion of states with $|K| = 3$.

Infrared depletion for $\mathbf{J = 3, 4, 5, 6, |K| = 3}$ The IRD scheme can easily be extended to incorporate also the $J = 5, 6$ rotational states as presented in section 4.1.2. Figure 4.8(b) shows the corresponding rate model and saturation measurement. The full IRD signal for depleting the manifold with $J = 3, 4, 5, 6, |K| = 3$ is given by the blue curve (blue circles). The population in the states $J = 5, 6, |K| = 3$ is deduced as explained in the following. By performing a second measurement without driving the vibrational excitation from $J = 5$ (green triangles) the states $J = 3, 4$, $|K| = 3$ are depleted as in (a) with, however, the MW couplings of the $J = 5, 6$, $|K| = 3$ states being additionally present. Thus, the effect of driving other K states with microwaves

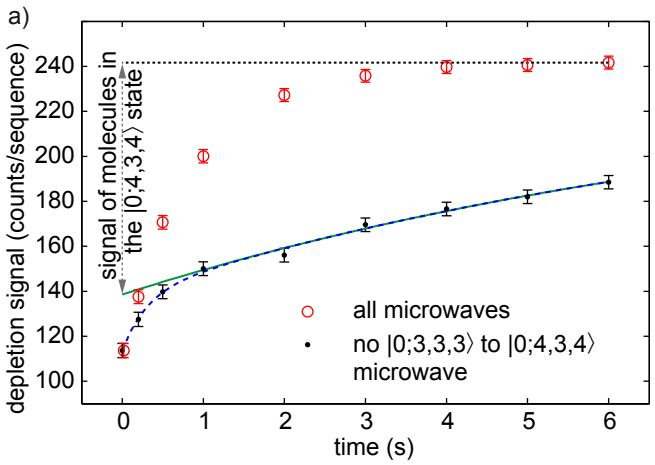

b)

duration(s)	experimental step
21	Sisyphus cooling to 150mK
1	accumulation
2	driving a ΔM=-1 vibrational transition from J=3
x	depletion
6-x	storage
12	unloading and molecule detection

Figure 4.9: Detection of the population in the $|0;4,3,4\rangle$ state. (a) The figure shows two saturation measurements. The red circles correspond to a full IRD measurement. The black dots are measured without driving the transition $|0;3,3,3\rangle \leftrightarrow |0;4,3,4\rangle$. The number of molecules in $|0;4,3,4\rangle$ is extracted from the difference of the two curves. Due to the Stark broadening of the spectral lines, the $|0;3,3,3\rangle \leftrightarrow |0;4,3,4\rangle$ transition is slightly driven by the other applied microwave frequencies. Measuring only at a single point with 2 s of depletion therefore underestimates the number of molecules in the $|0;4,3,4\rangle$ state as is explained in the main text. (b) Summary of the experimental sequence (see appendix A for more information about the individual experimental steps).

is contained in this measurement, and the difference of both measurements in (b) gives a $|K|$-selective signal for the molecule number in the states $J = 5, 6, |K| = 3$. IRD for $J = 3, 4, 5, 6, |K| = 3$ is in the following in few cases also applied for four seconds to better saturate the depletion.

4.2.3 Detection of the population in a single M substate

This subsection discusses the experimental results of the single M substate detection which was discussed in section 4.1.3. According to the results of the rate model, the scheme based on IRD is expected to work. With the means of a measurement of the depletion time dependence, an estimation of the error of the single M substate detection is obtained. Finally, a scheme to detect the population in the state $|0;3,3,3\rangle$ is presented.

Detection of the population in the $|0;4,3,4\rangle$ state The experimental sequence is summarized in Fig. 4.9(b). To improve statistics, an ensemble cooled to ≈ 150 mK is used. The subsequent one second of accumulation transfers all molecules of $J = 3, 4$, $|K| = 3$ to the two highest M substates of this manifold. Afterwards, the population in $J = 3$ was distributed among the $|0;4,3,M\rangle$ states by driving a $\Delta M = -1$ vibrational transition from $J = 3$. Then, the molecules were stored for 6 s, and an IRD saturation measurement was performed either with driving the $|0;3,3,3\rangle \leftrightarrow |0;4,3,4\rangle$ MW transition or without. To reduce the unwanted driving of the $|0;3,3,3\rangle \leftrightarrow |0;4,3,4\rangle$

transition and thus to improve the quality of the single state detection the MW power is reduced by about a factor of eight compared to the IRD measurements described above. The laser is left on during the whole 6 s.

The data is shown in Figure 4.9(a). The measurement with applying the $|0;3,3,3\rangle \leftrightarrow |0;4,3,4\rangle$ coupling (red circles) is equivalent to the full IRD signal (except for the reduced MW power). The measurement without (black dots) has to be separated into two regions: the fast increase yields the depletion signal of all molecules populating rotational states within $J = 3,4; |K| = 3$ except the state $|0;4,3,4\rangle$. The subsequent slower increase is caused by the unintended driving of the $|0;3,3,3\rangle \leftrightarrow |0;4,3,4\rangle$ transition in the inhomogeneous electric field regions of the trap as well as by blackbody induced population transfer.

The difference of both measurements yields a signal proportional to the number of molecules in the state $|0;4,3,4\rangle$ and thus the population of a state described by a single J, K and M quantum number. Due to the unintended depletion of the $|4;3;4\rangle$ state in the black curve, this difference underestimates the population in the state $|0;4,3,4\rangle$. To obtain an estimation of the error the black data points are fitted with a double exponential (blue, dashed). The slow part of this fit is plotted (solid green) and the difference of the fully saturated red curve and the extrapolation of the green curve to 0 s yields the signal of molecules in the $|0;4,3,4\rangle$ state. The fast increase saturates after about 2 s, meaning that the entire population of all states but the $|0;4,3,4\rangle$ state is depleted. For 2 s of single state detection, the number of molecules is thus underestimated by approximately 20 %. This measurement shows that it is clearly possible to distinguish between the $|0;4,3,4\rangle$ state and the other states in the $J = 3,4; |K| = 3$ manifold.

Detection of the population in the $|0;3,3,3\rangle$ state The $|0;3,3,3\rangle$ state can be detected with a similar scheme. The MW coupling stays the same but the vibrational driving is on the $J = 4$ states which has two consequences: First, the vibrational decay transfers population to the $J = 5$ state. Thus MWD or IRD for depleting the $J = 5,6$ state is additionally needed. Second, the spontaneous decay from the vibrational excited state $|1;4,3,3\rangle$ transfers population to the target state $|0;3,3,3\rangle$ with a branching ratio of 5 % which gives an additional error of the measurement.

4.2.4 Qualitative and quantitative investigation of the rotational-state depletion methods

In this section the quality of the state detection methods MWD and IRD is investigated by comparing the discussed methods with one another and with expected relative state populations. In addition, the ability of the depletion methods to deplete the total population within the states of interest is proven and the underestimation of the population while using K-selective IRD is measured.

Comparison of the depletion methods First, the number of molecules detected using MWD or IRD is compared for addressing either $J = 3,4, |K| = 3$ or the $J = 3,4,5,6 |K| = 3$ states. A summary of the experimental sequence is given in Fig. 4.10(a). An ensemble is used which is directly loaded from the electric quadrupole

(a)

duration(s)	experimental step
16	trap loading
1	storage
2	state-selective depletion
12	unloading and molecule detection

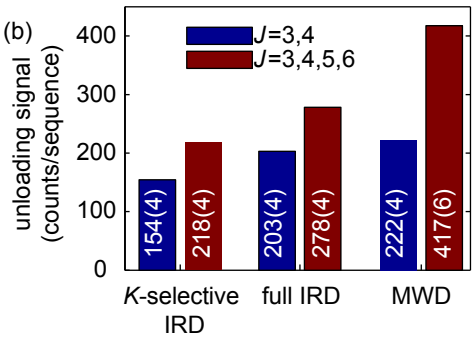

Figure 4.10: Comparison of the detection methods. (a) Summary of the experimental sequence. (b) MWD, IRD and K-selective IRD applied to a directly loaded ensemble in the trap where other J and K states are present. Note that the total signal of trapped molecules is 933(6) counts/sequence, if no depletion is applied.

depletion method	measured rel. population	set of states for comparison	expected rel. population
$\|K\|$-sel. IRD for $J = 3, 4, \|K\| = 3$	0.165(5)	$J = 3, 4, \|K\| = 3$	0.170
$\|K\|$-sel. IRD for $J = 3, 4, 5, 6, \|K\| = 3$	0.233(5)	$J = 3, 4, 5, 6, \|K\| = 3$	0.257
Full IRD for $J = 3, 4, \|K\| = 3$	0.217(5)	$J = 3, 4, \|K\| = 3$	0.170
Full IRD for $J = 3, 4, 5, 6, \|K\| = 3$	0.298(5)	$J = 3, 4, 5, 6, \|K\| = 3$	0.257
MWD for $J = 3, 4$	0.238(5)	$J = 3, 4, \|K\| = 1, 2, 3$	0.235
MWD for $J = 5, 6$	0.210(5)	$J = 5, 6, \|K\| = 1, 2, 3, 4, 5$	0.223

Table 4.1: Comparison of measured and expected relative state populations.

guide closely matching the rotational-state distribution shown in Fig. 2.3. The molecules are stored for 3 s and either the depletion or nothing is applied during the last 2 s. The difference of these two measurements gives the resulting state selected signal of molecules and is plotted for each method in Fig. 4.10(b), satisfying our expectations from the previous discussions. In particular it can be seen that the $|K|$-selective IRD measurement always results in the lowest signal as this method underestimates the number of molecules in the $|K| = 3$ states of interest. In contrast, MWD and full IRD overestimate the signal in $|K| = 3$ where the effect is stronger for MWD than for IRD due to the enhanced depletion of states with $|K| \neq 3$. All three methods differ less for the depletion of the states with $J = 3, 4$ than for the states with $J = 3, 4, 5, 6$ as the contribution of $|K| \neq 3$ is stronger for $J = 5, 6$ than for $J = 3, 4$.

Comparison of measured and expected relative state populations The results in Fig. 4.10(a) also allow a comparison with the expected rotational-state distribution in Fig. 2.3. For this purpose, the depletion signal for the various methods is divided by the total signal of trapped molecules of 933(6) counts/sequence, and the resulting measured relative populations are shown in Tab. 4.1. The expected relative populations were calculated taking into account those states listed in the third column of Tab. 4.1. In particular, for MWD the population in states with $|K| \neq 3$ is also included, following the discussion in section 4.1.1. The agreement between measured and expected populations is remarkable, with deviations conforming to the previous discussions.

(a)

duration (s)	experimental step
37	Sisyphus cooling to 30mK
8(a) or 2(b)	state-selective depletion
12	unloading and molecule detection

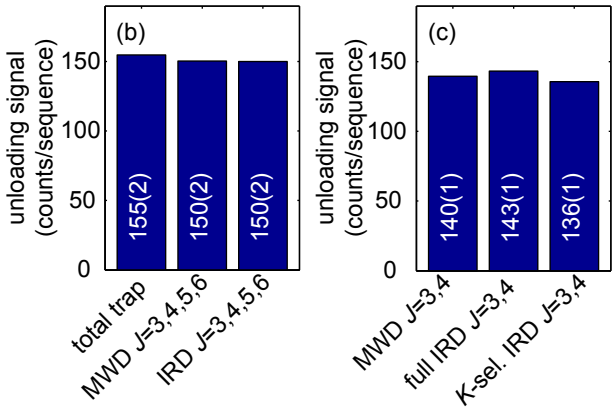

Figure 4.11: Tests of the detection methods. (a) Summary of the experimental sequence. (b) Proof that MWD and IRD deplete all molecules populating the states of interest. Here a molecular ensemble is used where no other J and K states are present (see main text). The detection is applied for 8 s to ensure full saturation. (c) Comparison of the K-selective IRD measurement with MWD and full IRD for an ensemble where no other K states are present. The K-selective measurement underestimates the signal of molecules by less than 5 %.

Validation of the depletion method To verify that all molecules within a certain set of states can be depleted an almost pure state ensemble produced by Sisyphus cooling is used. Due to the long trapping time during cooling, a reduced trap voltage for unloading, and the radio-frequency knife for cooling, almost only the cooled molecules (≈ 30 mK) in the states $|0;3,3,3\rangle$ and $|0;4,3,4\rangle$ are unloaded for detection at the end of the cooling sequence (see section 5.2). However, some molecules are pumped to the $J = 5, 6$ states due to blackbody radiation. In addition, a Fermi resonance with a doubly excited vibrational state can also lead to population of the $J = 5$ state. Thus most of the molecules should populate the $J = 3, 4; |K| = 3$ states and some the $J = 5, 6; |K| = 3$ states. Using this cold ensemble, testing the state-selective detection methods is possible. The depletion was applied to the states $J = 3, 4, 5, 6, |K| = 3$ for 8 s to ensure full saturation. Figure 4.11(b) shows the outcome of this measurement. Here, both methods, MWD and full IRD, give the same result which is almost equivalent to the total signal of trapped molecules of 155(2) counts/sequence. It can thus be stated that the depletion transfers all molecules populating the states of interest to untrapped states. A shorter depletion time leads to some error, however, already for two seconds of depletion this can most often be ignored.

Additionally, the Sisyphus-cooled ensemble can be used to compare the $|K|$-selective IRD measurement with MWD and full IRD, as states with $|K| \neq 3$ are hardly populated. The depletion is in each measurement applied for 2 s. Figure 4.11(c) shows that the K-selective IRD measurement underestimates the signal by less than 5 % compared to MWD and full IRD. However, in this measurement, the population was almost exclusively in the highest M substates of $J = 3, 4$. A higher population of lower lying M substates could lead to a higher underestimation when using $|K|$-selecitve IRD.

4.3 Discussion

In summary, this chapter presented a detailed investigation of rotational-state detection of trapped molecules based on rotational-state selective depletion. This depletion employs the driving of rotational and vibrational transitions to transfer molecules to untrapped states. As suitable transitions can be found in any molecule, this technique is extremely general and should be applicable to all trappable neutral molecule species. Moreover, with use of only a single microwave synthesizer and (optionally) a single infrared laser, the presented technique is simple to implement. Also an extension to other types of internal states is feasible. Detecting hyperfine states would require a sufficient spectral resolution, and detecting vibrational states could make use of different rotational constants in different vibrational states.

The current experimental setup could be advanced twofold. First, adding a second laser would allow to eliminate the need for MW coupling in IRD as these couplings could be replaced by driving P- or R-branch vibrational transitions. This in particular yields a K selective measurement that does not underestimate the population. Second, MW coupling of the rotational states $J = 4$ and $J = 5$ could be implemented. This would for example allow to measure the population within all M substates of the rotational state $J = 3$ by taking the difference of the signals obtained for depletion in $J = 3, 4, 5$ and $J = 4, 5$. It could also advance the detection of single M substates in $J = 3$ by applying MWD for $J = 4, 5$ and coupling only a single M substate of $J = 3$ to $J = 4$. In particular, this would also allow the detection of the population in lower lying M substates, which has multiple applications in the experiment. First, it would allow to study the unloading efficiency in more detail, as the Stark shift of the observed state can be varied of a larger range. Second, loss mechanism as for example Majorana losses which change the M quantum number can be investigated in more detail. Finally, searching for M changing collisions inside our trap could become possible.

Chapter 5

Rotational-state cooling

This chapter presents a comprehensive method for rotational-state control of polyatomic molecules. As a first step, rotational cooling by optically pumping CH_3F molecules in the states $J = 5$ and $J = 6$ into the state $J = 4$ is demonstrated and analyzed in section 5.1. Molecules in the states $J = 3$ and $J = 4$ can then be motionally cooled via optoelectrical Sisyphus cooling [Zep09, Zep12] which can be integrated seamlessly with the here presented rotational-state cooling. In particular, this combination allows for a simultaneous cooling of the internal and external degrees of freedom of polyatomic molecules. Section 5.2 briefly reviews optoelectrical Sisyphus cooling and discusses the results and the optimization of the combination with rotational-state cooling. A subsequent M sublevel-dependent optical pumping transfers a majority of the trapped molecules into a single M substate. This single state preparation is discussed in section 5.3 for optical pumping into the final states $|0; 4, 3, 4\rangle$ or $|0; 3, 3, 3\rangle$. Together with optoelectrical Sisyphus cooling, which eliminates all molecules in uncooled states from the trap, this leads to a cold ($\approx$30 mK) and almost pure state ensemble of trapped CH_3F molecules. The purity of this ensemble is studied in section 5.4 and compared to differently prepared ensembles in section 5.5. Finally, section 5.6 discusses possible extensions of rotational-state cooling to incorporate more states and possible schemes to improve the single state preparation.

5.1 Rotational-state cooling

5.1.1 The scheme for rotational-state cooling

General schemes The rotational-state cooling (RSC) scheme presented in this thesis is based on optical pumping via excitation of a vibrational mode using a scheme related

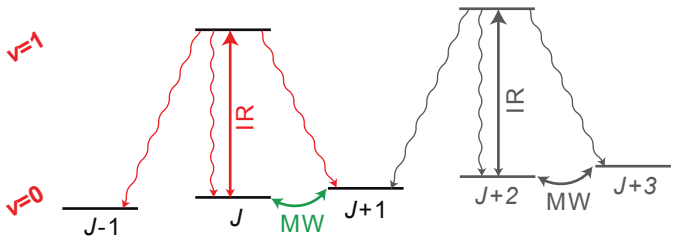

Figure 5.1: Simplified scheme for rotational-state cooling (RSC). Optical pumping via a vibrational excited state with infrared (IR) and microwave (MW) radiation is used to accumulate population in a lower rotational state.

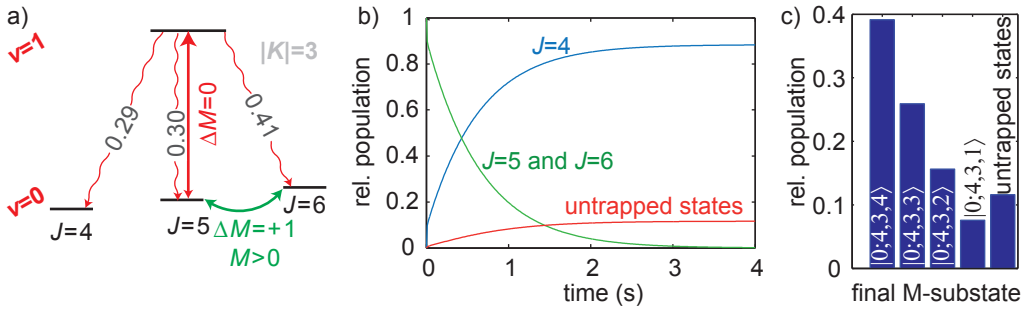

Figure 5.2: Implementation of rotational-state cooling (RSC) for CH_3F. (a) Scheme of the implemented RSC without resolving the M substates. (b) Result of a rate model simulating the dynamics of RSC. (c) Simulated population distribution within the final $J = 4$ rotational state for 4 s of RSC.

to those demonstrated for diatomic molecular ions [Sta10, Sch10]. The underlying idea is shown in Fig. 5.1. Driving a $\Delta J = 0$ vibrational transition from a given rotational state J results in spontaneous decay to the states $J \pm 1$. By coupling the states J and $J + 1$ with microwaves, the entire population in the states J and $J \pm 1$ accumulates in the dark state $J - 1$.

This scheme can easily be extended to incorporate larger sets of initial states by, e.g., applying the same couplings to subsequent pairs of rotational states as sketched in Fig. 5.1 or as discussed in the outlook in section 5.6. In principle, the dark state of such a scheme can be freely chosen.

Implementation for CH_3F All internal state manipulation presented in this thesis takes place in the homogeneous-field electric trap described in chapter 3. Thus, a key challenge of the implementation of RSC is to ensure that most molecules stay trapped during the optical pumping. Here, two features of the employed trap are of great advantage. First, the narrow electric-field distribution of the trap allows one to spectrally resolve all relevant transitions with minimal Stark broadening and thus minimizes accidental addressing of transitions that transfer the population to untrapped states. Second, the long trap lifetime of up to 30 s [Zep12] is crucial for the implementation of an optical pumping scheme based on spontaneous decays of vibrational excitations with typical decay times of more than 10 ms. Despite its slow decay rate the use of a vibrational mode is favorable due to strict selection rules as discussed in chapter 2.

RSC is implemented for CH_3F molecules by pumping the population of the rotational states with $J = 5, 6$, $|K| = 3$ to $J = 4, |K| = 3$. With this choice of rotational states, RSC can be combined with optoelectrical Sisyphus cooling which motioanlly cools molecules populating the rotational states $J = 3, 4, |K| = 3$ as will be discussed in the following section. Incorporating higher rotational states is of little gain for the relatively light molecule CH_3F as the population of higher J-states is rapidly decreasing (compare Fig. 2.3). Nevertheless, the implementation within the above mentioned rotational states already proves that RSC is applicable to polyatomic molecules.

Figure 5.2(a) shows the optical pumping scheme with all applied radiation fields. A $\Delta M = 0, \Delta J = 0$ vibrational transition from $J = 5$ is driven and transfers the popu-

lation to the vibrational excited state. The subsequent spontaneous decay brings the population with a probability of 29 % to our target state $J = 4$ and with another 41 % to $J = 6$. For $J = 4$ to become the only dark state of the pumping scheme, $J = 6$ and $J = 5$ are coupled with MW radiation. In particular, the rotational transitions $|0, 5, 3, M\rangle \leftrightarrow |0, 6, 3, M + 1\rangle$ are driven. Using the $\Delta M = +1$ rotational transitions has the advantage of relatively small Stark shifts and high Clebsch Gordan coefficients. Thus the needed MW power can be kept low which minimizes the problem of unintentionally driving rotational transitions to untrapped states (see section 3.5 for more details). The only state which is not incorporated is $|0, 6, 3, 1\rangle$, which is anyway hardly populated and due to the small Stark shift quickly lost from the trap.

The changes in population caused by RSC can be calculated with a rate model as detailed in section 2.4. The rate model used here simulates the driving of the MW and IR transitions needed for RSC by rate coefficients between appropriate states and the spontaneous decay from the vibrational excited state with a decay rate of 15 Hz. Note that it does not include unintenionally driving of rotational transitions in the inhomogeneous electric-field region of the trap. The initial state distribution consists of all trappable M substates in $J = 5, 6; |K| = 3$. The distribution over the M sublevels represents the conditions of the velocity filtered source as calculated in Fig. 2.3. Figure 5.2(b) shows the result of the rate model. The population of the state $J = 5, 6$ is transferred to $J = 4$ within slightly more than two seconds. The relatively long timescale of RSC is due to the slow spontaneous decay rate from the excited vibrational state, combined with a probability of at most $1/3$ for a molecule to be in the excited vibrational state and a branching ratio of 0.29 for a decay from the vibrational excited state to the states $|0; 4, 3, M\rangle$. The rate model also reveals about 10% losses, meaning that some molecules were pumped to untrapped states. Finally, the rate model yields the final population distribution within the $J = 4$ state, see Fig. 5.2(c). Most molecules, almost 40 %, end up in the highest M sublevel.

5.1.2 Experimental results of rotational-state cooling

For proof of RSC, two measurements are presented. First, the populations in the states $J = 3, 4$ and $J = 5, 6$ are examined versus the time for which RSC is applied. In a second measurement, the effect of the microwave radiation coupling $J = 5$ and 6 on the population of molecules transferred to $J = 3, 4$ is studied more closely and the contribution of individual M sublevels in $J = 6$ is identified.

5.1.2.1 Measurement of the time dependence of RSC

Sequence The experimental sequence is listed in Fig. 5.3(b). First, molecules are loaded for 16 s into the trap and are then stored for 8 s and unloaded for 12 s. During the last four seconds of storage the depletion necessary for $|K|$ selective detection of the state $J = 3, 4$, $J = 5, 6$ or all molecules in $J = 3, 4, 5, 6$ is applied. During the first four seconds of storage, RSC is applied for a varying amount of time. To reduce the problem of repopulation caused by blackbody radiation, RSC is applied directly before the depletion. How to optimize the MW power for driving the rotational transitions $|0, 5, 3, M\rangle \leftrightarrow |0, 6, 3, M + 1\rangle$ is shown in the next section. The MW power used in this measurement is the same as the marked value in Fig. 5.7(a).

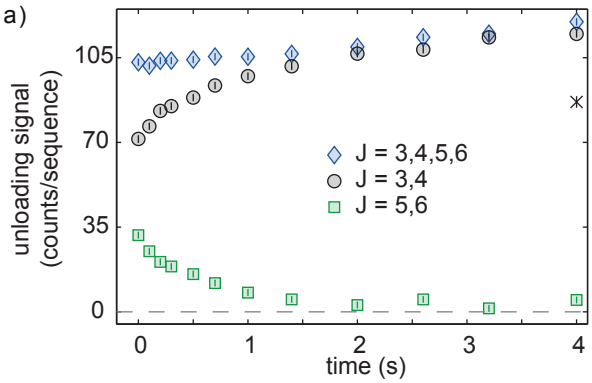

b)

duration(s)	experimental step
16	trap loading
(4-x)	storage
x	RSC
4	state-selective depletion
12	unloading and molecule detection

Figure 5.3: Results of RSC. (a) A saturation measurement of RSC. The rotational-state-discriminated unloading signal detected with the quadrupole mass spectrometer is plotted. The single black cross was measured while leaving the microwaves off (see main text). Vertical bars denote the 1σ statistical error. (b) Implemented experimental sequence. x is the time during which RSC is applied and varies from zero to four seconds.

Result of RSC-saturation measurement Figure 5.3(a) shows the experimental results of the implementation of RSC. A clear increase of the population in $J = 3, 4$ together with a decrease of population in $J = 5, 6$ to almost zero is observed. A comparison with the results of the rate model gives a nice agreement for the timescale of the process. In both cases, the population of the states with $J = 5, 6$ decreases by a factor of two within about 0.4 s. In addition, the rate model suggested about ten percent loss to untrapped states. However, the measurement shows an increase of molecules in the total set of states $J = 3, 4, 5, 6$.

The reasons for this discrepancy of the rate model and the measurement are described in the following. RSC on average increases the Stark shift of the molecule. For example, a spontaneous decay from the excited $|1; 5, 3, 5\rangle$ state to $J = 4$ has to end up in the $|0; 4, 3, 4\rangle$ state, where the Stark shift is a factor of 1.2 higher. The excited $|1; 5, 3, 3\rangle$ state can decay to the $|0; 4, 3, M = 2, 3, 4\rangle$ states. The lowest possible M sublevel $|0; 4, 3, 2\rangle$ has the same Stark shift as $|1; 5, 3, 3\rangle$. Therefore, the molecules, again, end up in rotational states with on average higher Stark shifts. As the lifetime in the trap increases with the Stark shift of the molecule [Eng11], one can expect to measure an increase in signal. This effect is particularly visible by comparing the results measured at 2 s and 4 s. Already after about 2 s almost all molecules from the states $J = 5, 6$ were pumped to $J = 3, 4$ (or lost to untrapped states), but the total signal still slightly increases for longer RSC times. The molecules have been pumped to higher Stark shifts earlier in the experimental sequence and hence the trap losses are slightly reduced. Another experimental subtlety is different detection efficiencies in different internal states which also might hide losses. As discussed in section 4.2.1, the detection efficiency of non-manipulated molecules depends on the ratio of temperature and Stark shift. However, RSC slightly changes the Stark shift possibly resulting in a slightly different detection efficiency. Both effects, the change in the molecule's lifetime and the possible different detection efficiency are hard to be included in the rate model but the outcome of the experiment can qualitatively be understood by the above considerations.

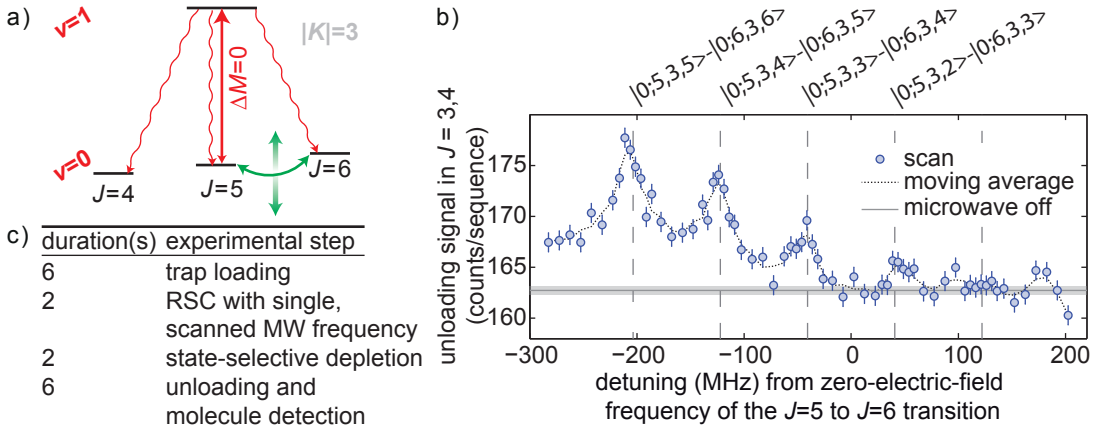

c)

duration(s)	experimental step
6	trap loading
2	RSC with single, scanned MW frequency
2	state-selective depletion
6	unloading and molecule detection

Figure 5.4: MW spectrum of the rotational transitions coupling $J = 5$ and $J = 6$. (a) Scheme for measuring the spectrum. Only a single MW frequency is applied and scanned across all relevant transitions coupling J=5,6. (b) Contribution of single M sublevels to RSC. The rotational-state-discriminated unloading signal detected with the quadrupole mass spectrometer. Dashed vertical lines show the calculated transition frequencies. Vertical bars denote the 1σ statistical error. (c) Summary of the experimental sequence.

While Fig. 5.3(a) shows an increase of molecules in the states $J = 3, 4$ closely tracking the decrease of molecules in $J = 5, 6$, it does not prove conclusively that the increased signal in $J = 3, 4$ originates from molecules populating initially the states $J = 5, 6$. Therefore, the effect of the microwaves coupling the states $J = 5$ and 6 on the rotational-state cooling is explored. Simply leaving these microwaves off leads to significantly less population in the states with $J = 3, 4$ for 4 s of cooling, as shown by the cross in Fig. 5.3(b). Since the microwaves only affect molecules in the states $J = 5$ and 6, the increase of population in $J = 3, 4$ over time clearly originates from molecules in the states $J = 5, 6$.

5.1.2.2 MW spectrum of the $J = 5 \leftrightarrow J = 6$ rotational transition

Contribution from single M sublevels in $J = 6$ can be identified by measuring a spectrum of the rotational transitions coupling the M sublevels of the J=5 and 6 states. The used scheme is shown in figure 5.4(a). As before, the number of molecules populating the states $J = 3, 4$ is detected while applying RSC. Compared to the measurement before, only one MW frequency is used, which is scanned across the transition frequencies of the M sublevels of the $J = 5$ and 6 states.

This measurement consists of many data points and to improve the statistics a shorter sequence is used. To optimize the short sequence, the voltage used during loading and the time for loading the molecules into the trap have to be adjusted. First the loading voltage, which influences the number and the temperature of the ensemble, was optimized with a saturated loading time. Second, the loading and unloading time was optimized to give the best statistical significance within the total length of the experimental sequence. To increase the spectral resolution,the offset field in the electric

trap is increased to obtain an electric-field distribution as in Fig. 3.5(b). This results in a reduced relative line width as explained in section 3.4.

The sequence to measure the spectrum of the $J = 5 \leftrightarrow J = 6$ rotational transition frequencies is given in Fig. 5.4(c). The trap is loaded and unloaded for 6 s. During the storage time of 4 s the first two seconds are used to apply the pumping scheme as described above. Each data point is measured twice, with and without applying IRD in $J = 3, 4$ during the last two seconds of storage and the full IRD signal is plotted in figure 5.4(b).

The Stark-shifted transitions coupling the three highest M sublevels can be clearly identified proving a transfer of molecules from $|0; 6, 3, M = 4, 5, 6\rangle$ to $|0; 4, 3, M'\rangle$. Lower lying M substates yield smaller or negligible peaks because these are less populated initially and the chance of losing the corresponding molecules to untrapped states during the pumping process is higher.

5.2 Combination of internal and motional cooling

A key advantage of the here presented RSC scheme is that it can be integrated straightforwardly with optoelectrical Sisyphus cooling and thus enables the simultaneous cooling of the internal and external degrees of freedom. Optoelectrical Sisyphus cooling is a newly in our group developed technique to cool the motion of electrically trapped polyatomic molecules. The idea is applicable to wide variety of molecule species and was first presented in a proposal on optoelectical cooling [Zep09] and experimentally realized in a proof a principle experiment in 2012 [Zep12]. In that work an ensemble of CH_3F molecules was cooled to a mean kinetic energy of $E_{\text{kin}} \approx 30\,\text{mK} \times \left(\frac{3}{2}k_B\right)$ purely limited by technical issues.

This section first briefly reviews optoelectrical Sisyphus cooling. Then, the results for adding RSC to the Sisyphus cooling sequence are presented together with a discussion about the optimization of the combined experimental sequence. Finally, a proof that RSC has hardly influences the motional degree of freedom is given. Specifically, the kinetic energy of the ensemble with and without RSC is determined by measuring the velocity distribution with a time-of-flight technique.

5.2.1 Optoelectrical Sisyphus cooling of CH_3F

In addition to the above mentioned publications, optoelectrical Sisyphus cooling is described in detail in the theses [Zep13, Eng13, Pre12]. Here a brief summary of the process, the sequence and the main result is given.

The scheme for motional cooling The scheme for optoelectrical Sisyphus cooling as used in [Zep12] is shown in Fig. 5.5. Kinetic energy is extracted by transferring a molecule in $|0; 3, 3, 3\rangle$ to the weaker trapped state $|0; 3, 3, 2\rangle$ via radio-frequency (RF) radiation in the edge region of the trap with high electric fields. The molecule is afterwards pumped back to $|0; 3, 3, 3\rangle$ by driving a $\Delta M = +1, \Delta J = 0$ vibrational transition from $J = 3$ in the homogeneous electric-field region of the trap. As the spontaneous decay can transfer population to the $J = 4$ rotational state, the rotational substates $|0;3,3,M\rangle \leftrightarrow |0;4,3,M+1\rangle$ $(M > 0)$ are coupled with MW radiation. This results in a closed cooling cycle which removes a large fraction of a molecule's kinetic

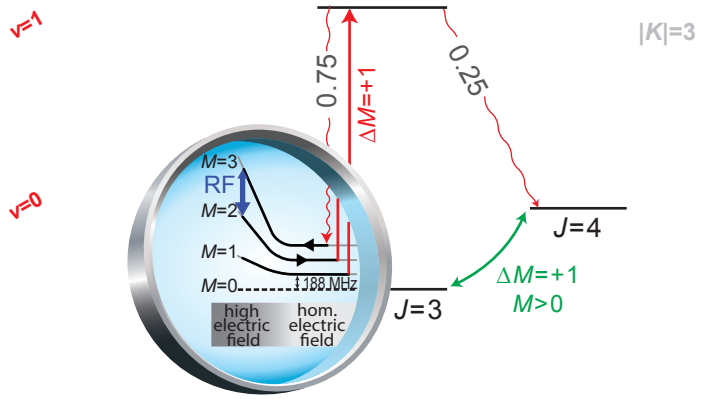

Figure 5.5: Scheme for optoelectrical Sisyphus cooling (not to scale). The zoom shows the Sisyphus process: Kinetic energy is extracted by applying RF radiation which transfers the population from $M = 3$ to $M = 2$ in the edge region of the trap with high electric fields. To repump the molecules to the $M = 3$ substate a $\Delta M = +1$ vibrational transition is driven in the homogeneous electric field region of the trap. The full scheme is described in the main text.

energy in each cycle of the cooling sequence. To achieve efficient cooling, the RF frequency is first as large as possible and then reduced as cooling progresses. The final kinetic energy of the molecular ensemble is hence determined by the last applied RF frequency.

The experimental sequence The experimental sequence for cooling a molecular ensemble to a mean kinetic energy of $E_{kin} \approx 30\,\mathrm{mK} \times \left(\frac{3}{2}\right) k_B$ as in [Zep12] works as follows. The molecules are loaded for 16 s while all radiation needed for Sisyphus cooling are already applied. In particular the RF is set to 3.4 and 1.6 GHz in turns with a duration of one second each. During storage Sisyphus cooling proceeds and the RF decreases (1220, 840, 640, 480, 390 MHz) with each frequency being applied for 4 s. Before unloading and detection of the molecules, state-selective depletion can be applied. The final velocity distribution of the ensemble has in the original work [Zep12] been deduced with a time-of-flight measurement by switching the last guide to a guiding configuration and recoding the arrival time of the molecules. The extracted mean kinetic energy is $E_{kin} = 29\,\mathrm{mK} \times \left(\frac{3}{2}k_B\right)$. Stopping Sisyphus cooling after applying a RF frequency of 1220 MHz leads to an ensemble of molecules with a mean kinetic energy of $E_{\mathrm{kin}} \approx 147\,\mathrm{mK} \times \left(\frac{3}{2}k_B\right)$. For comparison, the non-cooled ensemble has a mean kinetic energy of about $390\,\mathrm{mK} \times \left(\frac{3}{2}k_B\right)$. Note that the molecular ensemble in these experiments is not expected to have a thermal distribution as elastic collisions are missing. Thus temperatures given in this thesis are rather mean kinetic energies of the ensembles.

Consequences of Sisyphus cooling In addition to the reduction in kinetic energy, Sisyphus cooling has a few more effects, which are of importance for the results described in this thesis. First, Sisyphus cooling increases the 1/e trap lifetime of the molecules from initially ≈ 10 s to almost 30 s [Zep12]. Second, Sisyphus cooling depletes molecules

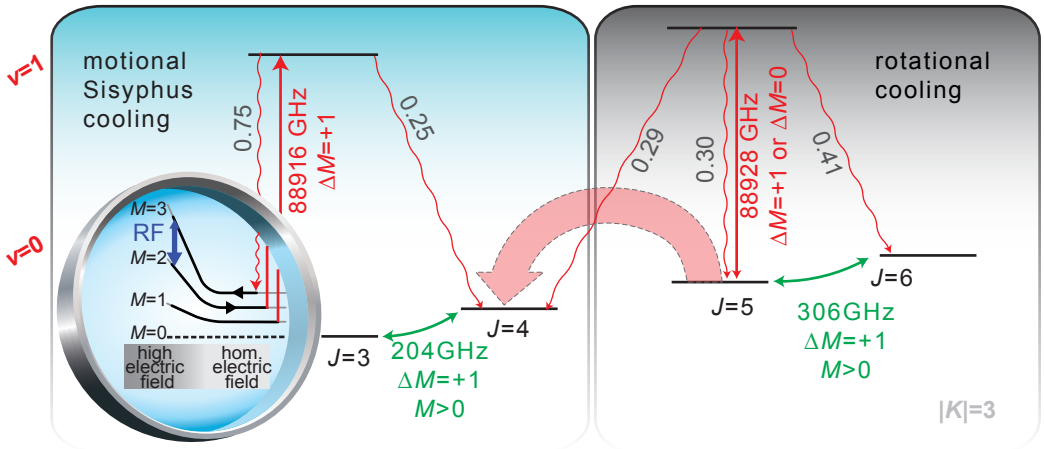

Figure 5.6: Scheme for the combination of optoelectrical Sisyphus cooling (left panel) and RSC (right panel).

populating rotational states outside of the closed level scheme ($J = 3, 4, |K| = 3$) due to the applied RF frequency. Obviously, the RF radiation is not state selective and thus couples the population to untrapped states unless there is repumping to higher M substates as present within the closed cooling cycle. In addition, the long trapping times and the low trapping potentials during unloading remove uncooled molecules from the trapped ensemble. In fact, after cooling to 30 mK almost only molecules populating the $J = 3, 4, |K| = 3$ states are unloaded. Third, within these states, mostly the highest M substates $|0; 3, 3, 3\rangle$ and $|0; 4, 3, 4\rangle$ are populated due to the $\Delta M = +1$ driving of the vibrational transition. Finally, two loss channels of Sisyphus cooling specific to CH_3F cause slow population transfer from the $J = 3, 4, |K| = 3$ states to the $J = 5$ rotational state: a Fermi resonance with the doubly excited vibrational v_5 mode of CH_3F and population transfer caused by blackbody radiation as discussed earlier.

5.2.2 Combination of rotational-state cooling and Sisyphus cooling

Figure 5.6 shows the scheme for the combination of RSC (right panel) and optoelectrical Sisyphus cooling (left panel). RSC transfers the population of the states $J = 5, 6$ to $J = 4$. As $J = 4$ is part of the closed cooling cycle of Sisyphus cooling, molecules initially populating the rotational states $J = 5, 6$ can now be motionally cooled, thus enhancing the number of cold molecules.

The combination is implemented by adding RSC to the above described optoelectrical Sisyphus cooling sequence. As Sisyphus cooling is already applied during trap loading the depicted radiation fields for both, RSC and Sisyphus cooling, have to be applied simultaneously. It is here of great advantage that the two vibrational transition lie within the tuning range of the laser system. The fast ramp and relock system (see chapter 2.2) allows one to switch the IR frequency quickly between both transitions and results in a quasi-simultaneous drive. For that, the switching should be fast compared to the decay time of the vibrational excited state. Also the ramp duration for a change of the frequency of several ms has to be taken into account. The optimal relative durations for the two IR frequencies have to be determined experimentally. In addition, it has to

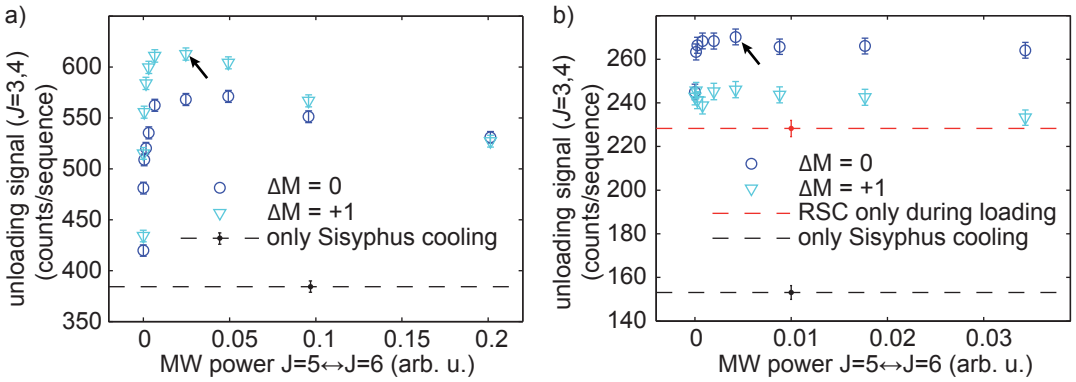

Figure 5.7: Optimisation of the MW power for the combination of Sisyphus cooling and RSC. Optimisation during loading (a) and during the storage phase of the experimental sequence (b). The MW power (duty cycle) is plotted for the $|0;5,3,5\rangle \leftrightarrow |0;6,3,6\rangle$ transition. Note that all needed $|0;5,3,M\rangle \leftrightarrow |0;6,3,6\rangle$ ($M > 0$) are applied, however, with a fixed relative power according to equation 3.1. The arrows point to the finally chosen values. $\Delta M = 0$ or $\Delta M = +1$ refers to the driving of the vibrational transition from $J = 5, |K| = 3$ as explained in the main text.

be deduced experimentally whether the driving of a $\Delta M = +1$ or $\Delta M = 0$ transition from $J = 5$ yields the better results. A $\Delta M = +1$ transition does not address molecules populating the states $|0;5,3,5\rangle$ and $|0;6,3,6\rangle$ which is the case for a $\Delta M = 0$ transition. However, the RF frequency applied for Sisyphus cooling transfers the population of these states to lower lying M substates. Driving a $\Delta M = +1$ vibrational transition transfers the population on average to higher M substates which minimizes losses. In the following, the main steps for an optimization of the combination of rotational and motional cooling are described prior to the discussion of the final results of the combination such as enhanced number of motionally cooled molecules. In addition, the influence of RSC on the final velocity distribution is measured.

Experimental optimization of the sequence At first, the power of the MW radiation used to couple the $J = 5, 6$ rotational states is optimized during the loading phase. The experimental sequence is based on Sisyphus cooling to $\approx 150\,\mathrm{mK}$. RSC is added during the whole time but the MW power is scanned during the loading phase and the subsequent second. As explained in chapter 2.2, the effective MW power is adjusted with the duty cycle of the applied MW frequency. The scan is performed twice with driving a $\Delta M = 0$ or a $\Delta M = +1$ vibrational transition from $J = 5$.

The result is shown in figure 5.7(a) and yields several information. First, adding RSC clearly enhances the number of molecules compared to only performing Sisyphus cooling (dashed line). Second, the optimal MW power has a clear maximum in signal of molecules populating the states $J = 3, 4$. With too low powers the $J = 5, 6$ rotational states are not coupled fast enough, and population is lost due to the effect of the RF, before it can be transferred to $J = 4$. Too high MW power causes unwanted driving of rotational transitions that couple the population to untrapped $M = 0$ states. Finally, the measurement clearly shows that the driving of a $\Delta M = +1$ transition is of advantage.

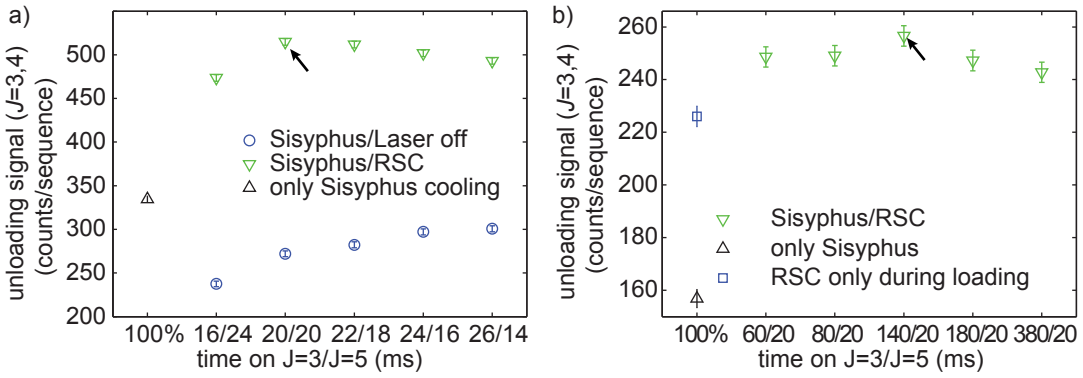

Figure 5.8: Optimization of cycling the two needed IR frequencies. Optimization during loading (a) and during the storage phase of the experimental sequence (b). 100% on the horizontal axis refers to a measurement, where the laser is always stabilized to match the transition frequency from $J = 3, |K| = 3$. This measurement equals the Sisyphus cooling sequence. Sisyphus/Laser off (blue cycles in (a)) refers to a measurement, where the laser is always stabilized to match the transition frequency from $J = 3, |K| = 3$ but where the laser light is blocked during the second interval. Sisyphus cooling/ RSC (green triangles) denotes a measurement, where the laser is stabilized to the frequency of the $J = 3, |K| = 3$ transition in the first interval and to the $J = 5, |K| = 3$ transition in the second interval. Note that the time of the interval includes the time needed to ramp the frequency which is $\approx 7\,\mathrm{ms}$. The arrows point to the finally chosen values.

Figure 5.7(b) shows the result of repeating the optimization during the storage phase of the sequence where the molecules are now motionally cooled to $E_{\mathrm{kin}} \approx 30\,\mathrm{mK} \times \left(\frac{3}{2} k_B\right)$. The number of molecules for performing only Sisyphus cooling (black dashed line) and for adding RSC during the loading phase (red dashed line) is given for reference. Compared to these numbers, a clear increase in signal of motionally cold molecules in $J = 3, 4$ is measured for continuing RSC also during the storage time. This continuation closes the loss channels of Sisyphus cooling specific to CH_3F. The measurement in addition reveals that driving a $\Delta M = 0$ IR transition from $J = 5$ yields a larger signal than driving a $\Delta M = +1$ transition. Here the RF does hardly transfer the population of the $|0; 5, 3, 5\rangle$ and $|0; 6, 3, 6\rangle$ states to lower lying M substates as the molecules are already precooled and the splitting in $J = 5, 6$ is noticeable smaller than in $J = 3, 4$. Thus driving a $\Delta M = 0$ is necessary to address molecules in these states. There is also no strong dependence on the applied MW power. As the RF has less effect on the molecules in $J = 5, 6$ it is not a problem if $J = 5, 6$ are coupled on a slightly slower timescale. Therefore, a lower MW power during cooling is used as indicated by the arrow in Fig. 5.7(b).

To optimize the timing of the IR frequency switching for a quasi-simultaneous driving of the vibrational transitions from $J = 5$ and $J = 3$ the number of molecules in $J = 3, 4$ was measured for different timings. Figure 5.8(a) shows the optimization during the loading phase of the sequence. As above, RSC is added to the Sisyphus cooling sequence which cools to $\approx 150\,\mathrm{mK}$. The horizontal axis shows the duration of the intervals where the laser is stabilized to the frequencies of the transition from $J = 3/J = 5$ in ms. Note that 6 ms for the frequency switch are needed within each interval, during which the

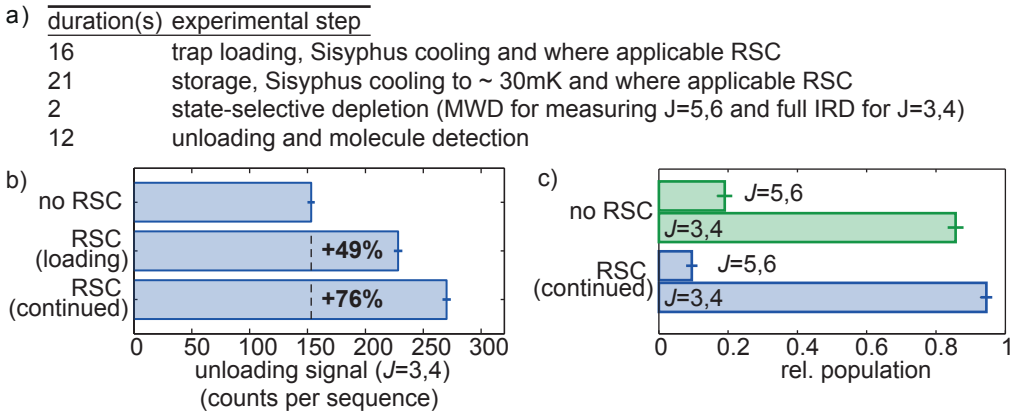

Figure 5.9: Combination of Sisyphus cooling and RSC. (a) Experimental sequence. (b) Measured number of motionally cooled molecules obtained by Sisphus cooling alone, with RSC added during the loading phase of the sequence and during the whole Sisyphus cooling. (c) Population distribution measured after Sisyphus cooling with and without RSC. Horizontal bars denote the 1σ statistical error. Note that the population in $J = 3, 4$ and $J = 5, 6$ adds to slightly more than 100% which can be explained by population transfer due to blackbody radiation during the depletion time.

laser light towards the experiment is blocked. For the combination of Sisyphus cooling and RSC (green triangles) the optimum signal is measured for being 20 ms on each of the transitions. If the laser light is blocked during the time when the laser is stabilize to the frequency of the transition from $J = 5$, effectively only apply Sisyphus cooling is applied, however, with a reduced effective laser power (blue circles). This results in a slightly reduced number of cooled molecules compared to the case where the laser addresses the vibrational transition used for Sisyphus cooling all the time (black single triangle). In summary, although it is of advantage for Sisyphus cooling to drive the needed vibrational transition all the time, the largest signal of cold molecules is obtained by adding RSC.

Figure 5.8(b) shows the optimization for the storage phase of the experimental sequence. In this measurement, the time interval for the IR frequency stabilized to the frequency for the $J = 3, |K|$ transition (including the ramp time) is always chosen to be 20 ms to ensure optimal Sisyphus cooling. The measurements reveals that the timing of the laser being stabilized to the frequency of the transition from $J = 5$ in not critical during the storage phase of the experimental sequence (green triangles). The finally chosen timing is indicated by the arrow in Fig. 5.8(b).

Experimental results of the combination The number of molecules is measured for three different experimental sequences (see Fig. 5.9(b)). First, Sisyphus cooling without RSC results in about 150 counts/sequence. By applying RSC during trap loading and the subsequent second, almost all molecules entering the trap in the states $J = 5, 6$ are pumped to $J = 4$. As expected from the initial rotational-state distribution, this increases the signal of cold molecules by 49 %. By continuing the optical pumping during the entire motional-cooling sequence the signal increases by 76 %. The above mentioned two loss channels of the Sisyphus scheme specific to CH_3F lead to a slow

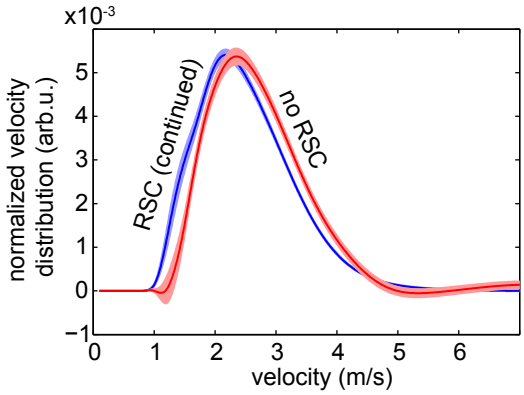

Figure 5.10: Comparison of measured velocity distributions. The velocity distribution (red, no RSC) is the result from the original publication [Zep12] and measured via a time-of-flight technique. The velocity distribution (blue, RSC (continued)) is measured equally. The shaded regions denote the 1σ statistical errors.

population transfer to the $J = 5$ rotational state which is repumped by RSC. This can be experimentally tested by measuring the population distribution of the ensembles (see Fig. 5.9(c)). One finds that the relative number of molecules populating the rotational states $J = 5, 6$ decreases if RSC is added to Sisyphus cooling. The remaining about 10 % population is an effect of the vibrational transition from $J = 5$, needed for RSC, being only applied for 20 ms every 160 ms. Thus the repumping is rather slow and not all the population can be transferred back to $J = 3, 4$. Furthermore, during the time used for state-selective depletion, about three percent of the population in $J = 3, 4$ is transferred to $J = 5, 6$ by blackbody radiation, which leads to an overestimation of the population.

Velocity distribution of combined motional and rotational cooling At the end of this section the influence of RSC on the velocity distribution is studied. Fig. 5.10 shows the normalized velocity distribution measured for the combination of Sisyphus cooling and RSC (blue) and the results obtained in the original publication of Sisyphus cooling (red, "no RSC") [Zep12]. The slight shift of the velocity distribution can be explained by newly optimized RF powers for Sisyphus cooling. The result proves that RSC does not hinder Sisyphus cooling and leads to an equally cold, but according to Fig. 5.9, larger ensemble of cold molecules.

5.3 Optical pumping into individual M sublevels

RSC as demonstrated thus far leaves molecules in a number of M sublevels in the states J=3,4, or, combined with Sisyphus cooling, in the two states $|0; 3, 3, 3\rangle$ and $|0; 4, 3, 4\rangle$ [Zep12]. As a final optical pumping step, the preparation of the motionally cooled molecular sample in a single rotational M substate is presented.

Schemes for single state preparation The population can be prepared in $|0; 4, 3, 4\rangle$ by appending the optical pumping scheme sketched in Fig. 5.11(a) to the experimental

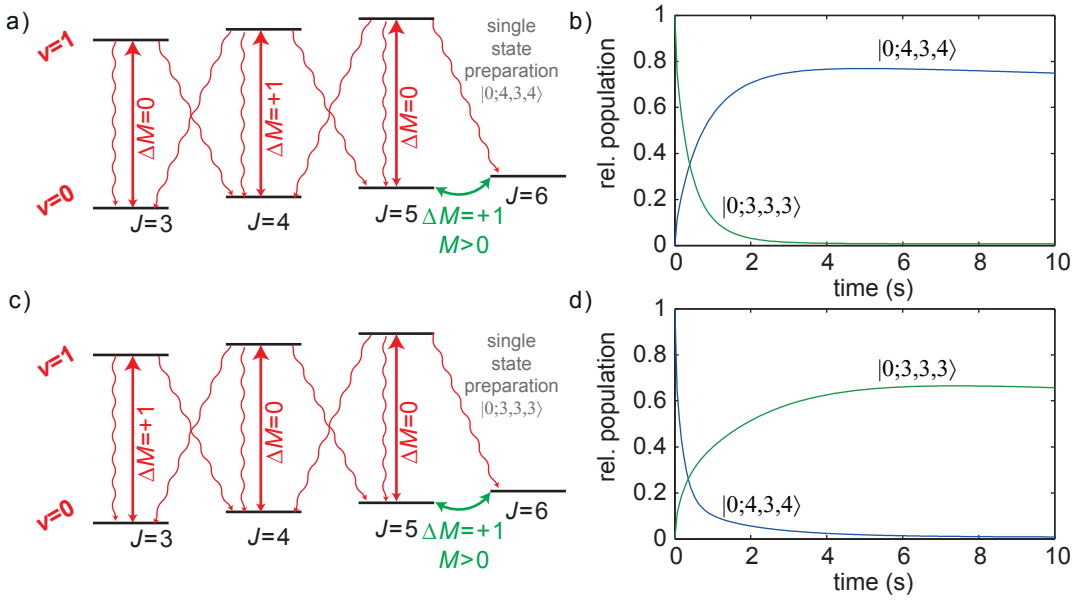

Figure 5.11: Optical pumping to a single M sublevel. Level scheme for single state preparation of the population in $|0;4,3,4\rangle$ (a) and $|0;3,3,3\rangle$ (c). Results of the rate model for the final state $|0;4,3,4\rangle$ (b) and $|0;3,3,3\rangle$ (d).

sequence for combined rotational and motional cooling. Here, the $|0;4,3,4\rangle$ rotational state is the only dark state and for long pumping times all molecules initially populating the $|0;3,3,3\rangle$ state are either transferred to $|0;4,3,4\rangle$ or to an untrapped state.

The efficiency and the time dependence of this process can be simulated with a rate model as described in section 2.4. It includes the driving of the shown transitions, the spontaneous decay from the vibrational excited states and population transfer caused by blackbody radiation. The rate model starts with the assumption that all the population is in the $|0;3,3,3\rangle$ state. After 2 s of optical pumping 71 % of the population is transferred from $|0;3,3,3\rangle$ to the $|0;4,3,4\rangle$ state as shown in Fig. 5.11(b). 13 % of the population ends up in untrapped states and 15 % still populate the other M sublevels within the manifold $J = 3,4,5,6$. The maximal population of 77 % in $|0;4,3,4\rangle$ is reached after about 5 s. On longer timescales the population again decreases due to losses caused by blackbody induced population transfer. The rate model shows that without this effect, the population in $|0;4,3,4\rangle$ would saturate at 85 % with 15 % losses to untrapped states.

A slight modification of the scheme also allows pumping from $|0;4,3,4\rangle$ to $|0;3,3,3\rangle$. Specifically a ΔM=+1 transition from J=3 and a ΔM=0 transition from $J = 4$ is driven (Fig. 5.11(c)) to obtain $|0;3,3,3\rangle$ as the only dark state. The result of the corresponding rate model is shown in Fig. 5.11(d). After 2 s, 51 % of the population is transferred from $|0;4,3,4\rangle$ to $|0;3,3,3\rangle$ with 6 % loss to untrapped states and 40 % still populating the other M sublevels of the $J = 3,4,5,6$ manifold. The maximal population of 67 % in $|0;3,3,3\rangle$ is reached after about 7 s. Without the effect of blackbody radiation the population in $|0;3,3,3\rangle$ would saturate at 77 %. The lower efficiency and the longer timescale compared to pumping into the $|0;4,3,4\rangle$ state is a consequence of less favorable branching ratios.

a)

duration(s)	experimental step
37	Sisyphus cooling+RSC
2	accumulation
2	SSP
2	state-selective depletion
12	unloading and molecule detection

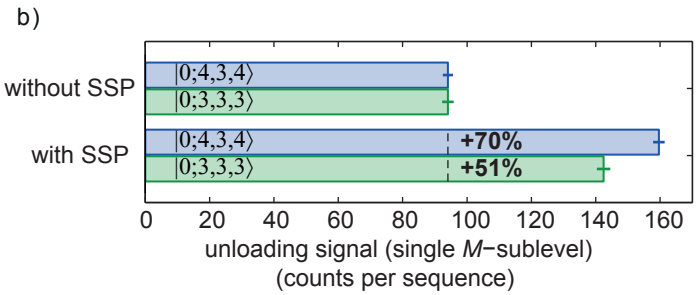

Figure 5.12: Optical pumping to a single M sublevel. (a) Experimental sequence. (b) Experimental results. Horizontal bars denote the 1σ statistical error.

Experimental sequence The experimental sequence is listed in Fig. 5.12(a). To characterize the single-state preparation (SSP) process first the experimental sequence for the combined Sisyphus cooling and RSC as explained above is performed. The population within the $J = 3, 4, 5, 6, |K| = 3$ manifold is thereby prepared in the $|0; 3, 3, 3\rangle$ and $|0; 4, 3, 4\rangle$ substates. To evenly distribute the population among the two M substates, accumulation (see appendix A) is applied for 2 s. Afterwards, either SSP according to the schemes shown in Fig. 5.11 is applied or nothing is done as a reference. 2 s for SSP were chosen, although according to the results of the rate model both schemes give a higher population of the single M sublevel for a longer pumping time. However, a longer pumping time also requires a longer trapping time and the trap losses quickly overcome the few percent that could be gained. State selective depletion during the last two seconds of storage allows for measuring the population within the single M substates (see section 4.2.3).

Experimental results Figure 5.12(b) shows the results of the measurement. By applying SSP according to the scheme in Fig. 5.11(a), the population in $|0; 4, 3, 4\rangle$ increased by 70 %. This number also yields the optical-pumping efficiency, as the populations in $|0; 3, 3, 3\rangle$ and $|0; 4, 3, 4\rangle$ were initially equal. By applying SSP according to the scheme in Fig. 5.11(c), the population in $|0; 3, 3, 3\rangle$ increased by 51 %. In both cases the outcome of the experiment fits nicely with the result of the rate model in Fig. 5.11(b) and (d). The presented experiments show that one can significantly increase the population in a highest M sublevel of choice. It can be estimated [Zep12] that finally about 10^6 cooled molecules populate this state.

5.4 A cold and pure state ensemble

All previous measurements examined optical pumping in the context of increasing the absolute number of molecules in a particular state or set of states. In this section, the state purity of the molecular ensemble is studied.

An internally pure-state ensemble can be produced by two techniques, transferring all the population to a single state or some sort of filter process. Both processes are used in this thesis as Sisyphus cooling filters the internal state (see section 5.2) whereas RSC and SSP decrease the rotational state distribution and thus also increase the phase-space density. As discussed in the previous section, this SSP process is not fully

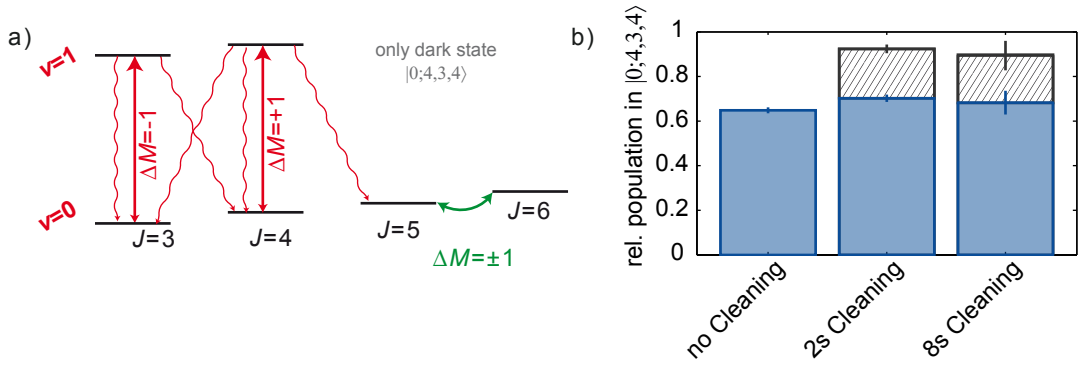

Figure 5.13: Enhancing the state purity by depleting molecules outside the target state (cleaning). (a) Scheme for cleaning. All molecules in the $J = 3, 4, 5, 6; |K| = 3$ manifold but the ones populating $|0; 4, 3, 4\rangle$ are depleted. (b) Measured relative population of the $|0; 4, 3, 4\rangle$ state (blue filled bar) or $J = 3, 4$ states (shaded bars) compared to the total trap signal. The basic sequence is the same as in Fig. 5.12(a) but with cleaning applied for two or eight seconds before the state-selective depletion where applicable. Vertical bars denote the 1σ statistical error.

saturated within the employed 2 s of optical pumping. The purity of the ensemble can be further enhanced by depleting all molecules in the $J = 3, 4, 5, 6; |K| = 3$ manifold but the ones populating $|0; 4, 3, 4\rangle$. This process is in the following referred to as cleaning.

The scheme for this cleaning is shown in Fig. 5.13(a). Driving a $\Delta M = -1$ vibrational transition from $J = 3$ depletes all molecules in this state. A $\Delta M = +1$ transition from $J = 4$ additionally empties the lower lying M substates in $J = 4$. Simultaneously, MWD in $J = 5, 6$ is applied to deplete all the population remaining in these states.

Figure 5.13(b) shows the resulting population in the single M substate $|0; 4, 3, 4\rangle$ compared to the total trap signal (blue filled bars). Without cleaning, at least 65 % of the molecules populate the $|0; 4, 3, 4\rangle$ substate. With 2 s of cleaning the relative population increases to 70 % and even a longer cleaning process does not increase the measured purity further for two reasons. First, the method for determining the number of molecules populating the single M sublevel $|0; 4, 3, 4\rangle$ underestimates the population by roughly 20 % (see section 4.2.3). However, a rate model for the process of cleaning suggests, that the other M substates in $J = 3, 4$ are populated by less than one percent after two seconds. If now the state $|0; 4, 3, 4\rangle$ is in good approximation the only one which is populated within the $J = 3, 4$ manifold, one can measure the total population with the $J = 3, 4$ states using full IRD which does not underestimate the population (see chapter 4). Doing so, indeed a higher relative population of 92 % (shaded bars) is measured which reveals that way more than 70 % of the molecules populate the $|0; 4, 3, 4\rangle$ state. Second, the achieved purity in the experimental system is mainly limited by blackbody induced population transfer which acts also during SSP, cleaning and state-selective depletion. During two seconds, already 10 % of the population is transferred from the $|0; 4, 3, 4\rangle$ state to other states. However, this limitation is of technical nature and can be overcome by cooling down the electric trap or choosing a molecule species not suffering from significant blackbody-radiation losses.

5.5 Population of a single M sublevel in differently prepared ensembles

In the last section before the outlook the population of the $|0;4,3,4\rangle$ state is studied for various ensembles. This analysis compares and contrasts all effects discussed in this chapter. In particular, we will see that the relative population of the $|0;4,3,4\rangle$ state is increased by one order of magnitude. The different preparation sequences are detailed in the following. Finally, the effect of the preparation on the absolute number of trapped molecules and the relative population in the state $|0;4,3,4\rangle$ is discussed.

The experimental sequences All sequences have a loading time of 16 s and an unloading and detection time of 12 s in common. In addition, the state-selective depletion for detecting the population of the $|0;4,3,4\rangle$ state is always applied for two seconds [1].

- Reference: An ensemble of non-manipulated molecules is studied. After loading and a subsequent second of storage the depletion and detection is appended. The total storage time is 5 s and the mean kinetic energy is about ≈ 390 mK) [Zep12].
- RSC: RSC as described in section 5.1 is implemented during the loading and the subsequent four seconds to transfer all the population from $J = 5,6;|K| = 3$ to $J = 4;|K| = 3$. The total storage time is 8 s.
- Sisyphus cooling: The used sequence is the same as in the original publication [Zep12], which is also described above in section 5.2. The total storage time is 25 s.
- RSC + Sisyphus cooling: To prepare the ensemble, a the sequence for combining RSC and Sisyphus cooling is used (see section 5.2). The total storage time is 25 s and the mean kinetic energy is about ≈ 30 mK.
- SSP: Two seconds of single state preparation (see section 5.3) are appended to the sequence of RSC + Sisyphus cooling. The target state of the optical pumping scheme is the $|0;4,3,4\rangle$ state. The total storage time is 27 s.
- SSP + cleaning: Two seconds of cleaning (see section 5.4) are added to the previous sequence. The total storage time is 29 s.

Experimental results Figure 5.14 shows the results of the various measurements. The non-manipulated reference ensemble consists of molecules populating many rotational states (compare Fig. 2.3) and yields as expected the highest total trap signal but the lowest population in the single M sublevel $|0;4,3,4\rangle$. Applying RSC leads to a reduction of trapped molecules as the storage time is increased by four seconds. In addition, the relative number of molecules populating the $|0;4,3,4\rangle$-substate increases as RSC transfers the population from $J = 5,6;|K| = 3$ to $J = 4;|K| = 3$.

In addition, Fig. 5.14 shows that Sisyphus cooling prepares a large fraction of the molecules in the $|0;4,3,4\rangle$ state. As both states, $|0;4,3,4\rangle$ and $|0;3,3,3\rangle$, are coupled

[1] After the state-selective depletion additional two seconds of storage are present in the experimental sequence which were used for cross checking the results with 4 s of state-selective depletion

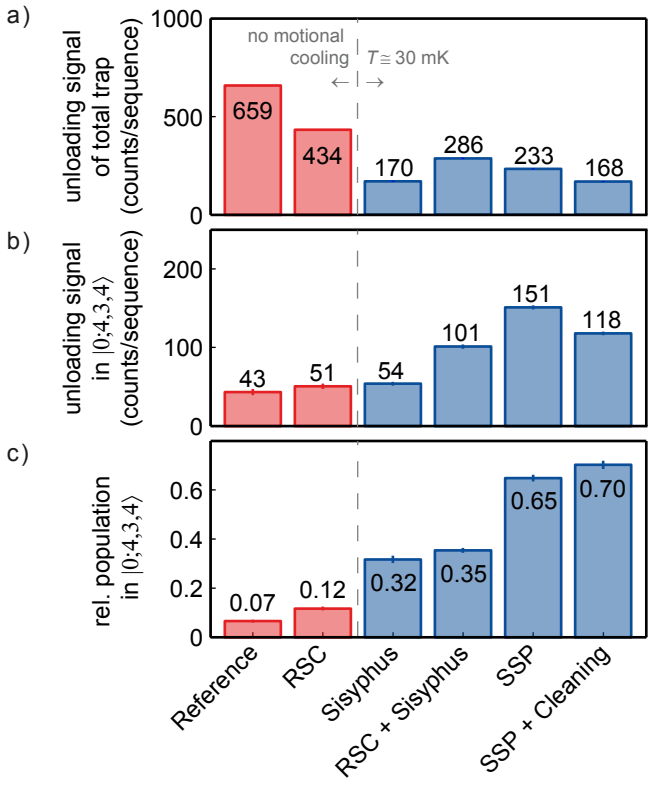

Figure 5.14: Analysis of differently prepared ensembles. (a) Total trap signal for variations of the experimental sequence as described in the main text. (b) Population of the $|0;4,3,4\rangle$. (c) Percentage of molecules populating the state $|0;4,3,4\rangle$. The vertical solid lines represent the 1σ statistical error (which is smaller than the edge of the bar if not visible). Note that the values for uncooled ensembles overestimate the population relative to the other sequences due to an imperfect state detection (see chapter 4).

with MW radiation, an equal distribution of the population among these two states is expected. Thus, most of the molecules populating states other than those which are addressed by Sisyphus cooling ($J = 3,4; |K| = 3$) are lost. This loss manifests itself as a drop of total trap signal. The effect of adding RSC to Sisyphus cooling is twofold: First, the total number of trapped molecules increases and second the fraction of molecules in the $|0;4,3,4\rangle$ state rises slightly as loss channels of Sisyphus cooling which transfer population from $J = 3,4$ to $J = 5,6$ are closed. The addition of the scheme for pumping population from $|0;3,3,3\rangle$ to $|0;4,3,4\rangle$ increases the population of the $|0;4,3,4\rangle$ state to 65 % and also yields the highest number of molecules in this state. The relative occupation is boosted a bit further by removing all molecules still populating states other than the $|0;4,3,4\rangle$ state. In total, the population of a single M sublevel is augmented from initially ∼7 % to at least 70 % while the molecular ensemble is motionally cooled by more than an order of magnitude. As discussed in the previous section, it is expected that even ∼90% of the molecules populate this M sublevel.

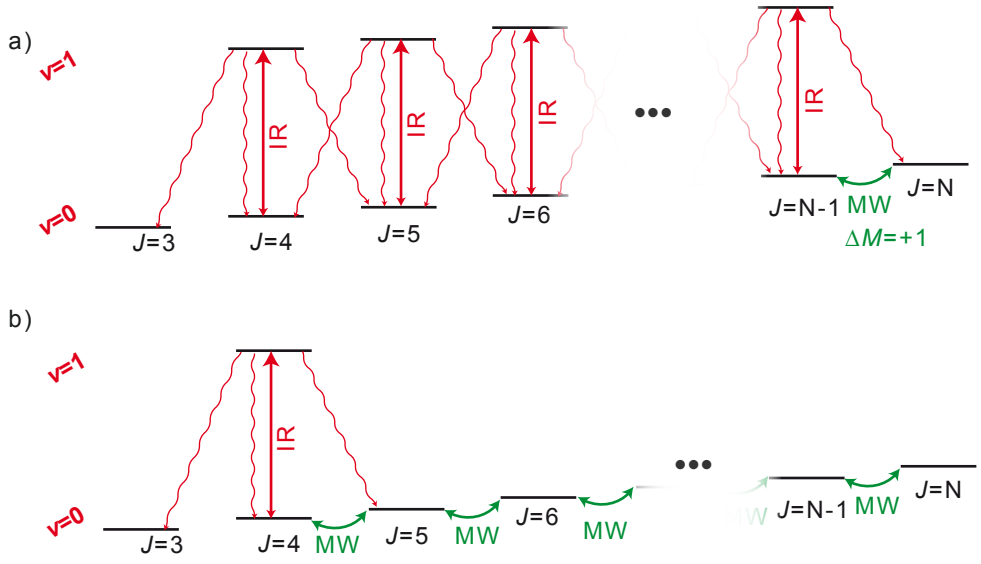

Figure 5.15: RSC extended to incorporate more states. (a) A possible extension involving the driving of several vibrational transitions. The MW coupling could also be replaced with a second laser, driving a $\Delta J = -1$ transition from the rotational state with $J = N$. (b) A possible extension involving only one vibrational transition but many rotational ones. Combinations of both schemes are of course possible.

5.6 Outlook

This chapter presented results of the first rotational-state cooling via optical pumping for trapped polyatomic molecules. Combined with optoelectrical Sisyphus cooling this has led to a concurrent cooling of the internal and external degrees of freedom. A subsequent additional pumping scheme allows finally to prepare the ensemble in a single M sublevel of choice. Thus, starting from a room temperature gas bottle, a motionally cold ($\approx 30\,\mathrm{mK}$) and almost pure state ensemble of polyatomic molecules was obtained. In the following, extensions to other states and possible improvements of the optical pumping schemes are discussed.

5.6.1 RSC extended to incorporate more states

Although extending RSC to incorporate higher rotational states is of little gain for the relatively light molecule CH_3F, it is still of interest to discuss suitable approaches for implementing RSC to other molecules species. Figure 5.15 depicts two potential schemes, which are described below, where also combinations of them are possible. Which one is better suited depends on the individual molecular properties, e.g. the spectral separation of the vibrational and/or rotational transitions as discussed for CH_3F in section 3.5.

The scheme in Fig. 5.15(a) shows an implementation which relies on the driving of several vibrational transition. MW coupling is only needed for the two highest rotational states. This MW coupling, however, could also be replaced with a second laser driving a $\Delta J = -1$ vibrational transition. To assess the value of this extension,

several aspects have to be discussed. First, driving the many vibrational transitions without huge financial and experimental effort is possible with the fast ramp and relock system as soon as the dark time needed for ramping the frequency can be decreased and as long as the transition frequencies lie within the tuning range of the OPO of currently about 100 GHz. The Q-Branch $\Delta J = 0$ transitions are in general close lying transitions and e.g. for the molecule CH_3F it is possible to drive all $\Delta J = 0$ transitions from $J = 3$ to $J = 11$ ($|K| = 3$) with a single laser. Other molecules have even more closely lying $\Delta J = 0$ transitions, e.g. formaldehyde with about 600 MHz separation of the frequencies, which allows for even larger sets of states. Also a larger tuning range of the OPO system can increase the number of accessible rotational states. Maybe also quantum cascade lasers which are rapidly developing could be an alternative in the future as they are expected to offer the possibilities for lasing on several freely chosen frequencies simultaneously. They are likely to be much cheaper than OPO systems and thus buying several might also be an option.

As a second aspect, losses to untrapped states have to be considered. The rate model for RSC shown above suggested about 10 % losses(see Fig. 5.2). These losses can be minimized by not only driving $\Delta M = 0$ vibrational transitions but by alternating the driving of $\Delta M = 0$ and $\Delta M = +1$ transitions. This, however, increases the duration of the optical pumping process as the highest M substates are not addressed while driving the $\Delta M = +1$ transitions. It thus depends on the trap lifetime and on the spontaneous decay rate of the vibrational excited state whether this option is better suited.

The scheme in Fig. 5.15(b) shows an alternative implementation which needs only the driving of one vibrational transition but several rotational ones. An advantage is that for the MW coupling of higher J states, several rotational transitions could be addressed with a single broad-band amplifier multiplier chain. However, a good spectral resolution is needed to avoid coupling of the rotational states to untrapped states. Which of the two schemes in Fig. 5.15 is the best suited one, thus depends on the molecular parameters, the spectral resolution, and the radiation sources available in the laboratory.

5.6.2 Single state preparation

There are quite a few possibilities to improve the efficiency of pumping the population to a single M substate. In the following some of these schemes are discussed in a bit more detail: The population transfer from $|0; 4, 3, 4\rangle$ to $|0; 3, 3, 3\rangle$ can for example be advanced by coupling the rotational states $J = 4$ and $J = 5$ with MW as shown in Fig. 5.16(a). With this scheme, the number of involved states decreases compared to the above demonstrated approach and thus losses decrease and the process is faster. However, the needed radiation sources were not available in the experimental setup. The efficiency can even be further increased by coupling the rotational states $J = 3$ and $J = 4$ in the vibrational excited state (Fig. 5.16(b)) which increases the branching ratio of the spontaneous decay to $J = 3$. It is also possible to transfer the population without applying any MW radiation but instead driving a $\Delta J = -1$ vibrational transition from $J = 4$(Fig. 5.16(c)). Unfortunately, this transition is red detuned by about 200 GHz and thus not within the tuning range of our current OPO system.

Another scheme to pump population from $|0; 3, 3, 3\rangle$ to $|0; 4, 3, 4\rangle$ employs selective driving of the MW transitions (Fig. 5.16(d)). Compared to the demonstrated ap-

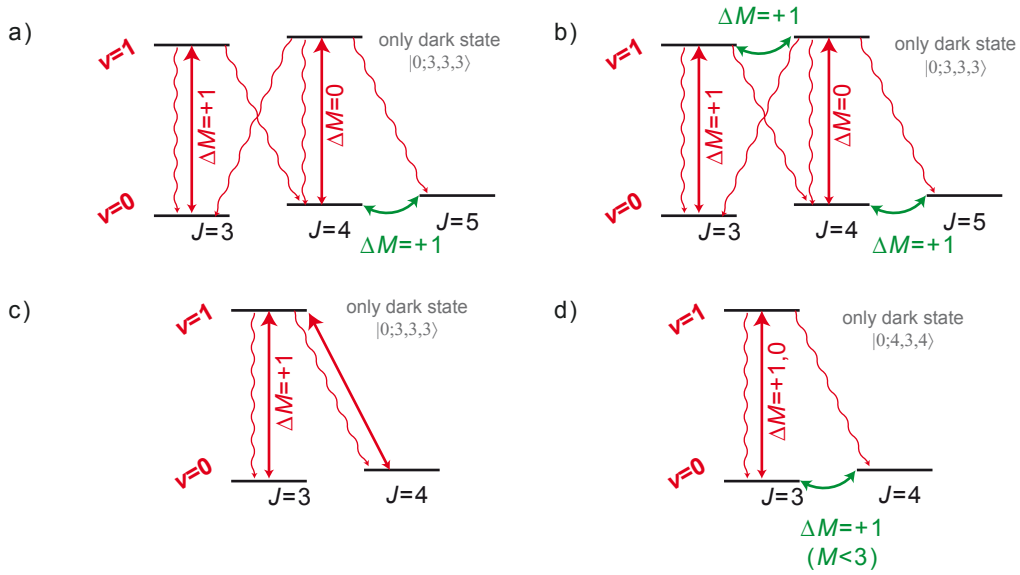

Figure 5.16: Schemes for advancing SSP. (a) The efficiency for pumping to the $|0;3;3;3\rangle$ substate can be increased by coupling the rotational states with $J = 4$ and $J = 5$. (b) In addition to (a) coupling the rotational states $J = 3, 4$ in the vibrational excited state while the laser is driven on $J = 4$ enhances the spontaneous decay to the $|0;3;3;3\rangle$ substate. (c) Accumulation in the $|0;3;3;3\rangle$ substate is possible without driving rotational transitions but instead driving a $\Delta J = -1$ vibrational transition on $J = 4$. (d) A scheme for efficient population transfer to $|0;3;3;3\rangle$ which relies on a sufficient spectral resolution for driving the rotational transitions selectively.

proach again much less internal states are involved. However, to use this scheme a very good spectral resolution is needed as the rotational transitions $|0;3,3,M = 0,1,2\rangle \leftrightarrow |0;4,3,M+1\rangle$ have to be driven without driving the $|0;3,3,3\rangle \leftrightarrow |0;4,3,4\rangle$ rotational transition. By additionally alternating the driving of the $\Delta J = 0$ and $\Delta J = +1$ vibrational transitions from $J = 3$, population is transferred to $|0;4,3,4\rangle$, which is the only dark state of this scheme. With this scheme, it should also be possible to prepare population in lower M substates, for example the $|0;4,3,3\rangle$. Here, the rotational transitions $|0;3,3,M = 0,1,3\rangle \leftrightarrow |0;4,3,M+1\rangle$ have to be driven without driving the rotational transition $|0;3,3,2\rangle \leftrightarrow |0;4,3,3\rangle$. Thus $|0;4,3,3\rangle$ is the only dark state.

Chapter 6

Outlook

In summary, a comprehensive approach to control the rotational states of trapped polyatomic molecules was presented in this thesis. It includes the development of a method to measure the spectral resolution inside the trap, the development of a rotational-state detection scheme for trapped polyatomic molecules and the first optical pumping for trapped polyatomic molecules demonstrating rotational-state cooling and the preparation of the population in a single M sublevel. The starting point of these results was the development of the motional cooling in previous theses [Zep13, Eng13]. Merging internal and external cooling yields a unified technique that allows one to prepare an ensemble of about 10^6 CH_3F molecules at about 30 mK in a single M sublevel of choice with a state purity of over 70%. Finally, the rotational-state control studied in this thesis represents a crucial step towards the cooling of polyatomic molecules to sub-mK temperatures, which was just realized in our lab [Pre15].

Further experiments with the current setup Beside the quest for even lower temperatures, the current temperatures should allow for the investigation of cold or ultracold collisions. Because of the homogeneous electric field present in a large part of the trapping volume, even the electric-field dependence of the collisions might be investigated. The collision properties of polyatomic molecules in the (ultra)low temperature regime are mostly unknown, but it is known that electric fields can dramatically change the collision properties. Reference [Avd02] for example shows that weak-field seeking OH molecules in small electric fields are stabilized against Stark relaxation which might provides prospects for evaporative cooling of electrically trapped molecules.

The possibility to detect the population in rotational states or to prepare the ensemble in a chosen internal state in combination with motional cooling also enables spectroscopy on trapped molecules with good resolution. As an example, the linewidth of the MW transition measured in this thesis has a FWHM of about 15 MHz. Cooling molecules to few tens of μK would allow to reduce the trapping fields by a factor of one thousand resulting in a FWHM of tens of kHz. By measuring the spectrum of a transition with no first-order Stark shift, the linewidth can be further reduced. In addition, the long storage time of the molecule this might open new possibilities for spectroscopy on very weak transitions.

Suitable molecule species The presented manipulation schemes only use generic properties of symmetric top molecules and it can thus be expected that similar schemes can be applied to other symmetric top molecules. However, to experimentally employ these molecules, further considerations have to be made, e.g, what are the properties for trapping and how does the trapping time compare to the time needed for the ma-

nipulation. Finally, a source that provides molecules below 1 K with a manageable internal-state distribution is needed.

The trapping properties of the molecules depend on the dipole moment and the trapping configuration. While the dipole moment is a molecular parameter, the trapping potential is solely a technical aspect. Thus, improving the trapping potential by closing electric field zeros and creating higher trap boundaries, should enable the use of molecules with a lower dipole moment than the current 1.85 D of CH_3F. The time needed for the optical pumping depends on the spontaneous decay rate of the vibrational excited state. This timescale must be compared to the trapping time and a better trap enables the use of molecule species with a slower spontaneous decay rate. An overview of symmetric top molecules with relatively large dipole moments and fast spontaneous decay rate is given in the original proposal of Sisyphus cooling of molecules [Zep09]. It includes the molecules CF_3H, CH_3CCH, CF_3CCH, $N(CH_3)_3$, CF_3Cl, CF_3Br, CF_3I, and BH_3CO. In addition, also slightly asymmetric molecules as H_2CO are suited because a small electric field already suffices to obtain a level structure similar to the one of symmetric top molecules [Pre15].

A new class of molecule species possibly opens up with the finding of polyatomic molecules possessing highly diagonal Franck-Condon factors [Isa15]. For these special molecules it might thus be possible to implement the manipulation schemes using electronic transitions, which would tremendously speed up Sisyphus and rotational-state cooling due to the orders of magnitude larger spontaneous decay rate. One example might be the symmetric top molecule $CaCH_3$ which has a large dipole moment of about two Debye.

Reaching quantum degeneracy The long term goal of the experimental approach presented in this thesis is to reach quantum degeneracy with an ensemble of polyatomic molecules. The most promising techniques to achieve this goal are evaporative or sympathetic cooling. Therefore trapping of the molecules in an internal state, that is stable against inelastic collisions is a prerequisite which often means that the molecules have to be trapped in the rotational ground state. In the following, some steps towards this goal are discussed and possible problems and open questions are unveiled.

The first discussion addresses the population transfer to the ground state. It is indeed not obvious whether pumping into the absolute ground state is possible as it involves driving a $\Delta K = 3$ transition. This transition is forbidden but can occur in polar symmetric top molecules of the point group C_{3v} due to a centrifugal distortion mechanism. This mechanism was already described by Watson in 1971 [Wat71]. The strength of these transitions depends on the individual molecular parameters and thus must be investigated individually [Oka76]. $\Delta K = 3$ transitions were experimentally found in several molecules as for example CH_3D [Ols72] or NH_3 [Lau76] indicating that suitable transitions can be found. In particular, the long storage times allow the driving of very weak transitions.

Trapping molecules at mK temperatures in the rotational ground state is e.g. possible with optical or microwave traps [DeM04]. Whether a MW or an optical trap is preferable depends on several aspects but the key issue is to achieve an efficient transfer of the molecules. Optical dipole traps are widely used to trap ultracold atoms [Gri00]. The trapping volumes are typically small, which is an advantage for evaporative or sympathetic cooling as high densities are needed. However, it is difficult to efficiently

load particles with initially low densities into dipole traps, and therfore a compression of the ensemble is be needed. The problem that arises is the high density of rotational excited molecules which could lead to rapid trap losses due to inelastic collisions.

MW traps offer a larger trapping volume and could for example be loaded via a fountain [Bet08, Tar13]. The MW fields can be switched on when the molecules launched from the fountain pass by, leading to pulsed loading of the MW trap. Continuous loading of the trap can be achieved with a spontaneous decay event which reduces the energy via a Sisyphus process and transfers the population into a trappable state. This process was demonstrated for Cr atoms [Fal11, Vol13] and for loading of CaF [Lu14] or NH [Rie11] molecules into a magnetic trap.

The success of evaporative or sympathetic cooling depends in general on the ratio of elastic to inelastic collisions. Evaporative cooling of $^1\Sigma$-type molecules trapped inside a MW trap has been theoretically studied in [Avd09]. They find that MW traps can provide successful evaporative cooling. The elastic and inelastic scattering rates of electrically trapped CH_3Cl molecules in the $|0;1,1,1\rangle$ state was theoretically investigated by M. Kajita [Kaj04]. In particular, the ratio of the two rates was calculated for bosonic and fermionic symmetric top molecules as a function of temperature, showing promising results for fermions. However, for bosons the ratio of inelastic to elastic collisions even increases for lower temperatures. A study of collisions of ultracold rubidium atoms and cold ammonia molecules unfortunately showed that the presence of electric fields speeds up inelastic processes [Par11], which might be a general problem for sympathetic cooling of symmetric top molecules with alkali atoms. Promising, however, is the fact that collisions between CH_3X (X=F,Cl,Br,I) and alkali atoms are in most cases non-reactive at low temperatures as was calculated in [Lut14].

In conclusion, there are still many open questions on the way to a quantum degenerate gas of polyatomic molecules. However, the overall concept of Sisyphus cooling and rotational-state manipulation via optical pumping now brings the experimental study of these questions into reach.

Appendix A

Summary of experimental steps and sequences

This appendix gives an overview of the experimental steps and sequences employed to obtain the results discussed in this thesis.

Trap loading For almost all data presented in this thesis, the experimental parameters are as follows: The voltage difference at the first quadrupole guide is $\Delta V_{1.Guide} = 3\,\mathrm{kV}$ and the voltages applied at the trap are $V_\mu = \pm 1800\,\mathrm{V}$,$V_{Offset} = \pm 90\,\mathrm{V}$ and $V_{Ring} = 5400\,\mathrm{V}$ (compare section 3.1). The unloading quadrupole guide is set to $\Delta V_{3.Guide} = 20\,\mathrm{V}$ to allow some molecules to reach the QMS during the loading phase for a monitoring of the whole sequence. If no other manipulation is applied, the molecular ensemble loaded with these parameters is expected to closely match the rotational-state distribution calculated in section 2.1 (compare also section 4.2.4 for experimental evidence). In addition, this ensemble has a mean kinetic energy of $E_{kin} \approx 390\,\mathrm{mK} \times \left(\frac{3}{2}k_B\right)$ [Zep12]. The only measurement, with different settings for loading ($V_{Offset} = \pm 450\,\mathrm{V}$ and $V_{Ring} = 4200\,\mathrm{V}$) is the MW spectrum of the $J = 5 \leftrightarrow J = 6$ rotational transitions in Fig. 5.4.

Storage During storage, a negative voltage and no voltage difference is applied at both quadrupole guides therewith closing the trap to both sides. The voltages applied during storage is in most cases $V_\mu = \pm 1800\,\mathrm{V}$,$V_{Offset} = \pm 90\,\mathrm{V}$ and $V_{Ring} = 5400\,\mathrm{V}$ (compare section 3.1). Only few measurements were performed with a higher offset voltage of $V_{Offset} = \pm 450\,\mathrm{V}$, namely the ones shown in Fig. 3.5(b) and in Fig. 5.4.

Sisyphus cooling to 30 mK Sisyphus cooling is discussed in section 5.2.1. Sisyphus cooling to 30 mK includes loading of the molecules and storage of the molecules while all involved transition are driven according to the scheme in Fig. 5.5. Sisyphus cooling is always performed with the following settings for loading and storage: $\Delta V_{1.Guide} = 3\,\mathrm{kV}$ for loading and the voltages applied at the trap are $V_\mu = \pm 1800\,\mathrm{V}$,$V_{Offset} = \pm 90\,\mathrm{V}$ and $V_{Ring} = 5400\,\mathrm{V}$ (compare section 3.1). The molecular ensemble, that is produced, is almost equally distributed between the $|0;3,3,3\rangle$ and $|0;4,3,4\rangle$ with some residual population in the $J = 5, 6, |K| = 3$ states. In particular the population in states with all other $J, |K|$ quantum numbers is removed from the trapped ensemble. The final ensemble has a mean kinetic energy of $E_{kin} \approx 30\,\mathrm{mK} \times \left(\frac{3}{2}k_B\right)$ [Zep12].

Sisyphus cooling to 150 mK Sisyphus cooling to 150 mK starts equally as Sisyphus cooling to 30 mK but is stopped earlier resulting in a hotter ensemble, with however

larger molecule numbers due to the shorter storage time. The population within the $J = 3, 4, |K| = 3$ states is almost equally distributed between the $|0; 3, 3, 3\rangle$ and $|0; 4, 3, 4\rangle$ with the population in all other $J, |K|$ states being reduced but not yet eliminated. The final ensemble has a mean kinetic energy of $E_{kin} \approx 150\,\mathrm{mK} \times \left(\frac{3}{2}k_B\right)$ [Zep12].

RSC Rotational-state cooling is discussed in section 5.1. Population of the $J = 5, 6|K| = 3$ states is transferred to $J = 4, |K| = 3$ via optical pumping with minimal control over the final M-substate.

Sisyphus cooling + RSC The combination of Sisyphus cooling and RSC is discussed in section 5.2.2. The produced ensemble is larger than an ensemble produced by only Sisyphus cooling in terms of molecule number and has almost no contribution of molecules in the $J = 5, 6, |K| = 3$ rotational states. Apart from that the achieved temperatures and settings for Sisyphus cooling apply.

Accumulation Accumulation denotes here an optical pumping technique, that transfers all molecules within the $J = 3, 4, |K| = 3$ state to the highest M substates $|0; 3, 3, 3\rangle$ and $|0; 4, 3, 4\rangle$ with equal population. It is implemented by driving a $\Delta J = 0, \Delta M = +1$ vibrational transition from $J = 3, |K| = 3$ together with the rotational transitions $|0; 3, 3, M\rangle \leftrightarrow |0; 4, 3, M + 1\rangle$ $(M > 0)$.

SSP Single-state preparation is discussed in section 5.3. Population of the $|0; 3, 3, 3\rangle$ state is transferred to $|0; 4, 3, 4\rangle$ or vice versa via optical pumping.

Cleaning Cleaning the state-purity of the ensemble is discussed in section 5.4. This is a depletion method, that removes all the population within the $J = 3, 4, 5, 6, |K| = 3$ states except the M substate of interest, e.g. the state $|0; 4, 3, 4\rangle$.

State-selective depletion State-selective depletion is discussed in chapter 4. State-selective depletion implies that the whole sequence was performed twice. In the first run, a state-selective depletion method (e.g. MWD or IRD) is applied to a specific set of rotational states. In the second run, no depletion at all is applied and the difference of the signals of both measurements yields the signal of the population in chosen specific set of states. Note that in the second run also state-selective depletion to a subset of this specific set of rotational states can applied. This gives a signal of population that is within this specific set of rotational states but not within the chosen subset.

Unloading and molecule detection Molecules are unloaded by switching the voltages of the exit guide to a guiding configuration and are afterwards detected with a QMS. The unloading voltage applied to the trap and the exit guide is adjusted to the temperature of the molecular ensemble (see discussion in section 4.2.1): The settings for unloading an ensemble motionally cooled to 30 mK is, independent of further manipulation, always $\Delta V_{3.Guide} = 300\,\mathrm{V}$ and the voltages applied at the trap are $V_\mu = \pm 300\,\mathrm{V}$,$V_{Offset} = \pm 15\,\mathrm{V}$ and $V_{Ring} = 300\,\mathrm{V}$. The settings for unloading an ensemble motionally cooled to 150 mK is, independent of further manipulation, always $\Delta V_{3.Guide} = 1400\,\mathrm{V}$ and the voltages applied at the trap are $V_\mu = \pm 1400\,\mathrm{V}$,$V_{Offset} =$

$\pm 70\,\mathrm{V}$ and $V_{Ring} = 1400\,\mathrm{V}$. The settings for unloading motionally uncooled ensemble is, independent of further manipulation, always $\Delta V_{3.Guide} = 3\,\mathrm{kV}$ and the voltages applied at the trap are $V_{\mu} = \pm 1800\,\mathrm{V}$,$V_{Offset} = \pm 90\,\mathrm{V}$ and $V_{Ring} = 3600\,\mathrm{V}$(in chapter 4),$V_{Ring} = 4200\,\mathrm{V}$(in chapter 5). The only measurement, with one different settings for unloading ($V_{Offset} = \pm 450\,\mathrm{V}$) is the MW spectrum of the $J = 5 \leftrightarrow J = 6$ rotational transitions in Fig. 5.4.

Bibliography

[And06] A. André, D. DeMille, J. M. Doyle, M. D. Lukin, S. E. Maxwell, P. Rabl, R. J. Schoelkopf, and P. Zoller. A coherent all-electrical interface between polar molecules and mesoscopic superconducting resonators. *Nat. Phys.* **2**, 636 (2006).

[Ant78] V. S. Antonov, I. N. Knyazev, V. S. Letokhov, V. M. Matiuk, V. G. Movshev, and V. K. Potapov. Stepwise laser photoionization of molecules in a mass spectrometer: a new method for probing and detection of polyatomic molecules. *Opt. Lett.* **3**, 37 (1978).

[Avd02] A. V. Avdeenkov and J. L. Bohn. Collisional dynamics of ultracold OH molecules in an electrostatic field. *Phys. Rev. A* **66**, 52718 (2002).

[Avd09] A. V. Avdeenkov. Collisions of bosonic ultracold polar molecules in microwave traps. *New J. Phys.* **11**, 055016 (2009).

[Bag13] J. Bagdonaite, P. Jansen, C. Henkel, H. L. Bethlem, K. M. Menten, and W. Ubachs. A Stringent Limit on a Drifting Proton-to-Electron Mass Ratio from Alcohol in the Early Universe. *Science* **339**, 46 (2013).

[Bar12] M. A. Baranov, M. Dalmonte, G. Pupillo, and P. Zoller, Condensed matter theory of dipolar quantum gases *Chem. Rev.* **112**, 5012 (2012).

[Bar14] J. Baron, W. C. Campbell, D. DeMille, J. M. Doyle, G. Gabrielse, Y. V. Gurevich, P. W. Hess, N. R. Hutzler, E. Kirilov, I. Kozyryev, B. R. O'Leary, C. D. Panda, M. F. Parsons, E. S. Petrik, B. Spaun, A. C. Vutha, and A. D. West. Order of magnitude smaller limit on the electric dipole moment of the electron. *Science* **343**, 269 (2014).

[Bel09a] M. T. Bell, A. D. Gingell, J. M. Oldham, T. P. Softley, and S. Willitsch. Ion-molecule chemistry at very low temperatures: cold chemical reactions between Coulomb-crystallized ions and velocity-selected neutral molecules. *Faraday Discuss.* **142**, 73 (2009).

[Bel09b] M. T. Bell and T. P. Softley. Ultracold molecules and ultracold chemistry. *Mol. Phys.* **107**, 99 (2009).

[Ber10] B. Bertsche and A. Osterwalder, State-selective detection of velocity-filtered ND_3 molecules *Phys. Rev. A.* **82**, 033418 (2010).

[Ber11] B. Bertsche and A. Osterwalder. Dynamics of individual rotational states in an electrostatic guide for neutral molecules. *Phys. Chem. Chem. Phys.* **13**, 18954 (2011).

[Bet99] H. Bethlem, G. Berden, and G. Meijer. Decelerating Neutral Dipolar Molecules. *Phys. Rev. Lett.* **83**, 1558 (1999).

[Bet08] H. L. Bethlem, M. Kajita, B. Sartakov, G. Meijer, and W. Ubachs. Prospects for precision measurements on ammonia molecules in a fountain. *Eur. Phys. J. Spec. Top.* **163**, 55 (2008).

[Blo08] I. Bloch, J. Dalibard, and W. Zwerger. Many-body physics with ultracold gases. *Rev. Mod. Phys.* **80**, 885 (2008).

[Blo11] J. H. Blokland, J. Riedel, S. Putzke, B. G. Sartakov, G. C. Groenenboom, and G. Meijer. Producing translationally cold, ground-state CO molecules. *J. Chem. Phys.* **135**(11) (2011).

[Boh09] J. L. Bohn, M. Cavagnero, and C. Ticknor. Quasi-universal dipolar scattering in cold and ultracold gases. *New J. Phys.* **11**, 055039 (2009).

[Bro52] J. Brossel and F. Bitter. A New "Double Resonance" Method for Investigating Atomic Energy Levels. Application to Hg $^3P_1$. *Phys. Rev.* **86**, 308 (1952).

[Bul91] J. Bulthuis, J. B. Milan, M. H. M. Janssen, and S. Stolte. Electric field dependence of reactivity of state-selected and oriented methylhalides. *J. Chem. Phys.* **94**, 7181 (1991).

[Bun06] P. R. Bunker and P. Jensen. Molecular Symmetry and Spectroscopy. NRC Research Press, Ottawa (2006), ISBN 0-660-1962-X.

[Car09a] L. Carr and J. Ye. Focus on Cold and Ultracold Molecules. *New J. Phys.* **11**, 055009 (2009).

[Car09b] L. D. Carr, D. DeMille, R. V. Krems, and J. Ye. Cold and ultracold molecules: Science, technology and applications. *New J. Phys.* **11**, 055049 (2009).

[Car15] L. D. Carr, D. DeMille, R. V. Krems, and J. Ye. Focus on New Frontiers of Cold Molecules Research. *New J. Phys.* (2015).

[Che14] S. Chervenkov, X. Wu, J. Bayerl, A. Rohlfes, T. Gantner, M. Zeppenfeld, and G. Rempe. Continuous centrifuge decelerator for polar molecules. *Phys. Rev. Lett.* **112**, 013001 (2014).

[Chi09] C. Chin, V. V. Flambaum, and M. G. Kozlov. Ultracold molecules: new probes on the variation of fundamental constants. *New J. Phys.* **11**, 55048 (2009).

[Cor07] P. B. Corkum and F. Krausz. Attosecond science. *Nat. Phys.* **3**, 381 (2007).

[Lid90] D. R. Lide (Editor) CRC Handbook of Chemistry and Physics, 71th Edition. CRC Press, Boca Raton (1990).

[Dau99] C. Daussy, T. Marrel, A. Amy-Klein, C. Nguyen, C. Bordé, and C. Chardonnet, Limit on the Parity Nonconserving Energy Difference between the Enantiomers of a Chiral Molecule by Laser Spectroscopy *Phys. Rev. Lett.* **83**, 1554 (1999).

[DeM02] D. DeMille. Quantum computation with trapped polar molecules. *Phys. Rev. Lett.* **88**, 067901 (2002).

[DeM04] D. DeMille, D. R. Glenn, and J. Petricka. Microwave traps for cold polar molecules. *Eur. Phys. J. D* **31**, 375 (2004).

[DeM08] D. DeMille, S. B. Cahn, D. Murphree, D. A. Rahmlow, and M. G. Kozlov. Using molecules to measure nuclear spin-dependent parity violation. *Phys. Rev. Lett.* **100**, 23003 (2008).

[Di 04] M. D. Di Rosa. Laser-cooling molecules: Concept, candidates, and supporting hyperfine-resolved measurements of rotational lines in the A-X(0,0) band of CaH. *Eur. Phys. J. D* **31**, 395 (2004).

[DIR37] P. A. M. DIRAC. The Cosmological Constants. *Nature* **139**, 323 (1937).

[Eng11] B. G. U. Englert, M. Mielenz, C. Sommer, J. Bayerl, M. Motsch, P. W. H. Pinkse, G. Rempe, and M. Zeppenfeld. Storage and adiabatic cooling of polar molecules in a microstructured trap. *Phys. Rev. Lett.* **107**, 263003 (2011).

[Eng13] B. G. U. Englert, Sisyphus-Kühlung von polyatomaren Molekülen, Ph.D. thesis (2013).

[Fal11] M. Falkenau, V. V. Volchkov, J. Rührig, A. Griesmaier, and T. Pfau. Continuous Loading of a Conservative Potential Trap from an Atomic Beam. *Phys. Rev. Lett.* **106**, 163002 (2011).

[Fit12] N. J. Fitch, D. A. Esteves, M. I. Fabrikant, T. C. Briles, Y. Shyur, L. P. Parazzoli, and H. J. Lewandowski. State purity of decelerated molecular beams. *J. Mol. Spectrosc.* **278**, 1 (2012).

[Ful04] R. Fulton, A. I. Bishop, and P. F. Barker. Optical stark decelerator for molecules. *Phys. Rev. Lett.* **93**, 243004 (2004).

[Gil06] J. J. Gilijamse, S. Hoekstra, S. Y. T. van de Meerakker, G. C. Groenenboom, and G. Meijer. Near-threshold inelastic collisions using molecular beams with a tunable velocity. *Science* **313**, 1617 (2006).

[Gin04] J. S. M. Ginges and V. V. Flambaum. Violations of fundamental symmetries in atoms and tests of unification theories of elementary particles. *Phys. Rep.* **397**, 63 (2004).

[Glö15a] R. Glöckner, A. Prehn, B. G. U. Englert, G. Rempe, and M. Zeppenfeld. Rotational Cooling of Trapped Polyatomic Molecules. *Phys. Rev. Lett.* **115**, 233001 (2015).

[Glö15b] R. Glöckner, A. Prehn, G. Rempe, and M. Zeppenfeld. Rotational state detection of electrically trapped polyatomic molecules. *New J. Phys.* **17**, 055022 (2015).

[Gór02] K. Góral, L. Santos, and M. Lewenstein. Quantum phases of dipolar bosons in optical lattices. *Phys. Rev. Lett.* **88**, 170406 (2002).

[Gra81] G. Graner and G. Guelachvili. Extensive high-resolution study of the crowded rovibrational CH3F spectrum around 3000 cm^{-1}. *J. Mol. Spectrosc.* **89**, 19 (1981).

[Gri00] R. Grimm, M. Weidemüller, and Y. B. Ovchinnikov,Optical Dipole Traps for Neutral Atoms, pp. 95–170, Academic Press (2000).

[Gri05] A. Griesmaier, J. Werner, S. Hensler, J. Stuhler, and T. Pfau. Bose-Einstein condensation of chromium. *Phys. Rev. Lett.* **94**, 1 (2005).

[Hal12] F. H. J. Hall and S. Willitsch. Millikelvin Reactive Collisions between Sympathetically Cooled Molecular Ions and Laser-Cooled Atoms in an Ion-Atom Hybrid Trap. *Phys. Rev. Lett.* **109**, 233202 (2012).

[Haw53] W. B. Hawkins and R. H. Dicke. The Polarization of Sodium Atoms. *Phys. Rev.* **91**, 1008 (1953).

[Hen12] A. B. Henson, S. Gersten, Y. Shagam, J. Narevicius, and E. Narevicius. Observation of Resonances in Penning Ionization Reactions at Sub-Kelvin Temperatures in Merged Beams. *Science* **338**, 234 (2012).

[Her45] G. Herzberg. Molecular Spectra and Molecular Structure. Vol. II, Infrared and Raman of Polyatomic Molecules. Van Nostrand Reinhold, New York (1945), ISBN 0-442-03386-9.

[Her66] G. Herzberg. Molecular Spectra and Molecular Structure. Vol. III, Electronic Spectra and Electronic Structure of Polyatomic Molecules. Van Nostrand Reinhold, New York (1966), ISBN 0442-03387-7 .

[Her08] E. Herbst, The Chemistry of Cold Interstellar Cloud Cores, in Low Temp. Cold Mol., editor I. W. Smith, chapter 1., Imperial College Press (2008), ISBN 184816209X.

[Her09] D. Herschbach. Molecular collisions, from warm to ultracold. *Faraday Discuss.* **142**, 9 (2009).

[Her13] D. Herschbach. Manipulating molecules via EM fields: a Festschrift for Bretislav Friedrich. *Mol. Phys.* **111**, 1631 (2013).

[Hin97] E. A. Hinds. Testing time reversal symmetry using molecules. *Phys. Scr.* **T70**, 34 (1997).

[Hoe07] S. Hoekstra, J. J. Gilijamse, B. Sartakov, N. Vanhaecke, L. Scharfenberg, S. Y. T. Van De Meerakker, and G. Meijer. Optical pumping of trapped neutral molecules by blackbody radiation. *Phys. Rev. Lett.* **98**, 133001 (2007).

[Hog11] S. D. Hogan, M. Motsch, and F. Merkt. Deceleration of supersonic beams using inhomogeneous electric and magnetic fields. *Phys. Chem. Chem. Phys.* **13**, 18705 (2011).

[Hos10] K. Hosaka, H. Shimada, H. Chiba, H. Katsuki, Y. Teranishi, Y. Ohtsuki, and K. Ohmori. Ultrafast Fourier Transform with a Femtosecond-Laser-Driven Molecule. *Phys. Rev. Lett.* **104**, 180501 (2010).

[Hud11] J. J. Hudson, D. M. Kara, I. J. Smallman, B. E. Sauer, M. R. Tarbutt, and E. A. Hinds. Improved measurement of the shape of the electron. *Nature* **473**, 493 (2011).

[Hüt10] W. Hüttner (Editor) Symmetric Top Molecules, *Landolt-Börnstein - Group II Molecules and Radicals*, volume 29C. Springer Berlin Heidelberg, Berlin, Heidelberg (2010), ISBN 978-3-540-56333-4.

[Hut12] N. R. Hutzler, H.-I. I. Lu, and J. M. Doyle. The buffer gas beam: An intense, cold, and slow source for atoms and molecules. *Chem. Rev.* **112**, 4803 (2012).

[Isa15] T. Isaev and R. Berger. Polyatomic candidates for cooling of molecules with lasers from simple theoretical concepts(2015). arXiv:1504.08326.

[Jan14a] J. Jankunas, B. Bertsche, and A. Osterwalder. Study of the Ne(3P2) + CH3F Electron-Transfer Reaction below 1 K. *J. Phys. Chem. A* **118**, 3875 (2014).

[Jan14b] P. Jansen, H. L. Bethlem, and W. Ubachs. Perspective: Tipping the scales: Search for drifting constants from molecular spectra. *J. Chem. Phys.* **140**(1) (2014).

[Jan15] J. Jankunas and A. Osterwalder. Cold and Controlled Molecular Beams: Production and Applications. *Annu. Rev. Phys. Chem.* **66**, 241 (2015).

[Jin12] D. S. Jin and J. Ye. Introduction to ultracold molecules: new frontiers in quantum and chemical physics. *Chem. Rev.* **112**, 4801 (2012).

[Jun04] T. Junglen, T. Rieger, S. A. Rangwala, P. W. H. Pinkse, and G. Rempe. Slow ammonia molecules in an electrostatic quadrupole guide. *Eur. Phys. J. D* **31**, 365 (2004).

[Kaj04] M. Kajita. Cold collisions between boson or fermion molecules. *Phys. Rev. A* **69**, 012709 (2004).

[Kaj09] M. Kajita. Sensitive measurement of m_p/m_e variance using vibrational transition frequencies of cold molecules. *New J. Phys.* **11**, 55010 (2009).

[Kas50] A. Kastler. Quelques suggestions concernant la production optique et la détection optique d'une inégalité de population des niveaux de quantifigation spatiale des atomes. Application à l'expérience de Stern et Gerlach et à la résonance magnétique. *J. Phys. le Radium* **11**, 255 (1950).

[Kin77] J. L. Kinsey. Laser-Induced Fluorescence. *Annu. Rev. Phys. Chem.* **28**, 349 (1977).

[Kre08] R. V. Krems. Cold controlled chemistry. *Phys. Chem. Chem. Phys.* **10**, 4079 (2008).

[Kre09] R. Krems, B. Friedrich, and W. Stwalley (Editors) Cold Molecules: Theory, Experiment, Applications. CRC Press Taylor & Francis Ltd (2009), ISBN 1420059033.

[Kuz08] E. Kuznetsova, R. Côté, K. Kirby, and S. F. Yelin. Analysis of experimental feasibility of polar-molecule-based phase gates. *Phys. Rev. A* **78**, 12313 (2008).

[Lah09] T. Lahaye, C. Menotti, L. Santos, M. Lewenstein, and T. Pfau. The physics of dipolar bosonic quantum gases. *Reports Prog. Phys.* **72**, 71 (2009).

[Lau76] D. Laughton, S. M. Freund, and T. Oka. Δk = $\pm$3 "forbidden" infrared transitions in the ν2-band of NH3. *J. Mol. Spectrosc.* **62**, 263 (1976).

[Lem13] M. Lemeshko, R. V. Krems, J. M. Doyle, and S. Kais. Manipulation of molecules with electromagnetic fields. *Mol. Phys.* **111**, 1648 (2013).

[Lu14] H.-I. Lu, I. Kozyryev, B. Hemmerling, J. Piskorski, and J. M. Doyle. Magnetic Trapping of Molecules via Optical Loading and Magnetic Slowing. *Phys. Rev. Lett.* **112**, 113006 (2014).

[Lut14] J. J. Lutz and J. M. Hutson. Reactions between cold methyl halide molecules and alkali-metal atoms. *J. Chem. Phys.* **140**(1) (2014).

[Man12] I. Manai, R. Horchani, H. Lignier, P. Pillet, D. Comparat, A. Fioretti, and M. Allegrini. Rovibrational cooling of molecules by optical pumping. *Phys. Rev. Lett.* **109**, 1 (2012).

[Man13] I. Manai, R. Horchani, M. Hamamda, A. Fioretti, M. Allegrini, H. Lignier, P. Pillet, and D. Comparat. Laser cooling of rotation and vibration by optical pumping. *Mol. Phys.* pp. 1–11 (2013).

[Mee09] S. A. Meek, H. Conrad, and G. Meijer. A stark decelerator on a chip. *New J. Phys.* **11**, 055024 (2009).

[Men15] C. Meng, A. P. P. van der Poel, C. Cheng, and H. L. Bethlem. Femtosecond laser detection of Stark-decelerated and trapped methylfluoride molecules. *Phys. Rev. A* **92**, 23404 (2015).

[Mer12] S. Merz, N. Vanhaecke, W. Jäger, M. Schnell, and G. Meijer. Decelerating molecules with microwave fields. *Phys. Rev. A* **85**, 063411 (2012).

[Met99] H. Metcalf and P. van der Straten. Laser Cooling and Trapping. Springer (1999), ISBN 0-387-98747-9.

[Mic06] A. Micheli, G. Brennen, and P. Zoller. A toolbox for lattice-spin models with polar molecules. *Nat. Phys.* **2**, 341 (2006).

[Mic07] A. Micheli, G. Pupillo, H. P. Büchler, and P. Zoller. Cold polar molecules in two-dimensional traps: Tailoring interactions with external fields for novel quantum phases. *Phys. Rev. A* **76**, 043604 (2007).

[Mie10] M. Mielenz, Speichern von polaren Molekülen in einer mikrostrukturierten elektrischen Falle, Diplomarbeit, Julius-Maximilians-Universität Würzburg (2010).

[Mos15] S. A. Moses, J. P. Covey, M. T. Miecnikowski, B. Yan, B. Gadway, J. Ye, and D. S. Jin. Creation of a low-entropy quantum gas of polar molecules in an optical lattice. *Science* **350**, 659 (2015).

[Mot07] M. Motsch, M. Schenk, L. D. Van Buuren, M. Zeppenfeld, P. W. H. Pinkse, and G. Rempe. Internal-state thermometry by depletion spectroscopy in a cold guided beam of formaldehyde. *Phys. Rev. A* **76**, 061402 (2007).

[Mot09] M. Motsch, C. Sommer, M. Zeppenfeld, L. D. Van Buuren, P. W. H. Pinkse, and G. Rempe. Collisional effects in the formation of cold guided beams of polar molecules. *New J. Phys.* **11**, 55030 (2009).

[Nag96] B. Nagels, M. Schuurman, P. L. Chapovsky, and L. J. F. Hermans. Nuclear spin conversion in molecules: Experiments on $^{13}CH_3F$ support a mixing-of-states model. *Phys. Rev. A* **54**, 2050 (1996).

[Nar12] E. Narevicius and M. G. Raizen. Toward cold chemistry with magnetically decelerated supersonic beams. *Chem. Rev.* **112**, 4879 (2012).

[Ni08] K.-K. Ni, S. Ospelkaus, M. H. G. de Miranda, A. Pe'er, B. Neyenhuis, J. J. Zirbel, S. Kotochigova, P. S. Julienne, D. S. Jin, and J. Ye. A high phase-space-density gas of polar molecules. *Science* **322**, 231 (2008).

[Ni09] K. Ni, S. Ospelkaus, D. J. Nesbitt, J. Ye, and D. S. Jin. A dipolar gas of ultracold molecules. *Phys. Chem. Chem. Phys.* **11**, 9626 (2009).

[Nor15] E. B. Norrgard, D. J. McCarron, M. H. Steinecker, M. R. Tarbutt, and D. DeMille. Sub-millikelvin dipolar molecules in a radio-frequency magneto-optical trap (2015). *Phys. Rev. Lett.* **116**, 063004 (2016).

[Oka76] T. Oka, Forbidden rotational transitions, in Mol. Spectrosc. Mod. Res. vol II, editor K. Rao, chapter 5.1, Academic Press, New York (1976).

[Ols72] W. Olson. The infrared spectrum of CH3D. Ground state constants and perturbation allowed transitions. *J. Mol. Spectrosc.* **43**, 190 (1972).

[Ort09] M. Ortner, A. Micheli, G. Pupillo, and P. Zoller. Quantum simulations of extended Hubbard models with dipolar crystals. *New J. Phys.* **11**, 055045 (2009).

[Ost10] A. Osterwalder, S. A. Meek, G. Hammer, H. Haak, and G. Meijer. Deceleration of neutral molecules in macroscopic traveling traps. *Phys. Rev. A* **81**, 051401 (2010).

[Par11] L. P. Parazzoli, N. J. Fitch, P. S. Żuchowski, J. M. Hutson, and H. J. Lewandowski. Large Effects of Electric Fields on Atom-Molecule Collisions at Millikelvin Temperatures. *Phys. Rev. Lett.* **106**, 193201 (2011).

[Per74] W. B. Person. Dipole moment derivatives and infrared intensities. I. Polar tensors. *J. Chem. Phys.* **61**, 1040 (1974).

[Pre12] A. Prehn, Cooling of an electrically trapped gas of Fluoromethane, Diploma thesis, Technische Universität München (2012).

[Pre15] A. Prehn, M. Ibrügger, R. Glöckner, G. Rempe, and M. Zeppenfeld. Direct cooling of polar molecules to sub-millikelvin temperatures (2015). *Phys. Rev. Lett.* **116**, 063005 (2016).

[QP14] M. Quintero-Pérez, T. E. Wall, S. Hoekstra, and H. L. Bethlem. Preparation of an ultra-cold sample of ammonia molecules for precision measurements. *J. Mol. Spectrosc.* **300**, 112 (2014).

[Qué12] G. Quéméner and P. S. Julienne. Ultracold molecules under control! *Chem. Rev.* **112**, 4949 (2012).

[Rab06] P. Rabl, D. Demille, J. M. Doyle, M. D. Lukin, R. J. Schoelkopf, and P. Zoller. Hybrid quantum processors: Molecular ensembles as quantum memory for solid state circuits. *Phys. Rev. Lett.* **97**, 33003 (2006).

[Rab07] P. Rabl and P. Zoller. Molecular dipolar crystals as high-fidelity quantum memory for hybrid quantum computing. *Phys. Rev. A* **76**, 42308 (2007).

[Ran02] S. A. Rangwala, T. Junglen, T. Rieger, P. W. H. Pinkse, and G. Rempe. A continuous source of translationally cold dipolar molecules. *Phys. Rev. A* **67**, 4 (2002).

[Rie05] T. Rieger, T. Junglen, S. A. Rangwala, P. W. H. Pinkse, and G. Rempe. Continuous loading of an electrostatic trap for polar molecules. *Phys. Rev. Lett.* **95**, 173002 (2005).

[Rie11] J. Riedel, S. Hoekstra, W. Jäger, J. J. Gilijamse, S. Y. T. Van De Meerakker, and G. Meijer. Accumulation of Stark-decelerated NH molecules in a magnetic trap. *Eur. Phys. J. D* **65**, 161 (2011).

[Rot06] B. Roth, P. Blythe, H. Wenz, H. Daerr, and S. Schiller. Ion-neutral chemical reactions between ultracold localized ions and neutral molecules with single-particle resolution. *Phys. Rev. A* **73**, 42712 (2006).

[Sal15] E. J. Salumbides, A. N. Schellekens, B. Gato-Rivera, and W. Ubachs. Constraints on extra dimensions from precision molecular spectroscopy. *New J. Phys.* **17**, 33015 (2015).

[San00] L. Santos, G. V. Shlyapnikov, P. Zoller, and M. Lewenstein. Bose-einstein condensation in trapped dipolar gases. *Phys. Rev. Lett.* **85**, 4 (2000).

[Sch10] T. Schneider, B. Roth, H. Duncker, I. Ernsting, and S. Schiller. All-optical preparation of molecular ions in the rovibrational ground state. *Nat. Phys.* **6**, 275 (2010).

[Sha03] M. Shapiro and P. Brumer. Coherent control of molecular dynamics. *Reports Prog. Phys.* **66**, 859 (2003).

[Smi08] I. W. M. Smith (Editor) Low Temperatures and Cold Molecules. Imperial College Press (2008), ISBN 978-1-84816-209-9.

[Sof09] D. Sofikitis, S. Weber, A. Fioretti, R. Horchani, M. Allegrini, B. Chatel, D. Comparat, and P. Pillet. Molecular vibrational cooling by optical pumping with shaped femtosecond pulses. *New J. Phys.* **11**, 055037 (2009).

[Sta10] P. F. Staanum, K. Højbjerre, P. S. Skyt, A. K. Hansen, and M. Drewsen. Rotational laser cooling of vibrationally and translationally cold molecular ions. *Nat. Phys.* **6**, 271 (2010).

[Stu05] J. Stuhler, A. Griesmaier, T. Koch, M. Fattori, T. Pfau, S. Giovanazzi, P. Pedri, and L. Santos. Observation of dipole-dipole interaction in a degenerate quantum gas. *Phys. Rev. Lett.* **95**, 1 (2005).

[Stu13] B. K. Stuhl, M. Yeo, M. T. Hummon, and J. Ye. Electric-field-induced inelastic collisions between magnetically trapped hydroxyl radicals. *Mol. Phys.* **111**, 1798 (2013).

[Tar13] M. R. Tarbutt, B. E. Sauer, J. J. Hudson, and E. A. Hinds. Design for a fountain of YbF molecules to measure the electron's electric dipole moment. *New J. Phys.* **15**, 53034 (2013).

[Tes02] C. M. Tesch and R. De Vivie-Riedle. Quantum computation with vibrationally excited molecules. *Phys. Rev. Lett.* **89**, 157901 (2002).

[Tie13] a. G. G. M. Tielens. The molecular universe. *Rev. Mod. Phys.* **85**, 1021 (2013).

[Ton10] X. Tong, A. H. Winney, and S. Willitsch. Sympathetic cooling of molecular ions in selected rotational and vibrational states produced by threshold photoionization. *Phys. Rev. Lett.* **105**, 1 (2010).

[Tow55] C. H. Townes and A. L. Schawlow. Microwave Spectroscopy (1955), ISBN 048661798X.

[Tre11] C. Trefzger, C. Menotti, B. Capogrosso-Sansone, and M. Lewenstein. Ultracold Dipolar Gases in Optical Lattices. *J. Phys. B* **44**, 56 (2011).

[Tru13] S. Truppe, R. J. Hendricks, S. K. Tokunaga, H. J. Lewandowski, M. G. Kozlov, and C. Henkel. A search for varying fundamental constants using hertz-level frequency measurements of cold CH molecules. *Nat. Comm.* **4**, 2600 (2013).

[Twy14] K. S. Twyman, M. T. Bell, B. R. Heazlewood, and T. P. Softley. Production of cold beams of ND3 with variable rotational state distributions by electrostatic extraction of He and Ne buffer-gas-cooled beams. *J. Chem. Phys.* **141**, 024308 (2014).

[Val02] J. Vala, Z. Amitay, B. Zhang, S. R. Leone, and R. Kosloff. Experimental implementation of the Deutsch-Jozsa algorithm for three-qubit functions using pure coherent molecular superpositions. *Phys. Rev. A* **66**, 62316 (2002).

[Van09] L. D. Van Buuren, C. Sommer, M. Motsch, S. Pohle, M. Schenk, J. Bayerl, P. W. H. Pinkse, and G. Rempe. Electrostatic extraction of cold molecules from a cryogenic reservoir. *Phys. Rev. Lett.* **102**, 33001 (2009).

[Van12] S. Y. T. Van De Meerakker, H. L. Bethlem, N. Vanhaecke, and G. Meijer. Manipulation and control of molecular beams. *Chem. Rev.* **112**, 4828 (2012).

[vdM05] S. Y. T. van de Meerakker, N. Vanhaecke, M. P. J. van der Loo, G. C. Groenenboom, and G. Meijer. Direct Measurement of the Radiative Lifetime of Vibrationally Excited OH Radicals. *Phys. Rev. Lett.* **95**, 13003 (2005).

[vH11] R. von Hahn, F. Berg, K. Blaum, J. R. C. Lopez-Urrutia, F. Fellenberger, M. Froese, M. Grieser, C. Krantz, K.-U. Kühnel, M. Lange, S. Menk, F. Laux, D. A. Orlov, R. Repnow, C. D. Schröter, A. Shornikov, T. Sieber, J. Ullrich, A. Wolf, M. Rappaport, and D. Zajfman. The electrostatic Cryogenic Storage Ring {CSR} – Mechanical concept and realization. *Nucl. Instruments Methods Phys. Res. Sect. B* **269**, 2871 (2011).

[Vit08] M. Viteau, A. Chotia, M. Allegrini, N. Bouloufa, O. Dulieu, D. Comparat, and P. Pillet. Optical pumping and vibrational cooling of molecules. *Science* **321**, 232 (2008).

[Vol13] V. V. Volchkov, J. Rührig, T. Pfau, and A. Griesmaier. Sisyphus cooling in a continuously loaded trap. *New J. Phys.* **15**, 93012 (2013).

[Wak12] A. Wakim, P. Zabawa, M. Haruza, and N. P. Bigelow. Luminorefrigeration: vibrational cooling of NaCs. *Opt. Express* **20**, 16083 (2012).

[Wal13] M. L. Wall, K. Maeda, and L. D. Carr. Simulating quantum magnets with symmetric top molecules. *Ann. Phys.* **525**, 845 (2013).

[Wal15] M. L. Wall, K. Maeda, and L. D. Carr. Realizing unconventional quantum magnetism with symmetric top molecules. *New J. Phys.* **17**, 025001 (2015).

[Wat71] J. K. G. Watson. Forbidden rotational spectra of polyatomic molecules. *J. Mol. Spectrosc.* **40**, 536 (1971).

[Wei10] Q. Wei, S. Kais, and Y. P. Chen. Communications: Entanglement switch for dipole arrays. *J. Chem. Phys.* **132**, 121104 (2010).

[Wei11a] Q. Wei, S. Kais, B. Friedrich, and D. Herschbach. Entanglement of polar molecules in pendular states. *J. Chem. Phys.* **134**, 124107 (2011).

[Wei11b] Q. Wei, S. Kais, B. Friedrich, and D. Herschbach. Entanglement of polar symmetric top molecules as candidate qubits. *J. Chem. Phys.* **135**, 154102 (2011).

[Wil08] S. Willitsch, M. T. Bell, A. D. Gingell, S. R. Procter, and T. P. Softley. Cold reactive collisions between laser-cooled ions and velocity-selected neutral molecules. *Phys. Rev. Lett.* **100**, 43203 (2008).

[Yam04] Y. Yamakita, S. R. Procter, A. L. Goodgame, T. P. Softley, and F. Merkt. Deflection and deceleration of hydrogen Rydberg molecules in inhomogeneous electric fields. *J. Chem. Phys.* **121**(3) (2004).

[Yan13] B. Yan, S. a. Moses, B. Gadway, J. P. Covey, K. R. a. Hazzard, A. M. Rey, D. S. Jin, and J. Ye. Observation of dipolar spin-exchange interactions with lattice-confined polar molecules. *Nature* **501**, 521 (2013).

[Yel06] S. F. Yelin, K. Kirby, and R. Côté. Schemes for robust quantum computation with polar molecules. *Phys. Rev. A* **74**, 50301 (2006).

[Zep09] M. Zeppenfeld, M. Motsch, P. W. H. Pinkse, and G. Rempe. Optoelectrical cooling of polar molecules. *Phys. Rev. A* **80**, 041401 (2009).

[Zep12] M. Zeppenfeld, B. G. U. Englert, R. Glöckner, A. Prehn, M. Mielenz, C. Sommer, L. D. van Buuren, M. Motsch, and G. Rempe. Sisyphus cooling of electrically trapped polyatomic molecules. *Nature* **491**, 570 (2012).

[Zep13] M. Zeppenfeld, Electric Trapping and Cooling of Polyatomic Molecules, Ph.D. thesis, Technical University of Munich (2013).

List of publications

- A. Prehn, M. Ibrügger, R. Glöckner, G. Rempe, and M. Zeppenfeld. Direct cooling of polar molecules to sub-millikelvin temperatures (2015). *Phys. Rev. Lett.* **116**, 063005 (2016).
- R. Glöckner, A. Prehn, B. G. U. Englert, G. Rempe, and M. Zeppenfeld. Rotational Cooling of Trapped Polyatomic Molecules. *Phys. Rev. Lett.* **115**, 233001 (2015).
- R. Glöckner, A. Prehn, G. Rempe, and M. Zeppenfeld. Rotational state detection of electrically trapped polyatomic molecules. *New J. Phys.* **17**, 55022 (2015).
- M. Zeppenfeld, B. G. U. Englert, R. Glöckner, A. Prehn, M. Mielenz, C. Sommer, L. D. van Buuren, M. Motsch, and G. Rempe. Sisyphus cooling of electrically trapped polyatomic molecules. *Nature* **491**, 570 (2012).

Danksagung

Die Ergebnisse, die mit dieser Doktorarbeit vorgestellt werden, sind am Ende auch das Resultat einer wunderbaren Zusammenarbeit vieler. An dieser Stelle möchte ich mich daher recht herzlich bei allen bedanken, die zum Gelingen beigetragen haben.

Zunächst möchte ich meinem Doktorvater Gerhard Rempe dafür danken, dass er mir die Möglichkeit gegeben hat, in seiner Gruppe an diesem spannenden Experiment zu promovieren. Seine spürbare Begeisterung und seine konstruktiven Fragen zum Thema haben mich die gesamte Zeit motiviert. Mit seiner Führungsart trägt er außerdem maßgeblich dazu bei, dass in der Abteilung Quantendynamik ein großer Zusammenhalt und eine positive Stimmung vorherrschen, was mir sehr viel Energie gegeben hat.

Diese Arbeit wäre auch ohne meine Kollegen am Experiment nicht möglich gewesen, bei denen ich mich hiermit herzlich bedanke. Martin Zeppenfeld, Post-Doc am Ultrastark Experiment, hat mit seiner Idee für das Sisyphuskühlen dieses Experiment erst möglich gemacht. Die Diskussionen über Physik haben immer wieder viel Spass gemacht, und von seinem Ideenreichtum werden sicherlich noch weitere Doktorandengenerationen profitieren. Eine besondere Freude war die Zusammenarbeit mit dem Masterstudenten Markus Krottenmüller sowie den Diplomanden Alexander Prehn und Martin Ibrügger, die mittlerweile beide als Doktoranden an dem Experiment arbeiten. Insbesondere bei Alex, mit dem ich meiste Zeit zusammengearbeitet habe, möchte ich mich für die tolle Stimmung und seine große Hilfsbereitschaft bedanken. Von meiner ehemaligen Kollegin, Barbara Englert, habe ich vieles über das Experiment gelernt und die fröhlichen Stunden, die wir im Labor verbracht haben, werden mir immer in guter Erinnerung bleiben. Über die Physik der Moleküle und die technischen Details im Labor konnte ich auch vieles von den anderen Wissenschaftlern der Molekülgruppe, Christian Sommer, Sotir Chervenkov, Xing Wu und Thomas Gantner lernen.

Ebenso gilt mein Dank allen anderen Gruppenmitgliedern der Abteilung Quantendynamik für die herzliche, hilfsbereite und anspornende Atmosphäre. Ich konnte hier eine inspirierende Zeit verbringen, auf die ich immer gerne zurückschauen werde. Besonders erwähnenswert ist hier, dass ich auch bei den Gruppenleitern der anderen Experimente Tatjana Wilk, Stephan Dürr und Stephan Ritter immer ein offenes Ohr gefunden und Ratschläge bekommen habe. Unsere Techniker Sepp Bayerl, Franz Denk, Helmuth Stehbeck, Thomas Wiesmeier, Tobias Urban und Florian Furchtsam haben mit ihrem Fachwissen, ihren handwerklichen Fähigkeiten und dem schnellen Helfen bei Problemen den Bau und Betrieb der Apparatur erst möglich gemacht. Iris Schwaiger hat mit ihrer freundlichen Art nicht nur immer wieder für gute Stimmung gesorgt, sondern war auch bei allen organisatorischen Fragen eine große Hilfe.

Die Möglichkeit, sich am MPQ ganz auf die Forschung zu konzentrieren, ergibt sich auch aus der großen Einsatzbereitschaft der nichtwissenschaftlichen Mitarbeiter am Institut, denen ich daher ebenfalls Danke sagen möchte.

Zum Schluss möchte ich mich bei meinen Eltern und Großeltern, meiner Schwester Charlotte, meinem Lebensgefährten Stephan und meinen Freunden bedanken. Sie sind

die Menschen, die mir das Rüstzeug gegeben haben, diese Aufgabe anzupacken und die mich jederzeit und bedingungslos unterstützt und gestärkt haben. Das ist keinesfalls selbstverständlich und ich bin dafür von ganzem Herzen dankbar.